FE-2248-17
Distribution Categories UC-90g and UC-93

DEVELOPMENT, TESTING AND EVALUATION OF MHD MATERIALS AND COMPONENT DESIGNS

Quarterly Report for the Period
July 1 - September 30, 1977

John W. Sadler
Raymond Calvo
Larry H. Cadoff*
James A. Dilmore*
Gary E. Driesen
Alfred G. Eggers
Edsel W. Frantti
Edward L. Kochka
John A. Kuszyk
Joseph Lempert*
Barry R. Rossing*
Stephen J. Schneider*
Abner B. Turner

* Westinghouse Research & Development Center

WESTINGHOUSE ELECTRIC CORPORATION
Advanced Energy Systems Division
P. O. Box 10864
Pittsburgh, PA 15236

February 1978

PREPARED FOR THE
UNITED STATES DEPARTMENT OF ENERGY

Under Contract No. EX-76-C-01-2248

APPROVED:

J. W. Sadler, Project Manager
Advanced Energy Systems Division

TABLE OF CONTENTS

TABLE OF CONTENTS (Continued)

TABLE OF CONTENTS (Continued)

LIST OF FIGURES

LIST OF FIGURES (Continued)

LIST OF FIGURES (Continued)

LIST OF FIGURES (Continued)

LIST OF TABLES

LIST OF TABLES (Continued)

I. ABSTRACT

Efforts during the July to September, 1977 quarter were directed toward the design, fabrication and evaluation of ceramic MHD electrodes for both clean fuel and coal fired environments.

Laboratory screening tests continued to evaluate the electrochemical corrosion encountered for coal-fired conditions. A series of tests were conducted on MAFF in an eastern synthetic slag which resulted in identification of the degradation mechanisms for anodes and cathodes. Torch testing was completed to evaluate several attachment techniques and to determine the resistance of $La_{.95}Mg_{.05}CrO_3$ to thermal shock.

Clean-firing tests of a cold copper electrode test assembly and a hot $LaCrO_3$ electrode test assembly were completed in WESTF. In addition installation, checkout and initial operation with oxygen was completed.

Primary emphasis was put on the design and analysis of electrode systems included in the Proof Test Series for the U-02 Phase III Module. Assembly of the initial proof test assembly is underway. This test is scheduled for October, 1977. Development and fabrication activities for the electrodes to be incorporated into the subsequent proof tests is proceeding.

II. OBJECTIVE AND SCOPE OF WORK

In continuation of the program to develop MHD power generation to commercial feasibility, Westinghouse is conducting a 36-month program to test and evaluate materials and component designs in both laboratory scale apparatus and in an integrated MHD system facility. Primary emphasis has been given to "hot generator wall" concepts under slagging conditions. The program provides a link between the basic and supportive materials development and testing and the applied testing in a facility that offers an adverse MHD environment for extended periods of time. The program carries forth the engineering development of selected MHD component(s), e.g., electrode and insulating wall systems, through design, materials fabrication, initial screening tests, construction and finally to an MHD system test. The entire sequence is reiterative; i.e., each stage will involve an optimization of both design and materials.

These objectives are being pursued in accordance with a statement of work which is consistent with the National Plan for MHD development formulated by DOE. The program consists of the following four tasks:

- Task 1 - Long Duration MHD Facility System and Component Test Evaluation
- Task 2 - Materials Design/Development
- Task 3 - Testing and Evaluation of Prototype Electrode Systems
- Task 4 - Technical Support for the Cooperative US-USSR Program on MHD

1.0 TASK 1 - LONG DURATION MHD FACILITY SYSTEM AND COMPONENT TEST AND EVALUATION (WALTZ MILL TEST FACILITY)

The engineering purpose of this task is to establish the basic chemical, thermal and electrical properties of the MHD gas stream and materials of construction in an integrated system on a component-by-component basis as well as on a system basis. The facility is a test bed for sub-scale generators of advanced design. The general technical approach to be adhered to is embodied in the "hot generator wall" concept.

1.1 Subtask 1.1 - Test and Evaluation with Existing Waltz Mill MHD Facility

Suspend all test activity effective January 1, 1977. Initiate tests during FY 1978 when the upgraded facilities become available. These tests shall be made on selected module designs and under selected electrical, thermal, and slagging conditions as stipulated in a DOE approved FY 1978 Work Plan with appropriate schedules.

1.2 Subtask 1.2 - Conversion and Upgrading of Waltz Mill Facility to Materials/Component Test Facility

Upgrading of the Waltz Mill Facility will be continued in FY 1977 at a reduced rate, using minimal supervision and craft personnel. In FY 1978, this effort will be increased to provide capability for 100 hr continuous testing of electrode modules under thermal, electrical, and chemical stress conditions representative of MHD power generation duty. Table 1 summarizes test capability objectives.

2.0 TASK 2 - MATERIALS DESIGN DEVELOPMENT (ELECTRODE SYSTEMS)

Deleted.

3.0 TASK 3 - TESTING AND EVALUATION OF PROTOTYPE ELECTRODE SYSTEMS

Complete material test facility modification, WESTF, including provision for oxygen enrichment to permit subsonic tests up to 2900K under imposed electrical loads, thermal fluxes, and seed environment simulating U-02 environmental conditions. Also provide ash injection capability to simulate coal-firing. Conduct three tests of up to 20 hours each of electrode module candidates per the Work Plan. The summary of test capability objectives is presented below. Continue laboratory bench test work is necessary to establish essential electrical, chemical, and thermal stability characteristics of selected electrode and insulator candidate materials.

MHD FACILITY CHARACTERISTICS

CHARACTERISTIC	WALTZ MILL TEST FACILITY (WMTF)	ELECTRODE SYSTEMS TEST FACILITY (WESTF)
Mass Flow	3 lb/sec design	0.5 lb/sec
Combustion Temperature	To 2850°K	To 2850°K
Combustor Pressure	2.6 - 3.0 atmospheres normal 6 atm peak	2-3 atmospheres normal 5 atm peak
Channel Velocity	Subsonic or Supersonic (Future)	Subsonic, 500 to 800 m/sec
Seeding	K_2CO_3 or K_2SO_4 dry with ash or char additions.	K_2CO_3 or K_2SO_4wet with ash or char additions.
B Field	3 Tesla flat over one meter	None (Future)
Magnet Opening	13.5 x 25.4 x 111.76 cm	N.A.
Fuel	Toluene	Toluene
Oxidant	Oxygen enriched preheated air	Oxygen enriched preheated air
Data Collection	240 channels	60 channels
Test Duration	up to 100 hrs or greater	up to 100 hrs
Test Frequency	1 per month	2 per month
Channel Configuration	16 or 48 electrode pairs	12 electrode pairs 1" x 2" flow cross section
Startup Ramp, Minimum	~10°K/min	~25°K/min
Load Bank	Lamps	N.A.

4.0 TASK 4 - TECHNICAL SUPPORT FOR THE COOPERATIVE US-USSR PROGRAM ON MHD

This task provides technical support to the activities of the cooperative US-USSR program.

Specifically this involves 1) USSR Testing in Westinghouse Facilities, 2) U-25 Module Testing in Westinghouse Facilities and 3) Materials Testing in U-02, Phase I and Phase II. Each of these activities are defined by DOE appointed committees.

- General liaison relative to the joint US/USSR committees active in the areas of materials and generators and monitoring USSR testing programs in US facilities, non-Westinghouse. This subtask does not include provisions for any development or hardware effort.

- Design, fabrication, assembly, and delivery of a U-02 Phase III test module to the U-02 facility in Moscow. Participate as directed by the DOE Program Manager in test operations and post-test analyses (to be performed by the National Bureau of Standards). Conduct a total of three tests of up to 20 hours on candidate electrode designs as approved by the DOE Project Manager as proof testing prior to final module selection. (Note: The U-02 program agreements are set forth in Meeting Record 08.0208.03, dated February 8, 1977, of the Joint US-USSR MHD Materials Working Group.)

III. SUMMARY OF PROGRESS TO DATE

Figure 1 summarizes the overall program schedule and status.

1.0 TASK 1 - LONG DURATION DUCT DEVELOPMENT - WALTZ MILL

No significant activity this quarter.

2.0 TASK 2 - MATERIALS/DESIGN DEVELOPMENT (ELECTRODE SYSTEMS)

This activity has been deleted.

3.0 TASK 3 - TESTING AND EVALUATION OF PROTOTYPE ELECTRODE SYSTEMS

Laboratory scale electrochemical experiments were continued with MAFF-31 electrodes. Analysis of these tests indicate that electrochemical corrosion is a result of two separate but interrelated reactions that occur within the slag due to the passage of current and reactions between the "reacted" slag and the electrode materials themselves. Details of these investigations are presented in Section 3.1

A series of five laboratory oxygen-propane torch tests of electrode systems were completed to investigate the performance of different electrode attachment methods and to determine the thermal shock resistance of $La_{.95}Mg_{.05}CrO_3$. Results of this continuing investigation are presented in Section 3.3.

During this quarter the Westinghouse Electrode Systems Test Facility (WESTF), formerly identified as the Materials Test Facility (MTF), performed satisfactorily for a series of test runs in the clean-firing mode with a cold wall test assembly, copper electrodes, and a hot wall test assembly, lanthanum chromite electrodes. These runs, Tests 35 and 36, are the final runs prior to the U-02 Proof Test Series scheduled for the next quarter. The test time at design conditions, seed on to seed off, was 42 hours and the longest continual run

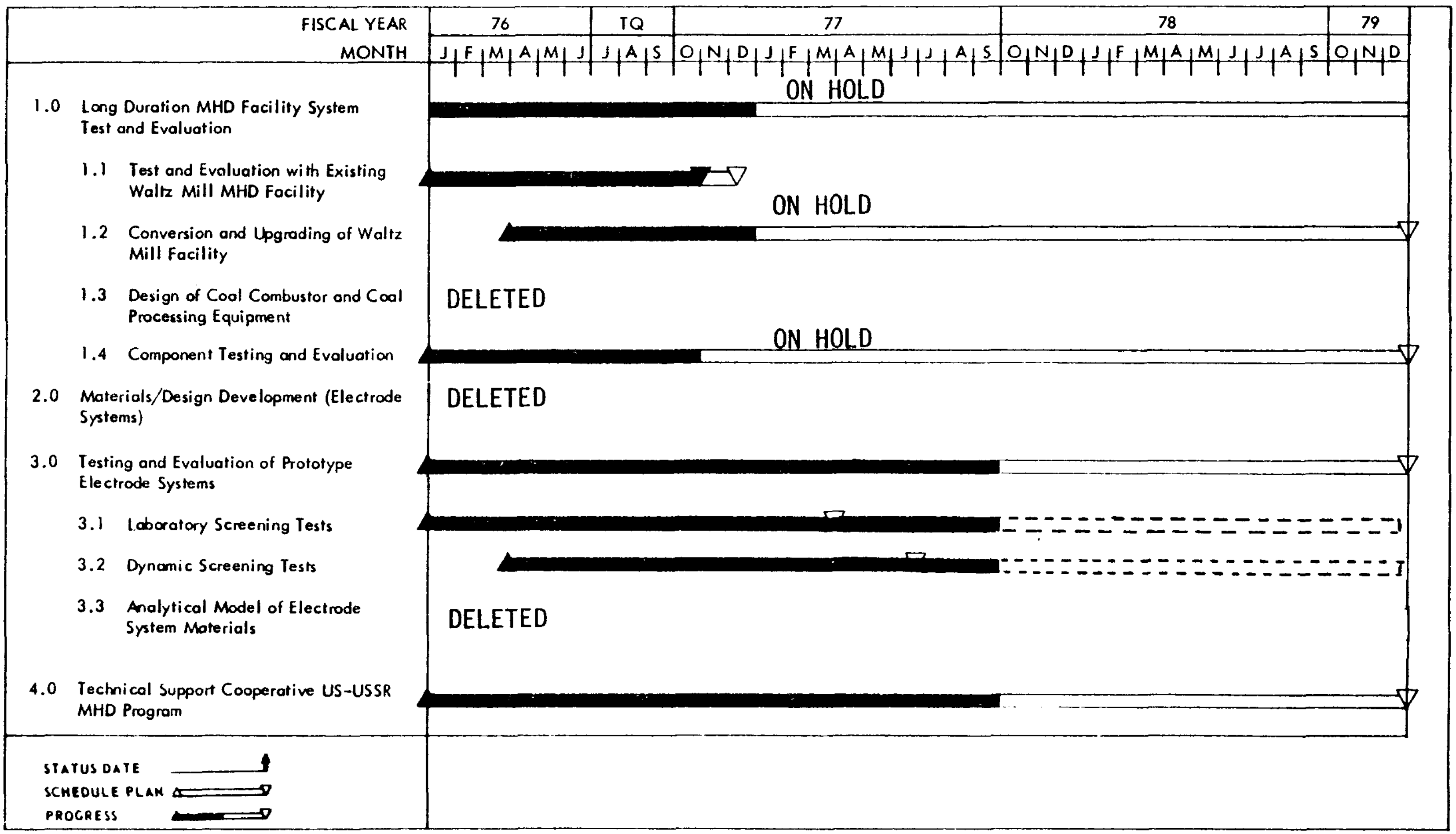

Figure 1. Program Schedule and Status

was 20 hours, Test 36. Installation and checkout of the oxygen system was completed and oxygen was initially used in Test 35-3. This series of runs, discussed in Section 3.5, has shown WESTF to operate very reliably as a long duration test facility for the testing of candidate electrode materials and systems.

4.0 TASK 4 - TECHNICAL SUPPORT FOR THE US-USSR PROGRAM ON MHD

Work on the U-02 Phase III Module Test is continuing with current emphasis placed on the design and fabrication effort associated with the upcoming Proof Test Series. The proof tests will provide for the comparitive evaluation of 11 electrode/insulator systems including seven based on $LaCrO_3$, three upon MAFF and one upon a HfO_2-metal composite. Magnesium oxide, MgO, and magnesium aluminate spinel, $MgAl_2O_4$, are included as interelectrode insulators; strontium zirconate was eliminated as an insulator on the basis of poor high temperature resistivity.

Pre-test property measurements are being completed by Battelle-Northwest Laboratories (BNW), National Bureau of Standards (NBS) and Westinghouse to support the electrode detail design. Extensive coupled thermal-structural design analyses are being completed to support the detail design of electrode systems to be incorporated into the Proof Test Series. As a result of these analyses a number of design optimizations have been identified for inclusion in the proof test hardware.

The first three sets of electrodes have been received and are in the process of being assembled into electrode walls for the first proof test. This test includes: MAFF-41 on a proprietary "FLEXBED" structure, supplied by General Electric, Argonne National Laboratory's CeO_2OHfO_2-Y_2O_3-metal composite and MAFF-31 on Hoskins 875 BRUNSBOND mesh. The remaining eight sets of electrodes are in various stages of development or fabrication. Details relative to the U-02 Phase III effort are presented in Section 4.0.

IV. DETAILED DESCRIPTION OF TECHNICAL PROGRESS

1.0 TASK 1 - LONG DURATION MHD DUCT DEVELOPMENT - WALTZ MILL

No significant activity was undertaken this quarter.

2.0 TASK 2 - MATERIALS/DESIGN DEVELOPMENT (ELECTRODE SYSTEMS)

No activity - task deleted.

3.0 TASK 3 - TESTING AND EVALUATION OF PROTOTYPE ELECTRODE SYSTEMS

The objective of this task is to evaluate candidate electrode and insulator materials under the thermal, chemical and electrical conditions realized in future base load, coal fired MHD generators. Candidate materials will cover the full range of channel operating conditions, i.e., from cold wall-slagging to hot non-slagging. Basic material property data will be generated in this task. For clean firing conditions materials data is presented under Task 4.0.

3.1 Electrochemical Corrosion

A number of laboratory-scale electrochemical experiments have been run with $3MgAl_2O_4 \cdot 1Fe_3O_4$ electrodes to ascertain corrosion mechanisms and to elucidate the role of current density on corrosion in a synthetic eastern slag, E-03*. The tests were run in a manner described earlier, at constant current, using $3MgAl_2O_4 \cdot 1Fe_3O_4$ electrode material obtained from Battelle North West.[(1)] The test conditions and results of this series of experiments are summarized in Table 1.

For all tests the cathode is characterized by a highly recrystallized multi-phase structure at the slag interface which consists mainly of slightly Fe depleted $3MgAl_2O_4 \cdot Fe_3O_4$, FeO particles and sometimes includes particles of a (Fe, Ca, Mg)

---

* E-03 slag composition in weight percent is: 48 SiO_2, 20 Al_2O_3, 21 Fe_2O_3, 8 CaO, 1 MgO, .8 TiO_2, 1.1 Na_2O and 1.5 K_2O.

TABLE 1

SUMMARY OF ELECTROCHEMICAL CORROSION TESTS
OF $3MgAl_2Oy \cdot 1Fe_3O_4$ IN E-03 SLAG

Electrode Material	$3MgAl_2O_4 \cdot Fe_3O_4$			
Test ID#	105,* 106	123	116	1S3
Temperature, °C	1390	1390	1390	1000
Duration, min	26	43	30	60
Electrode Separation, cm	0.45	0.64	0.64	0.32
Current Density, amp/cm^2	1.2	2.4	3.0	1.1
Voltage Drop Across Slag, Calculated				
Start	9	29	31	
End	2.7	16	26	
Corrosion, ΔW, mg/coulomb				
Cathode, ΔW_c	64	34‡	34‡	3.8
Anode, ΔW_a	10	104	194	1.9
$\Delta W_c/\Delta W_a$	6.4	.33	.18	2

*Identical test conditions. Results were within 10% of each other.

‡Extensive cathodic grain boundary penetration by slag.

silicate phase and metallic Fe globules, especially at the higher current densities. Figure 2 illustrates the nature of this microstructure. With time or increasing current density, the surface structure becomes more and more infiltrated with slag, due perhaps to the preferential dissolution of the FeO phase and the fluxing of large grains off the surface. In nearly all cases, metallic Fe globules or dendrites are found at the slag/electrode interface. A small distance into the electrode from the slag interface is a region of partially dissociated $3MgAl_2O_4 \cdot Fe_3O_4$ which contains FeO particles at most grain boundaries and pores. The shape of the FeO phase, as shown in Figure 2, suggests that a liquid phase was present during its formation. No FeO is found at locations other than grain boundaries or pores. SEM-EDAX analysis shows that the $3MgAl_2O_4 \cdot Fe_3O_4$ is depleted in iron around the FeO particles, indicating that the iron has come from the matrix, i.e., $3MgAl_2$ $3MgAl_2O_4 \cdot Fe_3O_4 \rightarrow FeO + 3MfAl_2O_4 \cdot 1Fe_2O_3$. Still further into the cathode from the slag interface, a region of iron-depleted but calcium-enriched slag penetrates pores and grain boundaries of the matrix. The depth and extent of the various corrosion (reaction) regions increases with the number of coulombs passed. All indications are that cathodic corrosion is first triggered by the penetration into the matrix, via grain boundaries and pores, of a highly fluid slag which is formed by the preferential transport of Fe^{+2}, Ca^{+2} and K^{+1} ions towards the cathode. The role of metallic iron in corrosion at the cathode appears to be quite passive--the metallic iron, being much denser than the surrounding slag, generally falls away from the interface after it is formed.

Analysis of these tests indicate that electrochemical corrosion is, in the main, a result of two separate but interrelated reactions--reactions that occur within the slag itself due to the passage of current and reactions between the "reacted" slag and the electrode materials themselves.

The predominant reaction occurring in the slag involves electrolysis. This is evidenced by the formation of metallic α-iron at the cathode as shown in Figure 2 and oxygen gas at the anode. Bubble evolution can be readily viewed during a run and is responsible for the large and frequent fluctuations in

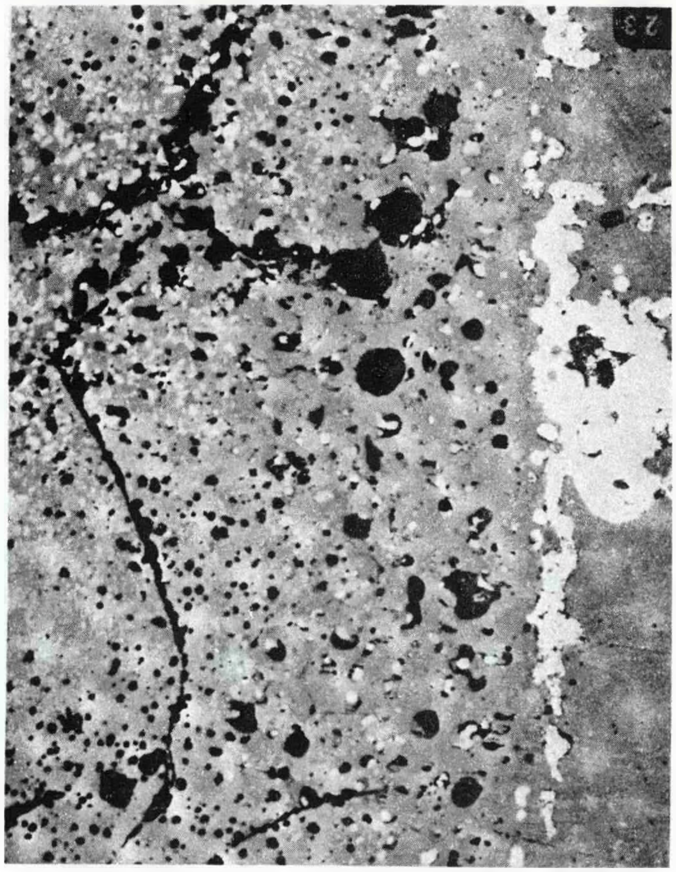

$3MgAl_2O_4 \cdot 1Fe_3O_4$ [Slag]

Figure 2. Photomicrograph showing typical cathodic corrosion of $3MgAl_2O_4 \cdot 1Fe_3O_4$ (Test 116). White particles in slag at interface are α-Fe, lighter colored particles in matrix are FeO.

voltage during the course of a constant current test. Fluctuations usually amount to ≈± 6-10% of the interelectrode voltage drop with a frequency of about 15-30 seconds at 1 amp/cm^2. The frequency of voltage fluctuations as well as the rate of bubble formation increases rapidly with increasing current density.

SEM-EDAX scans across the interelectrode slag indicated that all test cells in Table 1 exhibited an enrichment in aluminum and silicon near the anode and iron, calcium and potassium (Fe^{+2}, Ca^{+2}, K^{+1}) at the cathode. These regions of segregation are usually limited to a zone within 0.5 mm of the electrodes; the slag is generally homogeneous outside of these areas.

The reaction scheme at the anode differs considerably from that at the cathode. The more viscous SiO_2 and Al_2O_3 rich slag apparently does not wet nor penetrate to a significant degree into the matrix. Surface chemical reactions dominate and a nonadherent readily fluxed iron-rich spinel layer (probably hercynite, $FeAl_2O_4$) is found at the surface at low current densities. At current densities much greater than 1 amp/cm^2, the anode is rapidly machined or cavitated away by the action of oxygen bubbles. Catastrophic anodic attack is illustrated in Figure 3 for a test cell run at 3 amp/cm^2 for 30 minutes.

The rapidly increasing severity of cavitation/corrosion in $3MgAl_2O_4 \cdot Fe_3O_4$ anodes with increasing current density is evident in Figure 4. Cathodic corrosion is also included in Figure 4 for comparison purposes. Corrosion at both electrodes, (W/It) does not obey Faraday's Law, indicating non-Faradaic processes are dominating the corrosion reactions.

3.2 Electrode/Insulator Development

Primary emphasis during this period was placed on support of the U-02 Phase III Module and results are reported in Section 4.1.1 for clean firing.

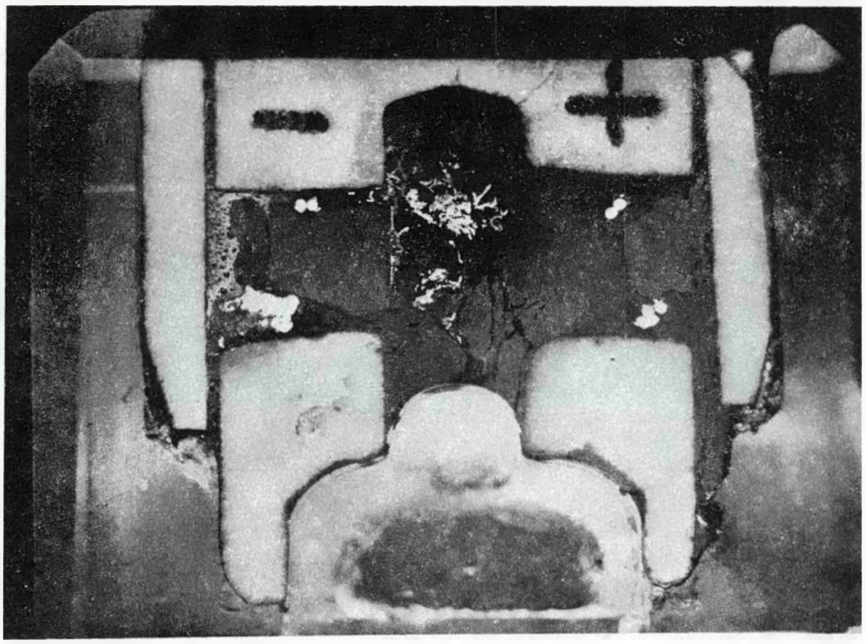

Figure 3. Cross-section of test cell (Test #116) illustrating catastrophic anodic erosion at high current density (3 Amp/cm^2).

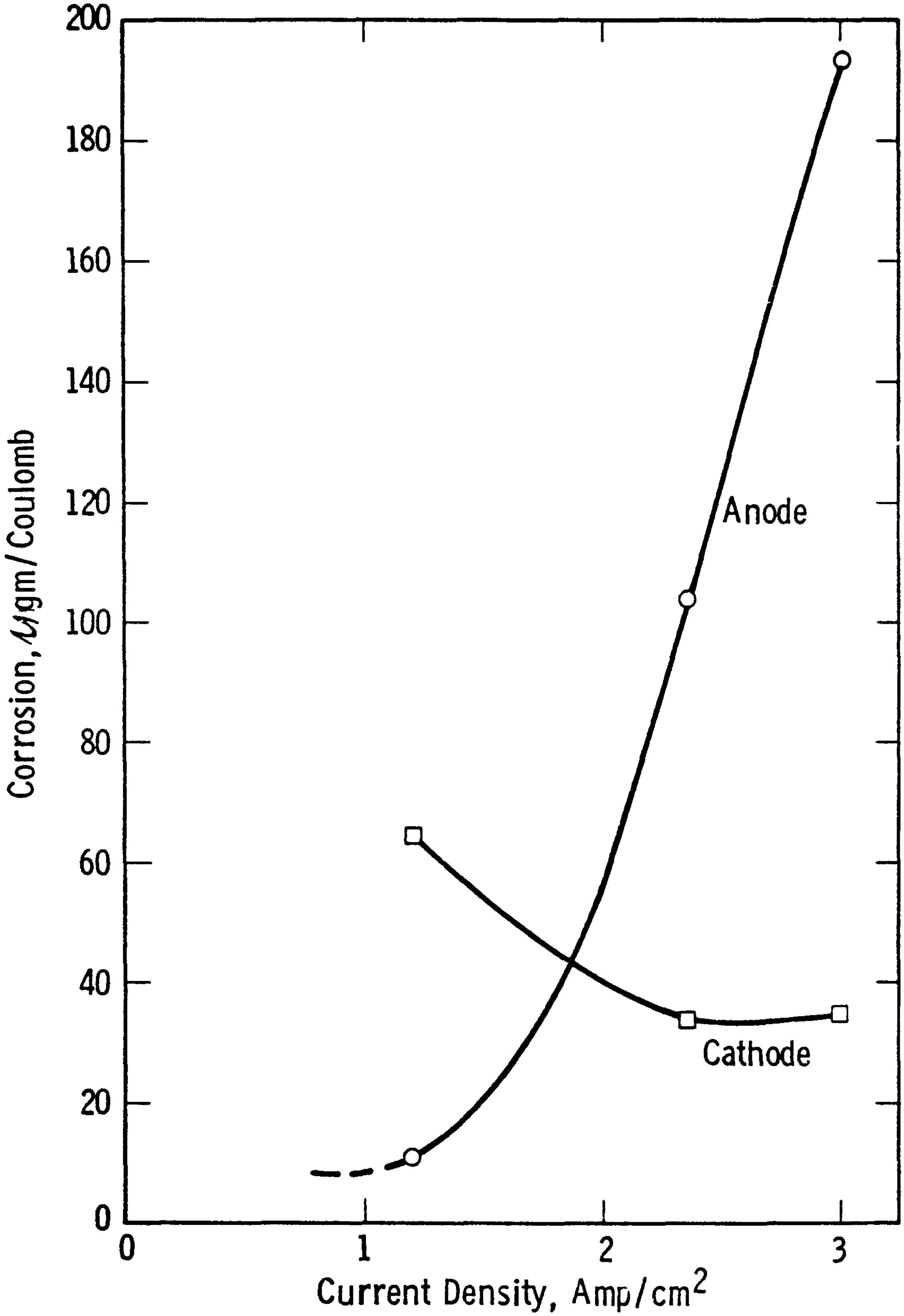

Figure 4. Dependence of anodic and cathodic corrosion losses in $3MgAl_2O_4 \cdot 1Fe_3O_4$ on current density

3.3 Electrode/Insulator Structure

A number of torch (oxygen-propane) tests were continued during this quarter to primarily evaluate two MHD material areas: 1) to determine the performance of differene electrode attachment methods under commercial channel thermal stresses and 2) to determine the thermal shock resistance of $La_{.95}Mg_{.05}CrO_3$ ceramics. The electrode/insulator assemblies and the test rig were comparable to those described in previous quarterlies. The results of Test 7 through 11 are shown in Table 2.

For Tests 7 through 9, $12Y_2O_3$-$88ZrO_2$ was used as the electrode material and hot-pressed $MgAl_2O_4$ was the insulator. These three tests were conducted to primarily evaluate the attachment method. The Techfelt attachment used in Test 7 held up reasonably well during the run, although small fissures were observed in the electrode just above and parallel to the brazed interface. The corrugated nickel attachment used in Tests 8 and 9 held up extremely well, with no detectable signs of the braze joint failing. After air quenching, the whole electrode assembly from a surface temperature of 1770°C, no deleterious effects were apparent.

Tests 10 and 11 were conducted to ascertain a qualitative estimate of the thermal shock resistance of $La_{.95}Mg_{.05}CrO_3$. The height of the electrode was set to correspond to a surface heat flux of ~15 w/cm^2. For both tests the electrode maintained a surface temperature of 1700°C prior to an immediate air quench to a surface temperature of 500°C. In both cases the electrode was then brought back up to a surface temperature greater than 1750°C prior to a second air quench. In test No. 10 the post test observations revealed no failure of the silver epoxy attachment. The electrode did however, crack into two pieces parallel to the surface of the electrode halfway between the surface and backface. Test No. 11 was run in an identical manner to Test No. 10 to determine if the same cracking pattern would prevail. This time no fractures

TABLE 2

MATERIALS/ATTACHMENT TORCH TEST (OXYGEN/PROPANE)

Test	Electrode	Insulator	Attachment	Thermal w/cm°C Conductivity (Electrode)	Max. Surface Temp. (°C)	Electrode Thickness	Heat Flux w/cm^2	Observations
7	$12Y_2O_3$-$88ZrO_2$	$MgAl_2O_4$ (W)	Nichrobraze 10 between Cu and Techfelt*, Techfelt brazed to electrode with Nicosil	$K_{av} \simeq 0.0123$	1720	1 cm	10.6	Backface temperature reached 853°C; Attachment held but air gaps evident between Techfelt and electrode; Observable cracking of electrode near braze. Electrode at maximum temperature for 1 hour.
8	$12Y_2O_3$-$88ZrO_2$	$MgAl_2O_4$ (Transtech)	Nickel corrugated sheet brazed to electrode and Cu with Ticosil	$K_{av} \simeq 0.0123$	1715	1 cm	12.7	Backface temperature reached 682°C; Corrugation stayed brazed to Cu and electrode; Insulator cracked across its width; Electrode at max. temperature for 1 hour.
9	$12Y_2O_3$-$88ZrO_2$	$MgAl_2O_4$ (Transtech)	Nickel corrugated sheet brazed to electrode and Cu with BT.	$K_{av} \simeq 0.0123$	1770	1 cm	14.0	Backface temperature reached 567°C; After 1 hour at 1700°C surface, torch was taken away until surface reached 500°C, Torch was then refired, surface taken up to 1770° for 15 min. then taken away as before - No visible signs of cracking and attachment was still good after this test.
10	$La_{.95}Mg_{.05}CrO_3$	$MgAl_2O_4$ (Transtech)	Silver epoxy	$K_{av} \simeq 0.0225$	1775	0.70"	14.5	Backface temp. reached 555°C; After 1 hour at 1700°C torch taken away until 500°C surface reached; then torch refired to 1775°C surface for 15 min.; $LaCrO_3$ electrode totally cracked halfway up the material laterally from the backface.
11	$La_{.95}Mg_{.05}CrO_3$	$MgAl_2O_4$ (Transtech)	Silver epoxy	$K_{av} \simeq 0.0225$	1780	0.70"	16.4	Backface temp. reached 418°C; After 1 hour at 1715°C torch taken away until surface reached 480°C, torch refired to 1780°C surface for 15 min; No observable cracking of electrode or insulator; Attachment remained good after test.

* Stainless Steel Mesh, Technical Wire Products, Inc., Crawford, N. J. 07016

occurred in the electrode and the epoxy attachment again maintained a good bond. Finite element stress analysis reveals that for this model (lanthanum chromite bonded with epoxy) the greatest stresses are concentrated near the attachment interface, not in the interior of the electrode where the fracture had occurred. Therefore, the fracture in the electrode in Test 10 was most likely initiated by a flaw (either a pore or low density area) in the interior of the ceramic piece.

3.4 Test Section Fabrication

3.4.1 Hot Wall Test Assembly - (Lanthanum Chromite Electrodes)

The first hot wall ceramic electrode channel was assembled for test in WESTF, Test #36. The electrodes were lanthanum chromite; interelectrode insulators were either magnesia, spinel, or strontium zirconate; and attachments were made either directly by an adhesive or through a compliant layer using an adhesive or brazing. Figures 5 through 10illustrate the construction of the test assembly.

Figure 5 shows a view of an electrode wall. There are twelve identical electrodes in the anode and cathode walls. The electrodes are one centimeter wide in the direction of plasma flow and about six centimeters long with an area of about five square centimeters exposed to the plasma flow. The pitch between electrode is about 1.4 centimeters. Each electrode is made up of three pieces, nominally 1 x 2 x 2 cm, of hot pressed lanthanum chromite. Attachments and insulators differ from electrode to electrode. These are identified in Table 3.

Electrodes in channel positions 201, 209, 109 and 112 were joined to the copper base with a conductive silver-filled silastic adhesive cured at room temperature. The electrodes in positions 101, 205, 105, 206, 106 and 212 were joined to copper with a conductive silver-filled epoxy adhesive cured overnight at 130^{o}C. Electrodes in positions 202, 102, 207, 107, 208, and 108 were attached to the copper through a stress-absorbing corrugated nickel part. The lanthanum chromite surface was metallized with plasma sprayed nickel and brazed at high temperatures to the corrugated nickel. This assembly was then soldered to the copper base where, if

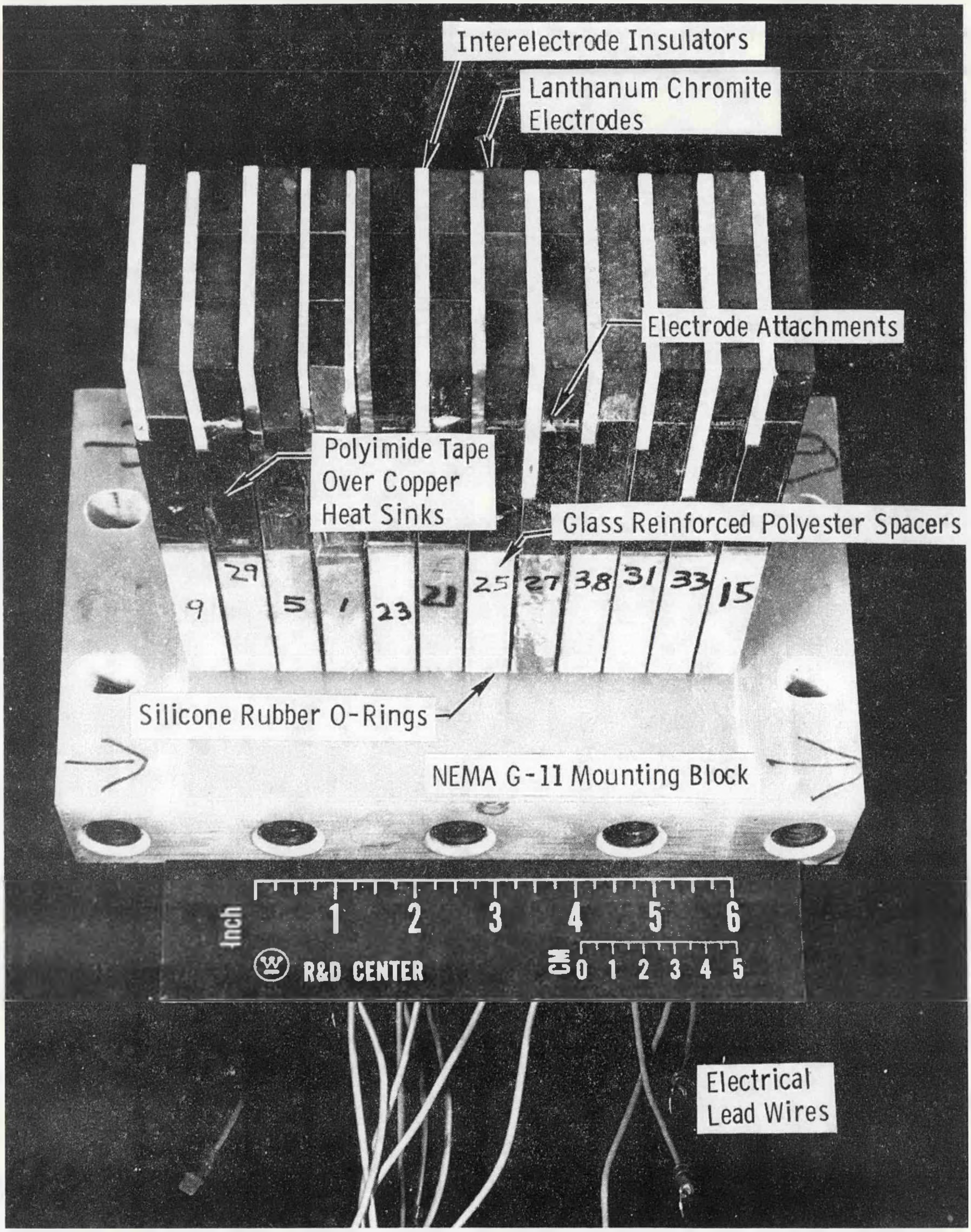

Figure 5. View of Electrode Wall

TABLE 3

DESCRIPTION OF HOT CHANNEL ELECTRODE WALLS

Electode No.	Channel Position	Electrode Height (mm)	Attachment Type	Attachment Size (mm)	Interelectrode Insulators Type	Interelectrode Insulators Size (mm)
9,16	201,101	17,17	Silastic, Epoxy	.25, .25	MgO, MgO	24.7, 24.8
29,30	202,102	18	Corrugated Nickel	2.8	$MgAl_2O_4$	28.6
5,6	203,103	21	Mechanical/Silastic	0.7	MgO	14.1
1,2	204,104	21	Mechanical/Techfelt	1.9	MgO (2 sides)	13.8
23,24	205,105	17	NBS Mechanical/Epoxy	.25	MgO	24.8
21,22	206,106	17	Epoxy	.25	MgO	24.8
25,26	207,107	18	Corrugated Nickel	2.8	$MgAl_2O_4$	28.6
27,28	208,108	18	Corrugated Nickel/Epoxy	2.8	$MgAl_2O_4$	28.6
38,37	209,109	17	Silastic	.25	$SrZrO_3$	24.7
31,32	210,110	19	Monel/Braze	1.5	$MgAl_2O_4$	28.6
33,34	211,111	19	Monel/Braze	1.5	$MgAl_2O_4$	28.6
15,12	212,112	17,17	Epoxy, Silastic	.25, .25	MgO, MgO	24.8, 24.7

separation occurred in the bond between the lanthanum chromite and nickel, the assembly was repaired using silver-filled epoxy for the particular electrode segment rather than by rebrazing. Electrode positions 210, 110, 211 and 111 employed a soft Monel mesh as a compliant layer brazed to the lanthanum chromite and soldered to the copper base. As above, if a bonded electrode segment detached it was repaired with silver-filled epoxy. Mechanical attachments were employed in electrode positions 203, 103, 204, and 104. Electrodes 203 and 103 used 0-80 brass screws through holes near the base of the lanthanum chromite into threaded holes in an extension of the copper base. Silver-filled silastic was used to provide a conductive connection between the ceramic electrode and the copper base. Electrodes 204 and 104 used 0-80 brass screws threaded through extensions of the copper base into shallow blind holes on both sides of the ceramic electrodes. Techfelt (a nickel filled silicone rubber pad) was used to provide continuity between the ceramic electrode and the copper base. Electrodes 205 and 105 also had a mechanical attachment provided by the National Bureau of Standards. However, in this case the mechanical attachment was between a copper section holding the electrodes and the copper base. The ceramic electrodes were attached to the copper section with silver-filled epoxy adhesive.

Interelectrode insulators consisted of either dense fused-grain magnesia, spinel, or, in one case strontium zirconate as indicated in Table 3. These insulators were cemented to the step in the copper electrode base with silver-filled epoxy adhesive. (In the case of the two mechanical attachments the insulator was cemented to the top of the copper extension and to an inner metal shim). Additional insulation on the electrodes consisted of 10 mils of polyimide tape on the copper surfaces. A glass fiber reinforced polyester block was used as a spacer between the copper cooling block and a NEMA G-11 laminated phenolic mounting block that is the main structural element that both holds the electrodes and supports the top and bottom insulating walls.

Two rods are threaded into the base of the copper portion of the electrode. These extend through the spacer and sidewall. Silicone rubber "O" rings placed over these rods and over the water coolant tube seal the electrode assembly to the inner surface of the wall by compression applied by hexagonal nuts against the outside surface of the electrode wall. The outside surface of an electrode wall, prior to sealing around all pass-throughs with RTV silastic, appears in Figure 6. One of the two threaded rods used to fasten the electrode assembly to the mounting block also serves as an electrical connection and this view shows the electrical wiring beneath the hexagonal nuts holding a crimped ring terminal leading to a rectangular quick-connect terminal used for final hook-up in WESTF. Cooling water flow is supplied through flexible tubing clamped to the copper tubes brazed to the electrode coolant passages.

Thermocouples (three per each set of three electrode pairs) are also visible in the photograph. Two of these (Type R exposed junction thermocouples) terminate in wells drilled into the electrode near its surface and near its base and one (Type K, ungrounded, sheathed) terminates in a well drilled in the copper electrode base. Both the anode and cathode walls are of identical construction.

The insulating walls are shown in Figures 7 through 10. The bottom insulating wall is the simpler of the two walls in that it does not have a view port or other instrumentation. As seen in Figure 7, it consists solely of magnesia brick insulation attached to copper heat sinks. The center blocks, over which the plasma will flow, are metallized with plasma sprayed Inconel and brazed to a corrugated Inconel sheet that is in turn soldered to a tinned surface of a copper cooling block. A typical center block is shown in Figure 8. The corrugated Inconel sheet serves as a thermal barrier to raise the surface temperature to the desired value. Several different types of magnesia insulating blocks were used in the center section to evaluate their performance in the seeded plasma. The side insulators are machined from an inexpensive, course-grained, magnesia brick. These insulators are bonded to the copper heat sinks with RTV silastic adhesive. The copper heat sinks are all covered with four layers of 0.0025 inch thick polyimide tape. These insulating assemblies are backed up with a flat silicone rubber gasket and attached to the NEMA G-11 mounting block with machine screws. The rear view of the wall (Figure 6) shows this attachment and the copper tubes for the connection of the cooling water lines.

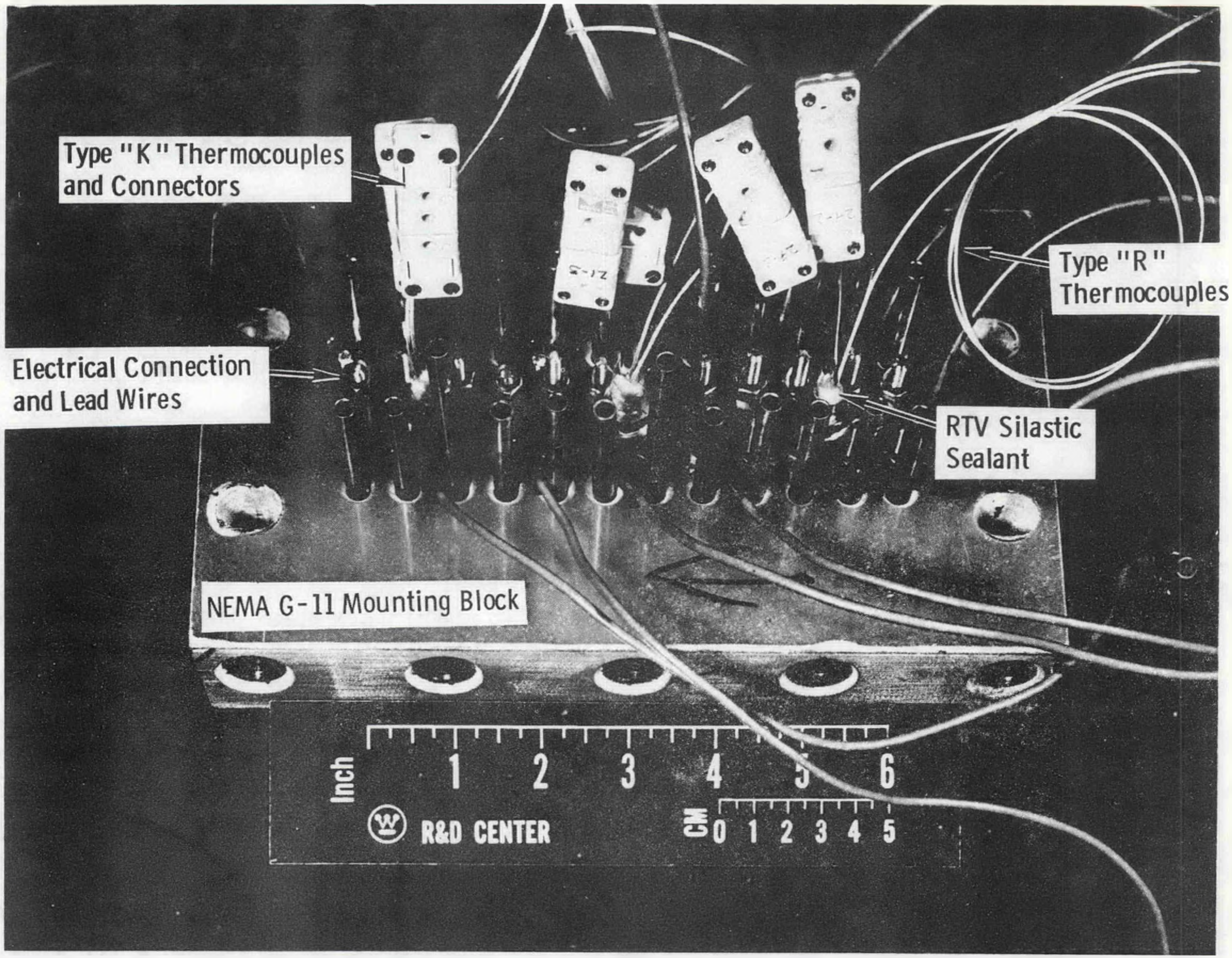

Figure 6. View of Outer Surface of Electrode Wall

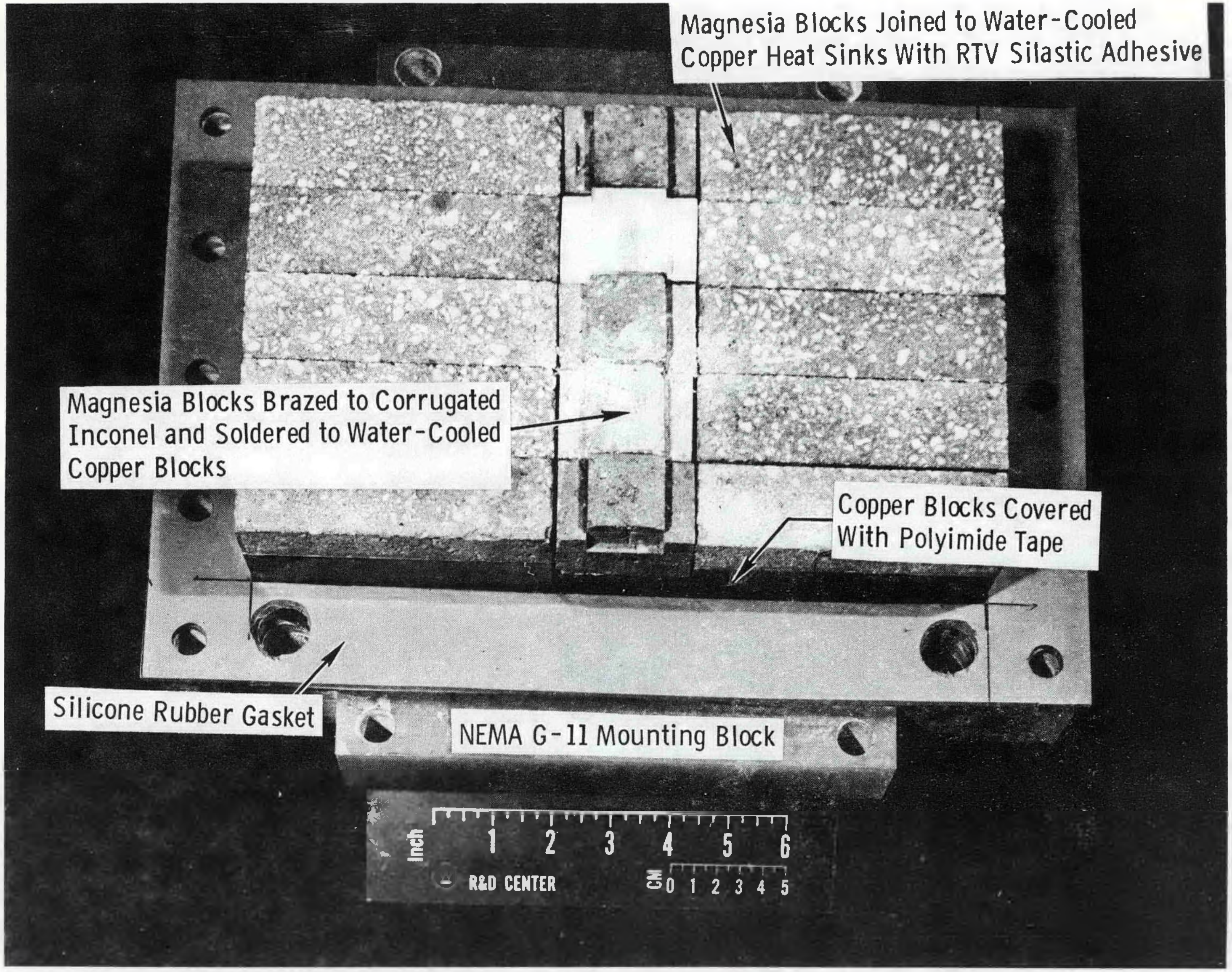

Figure 7. View of Bottom Insulating Wall

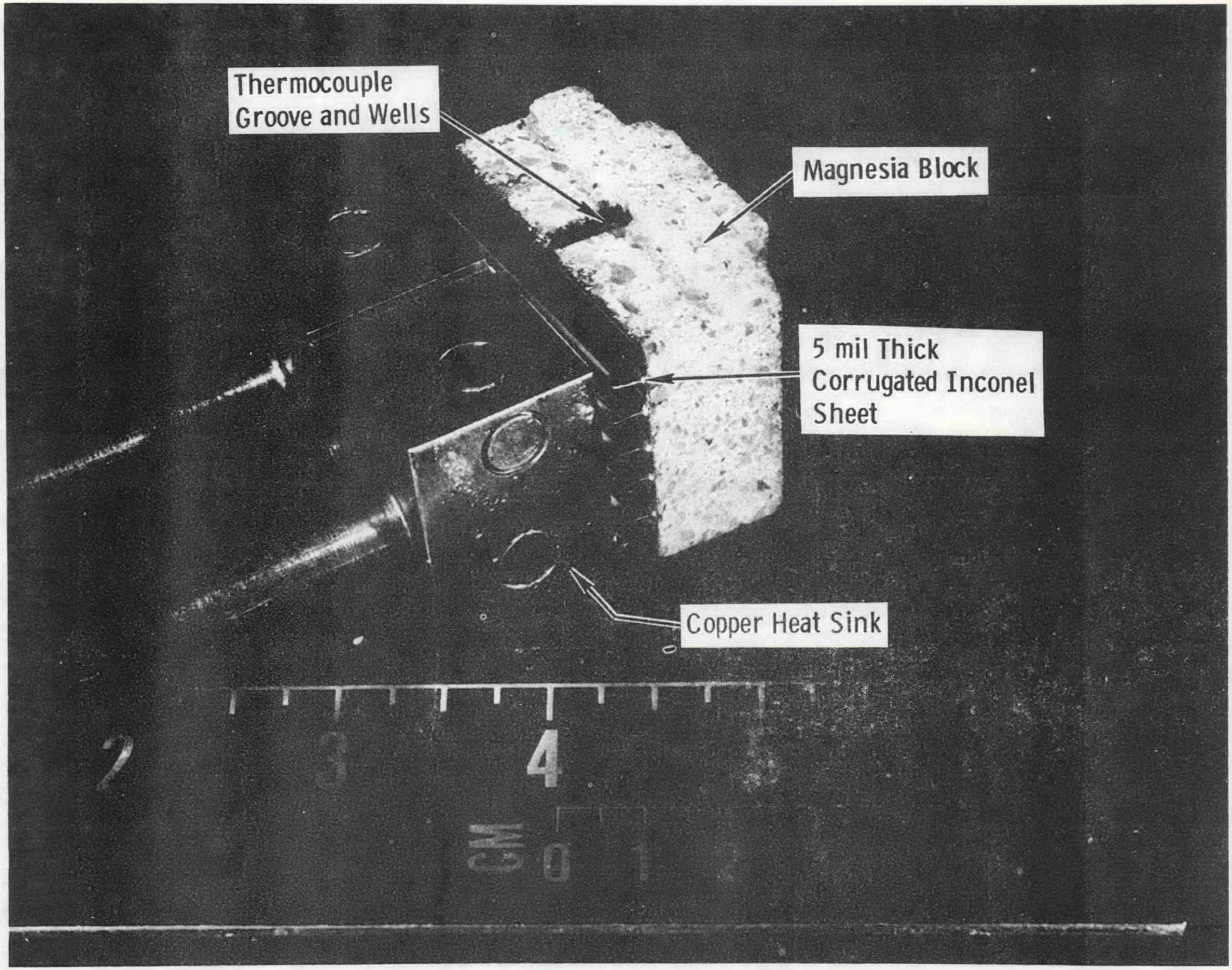

Figure 8. Typical Construction of Center Block in Insulating Walls

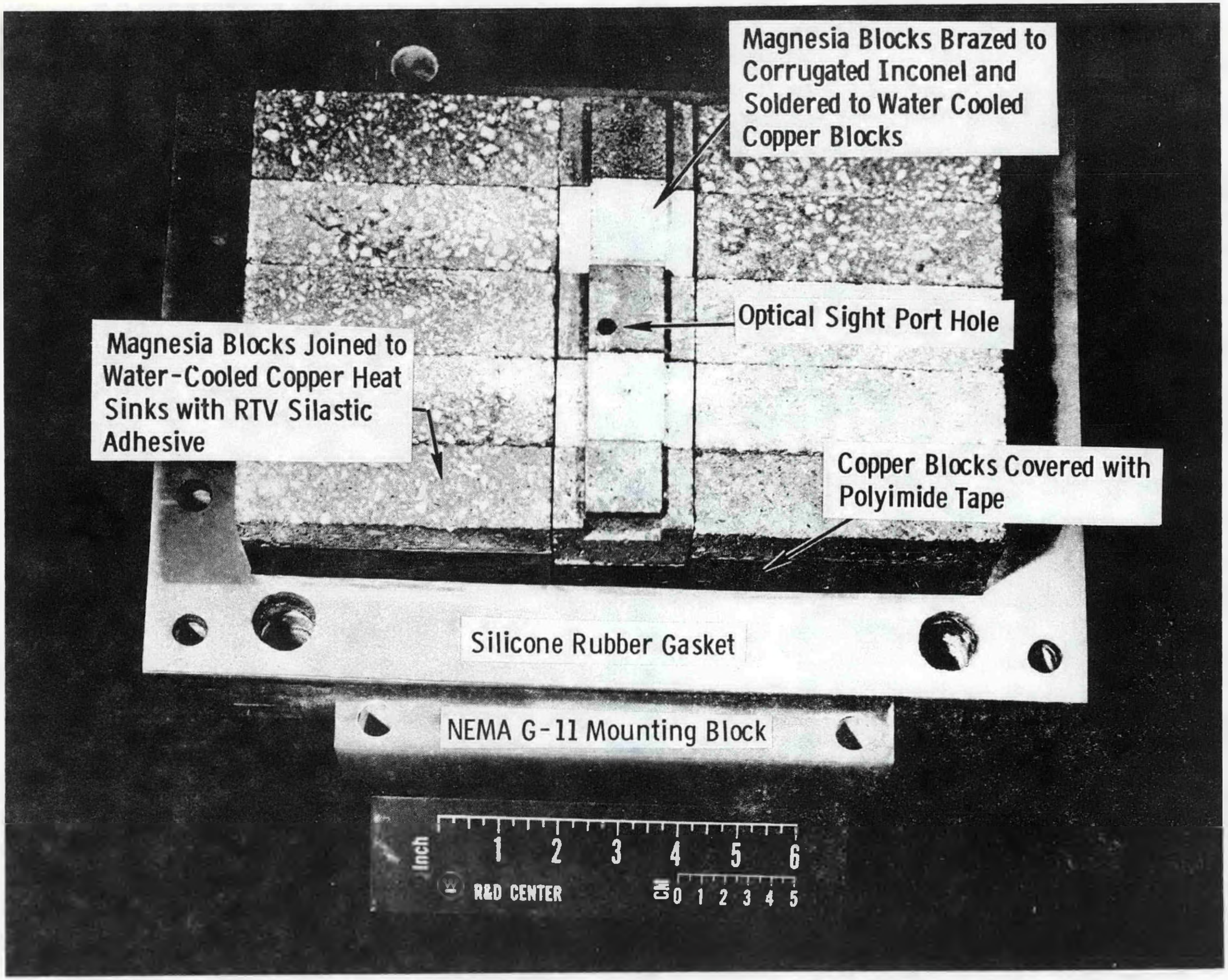

Figure 9. View of Top Insulating Wall

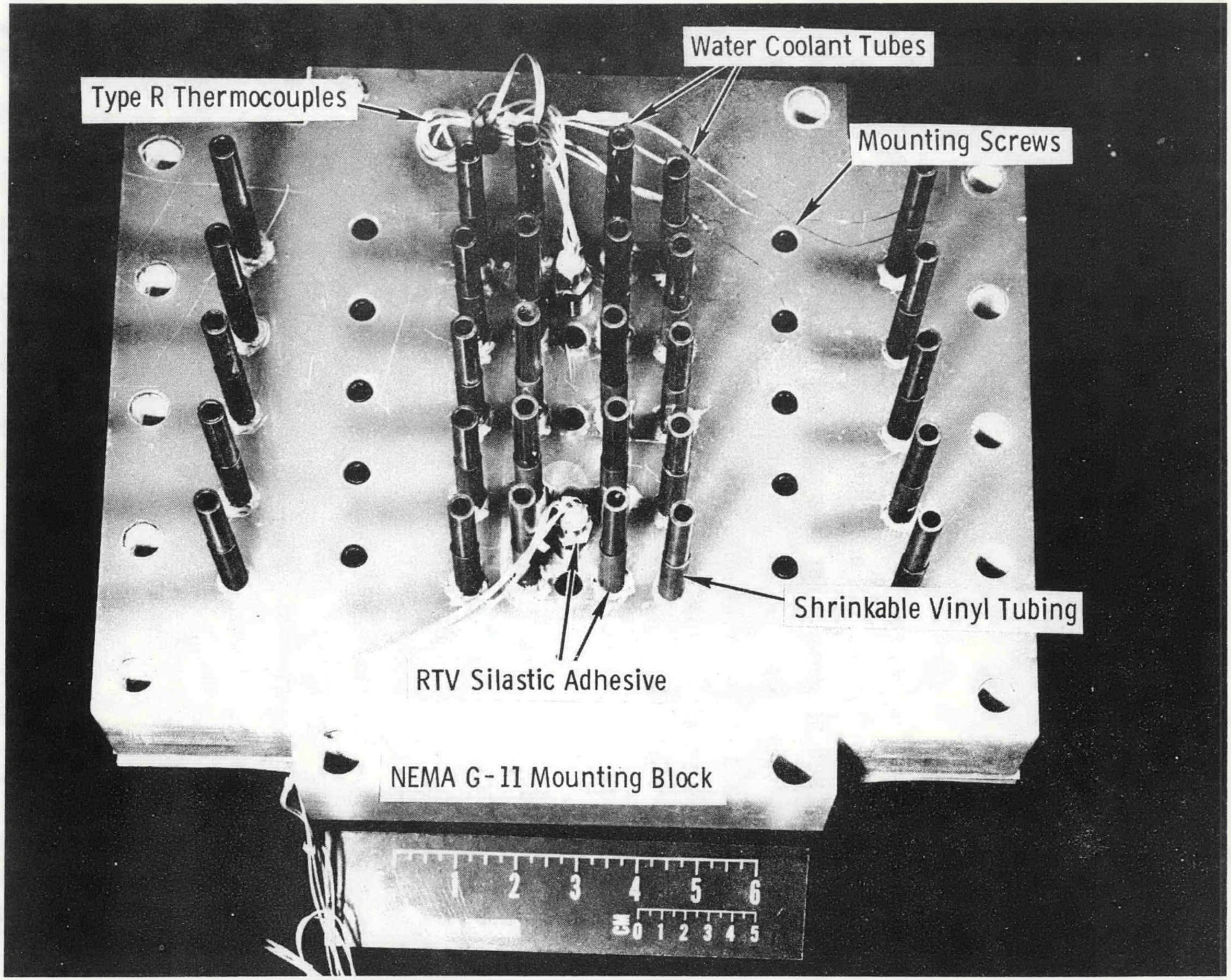

Figure 10. View of Outer Surface of Top Insulating Wall

The top insulating wall contains a hole drilled at a compound angle to provide visual access to the channel-interior. Figure 9 shows the location of this hole in the center insulating blocks. There are two thermocouples each in the second and fourth insulating block (they are all Type R exposed junction thermocouples made in the laboratory); one thermocouple is located near the surface of the ceramic and the other closer to the base of the ceramic. Except for the instrumentation, the construction of the top and bottom insulating walls is the same.

A raised portion of the center insulators cover a portion of each edge of the electrode to give a channel that has a nominal cross-section of one by two inches. The channel is contained between inlet and outlet transition sections that also have a nominal cross-section of one by two inches. These inlet and outlet transition sections are essentially water cooled copper sections lined with magnesia brick. The ceramic blocks are joined to the housing with RTV silastic adhesive. A pair of thermocouples are inserted in the center block of one of the walls. A pressure tap is available on the opposite wall.

The transition sections, the insulating walls, and the method of assembly are similar in many respects to those of the cold channel discussed in the previous quarterly report. As before, the electrode and insulating walls are bolted to each other and to the transition sections. Any minor alignment problems encountered in assembling the component parts due to the gasketing and also due to interference between ceramic-to-ceramic and ceramic-to-metal surfaces are adjusted during final assembly. All penetrations through the NEMA G-11 laminate and gasketed joints are sealed with RTV silastic sealant and made leaktight. Electrical measurements are taken on the interelectrode insulation during assembly and prior to delivery to WESTF.

3.5 Westinghouse Electrode System Test Facility (WESTF)

During the quarter the Materials Test Facility was redesignated the Westinghouse Electrode System Test Facility (WESTF) to reflect its expanded capabilities. Testing of the Cold Wall Test Assembly (copper electrodes), initiated during the prior quarter, was completed; installation of the cryogenic oxygen facility was completed, and the test of the initial Hot Wall Test Assembly ($LaCrO_3$ electrodes) was completed. In view of the upcoming U-02 Proof Tests, these tests were completed under clean-firing conditions.

Table 4 summarizes the current WESTF Test Program.

3.5.1 Facility

Installation and checkout of the oxygen facility was completed in early August. A 7000 gallon cryogenic oxygen tank supplies up to 300 SCFM at 125 psig to the facility. The oxygen system has automatic mass flow controls, safety check valves to prevent reverse flow from the combustor into the oxygen line, and several safety solenoids for emergency shutdown. The oxygen is not preheated, but is injected counterflow to the combustion air in the combustor plenum to achieve enrichment of the oxidant before combustion is initiated. Initial oxygen enrichment was achieved in Test No. 35-3.

3.5.2 Test Conditions

3.5.2.1 Test No. 35 (Copper, Cold Wall Electrodes)

Testing of the Cold Wall Test Assembly (copper Electrodes), Test No. 35, which was initiated during the prior quarter was completed. This test included a series of five runs designated 35-1 through 35-5. The test incorporated 8 cold copper electrodes operating in the surface temperature range of 100 to 400°C at impressed currents to 1 A/cm^2. The cryogenic oxygen system was not operable prior to Test No. 35-3 and as a result there was no oxygen enrichment of the combustion air. The test was run with preheated air and toluene (C_7H_8), thru 35-2, at 0.5% potassium seeding level and a flame temperature of 2500°K. This test was run for 10 hours at conditions and a representative electrode temperature history can be seen in Figure 11. Materials temperature drops and decreases in heat flux were noted when seed was introduced. This has been assumed to be due to the condensation of seed in all of the cracks in the channel: electrode-interelectrode insulator cracks and electrode wall-insulator wall cracks.

TABLE 4

SUMMARY OF WESTF TESTS (DESIGN DATA)

Test No.	35-1	35-2	35-3	35-4	35-5	36
Date	6/30	7/11	9/8	9/12	9/15	9/28/77
Cathode Materials	<———	———	Copper	———	———>	$LaCrO_3$
Anode Materials	<———	———	Copper	———	———>	$LaCrO_3$
Attachment Materials	<———	———	None	———	———>	Various
Insulator Materials	<———	———	$MgAl_2O_4$	———	———>	$MgAl_2O_4$ MgO
Twall - °C	<———	———	400 - 100	———	———>	1700
Mass Flow kg/sec	<———	———	0.12	———	———>	0.15
Current, Amp/cm^2	.1-.2	.1-.2	1.0	0	1.0	1.0
Heat Flux, W/cm^2	<———	———	96 - 86	———	———>	34 - 26
Axial Field, Kv/m	<———	———	0	———	———>	0
Fuel	<———	———	Clean	———	———>	Clean
Duration, -Hrs	2	10	5	1	4	20

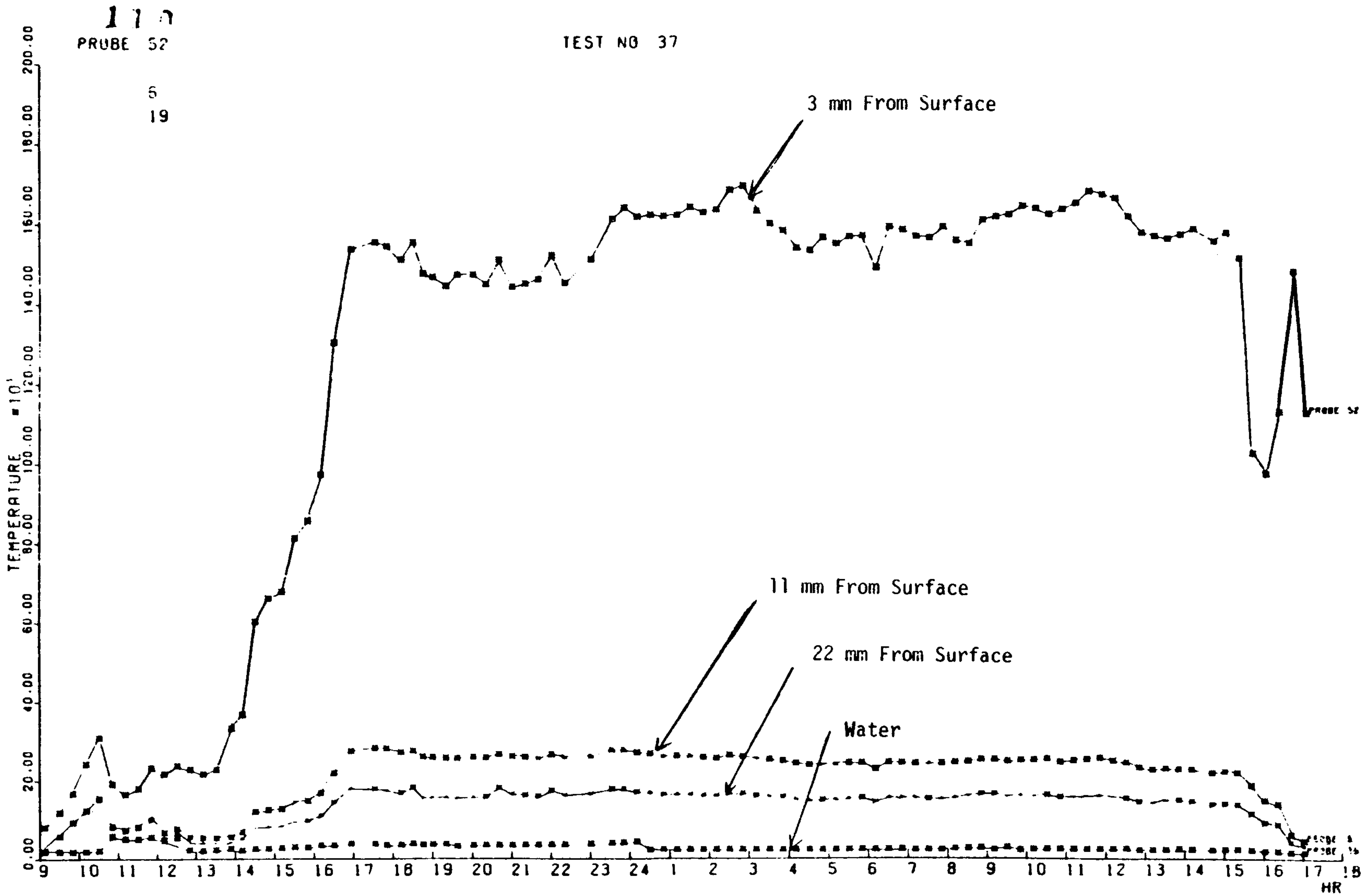

Figure 11. Test 35 T/C Data

Tests conducted on this channel were designated Tests 35-1 through 35-5. After the initial long duration test was completed (Test 35-1) and visual inspection completed, the additional tests on the copper channel (tests 35-2 through 35-5) were run as diagnostic tests and to further debug the facility.

The copper electrode channel was designed so that copper electrodes could be tested over a range of surface temperatures (400°C at the inlet linearly dropping to 100°C at the exit.) It was designed to run in the heat transfer coefficient range of .051 watt/cm^2°K at the inlet to .041 watt/cm^2°K at the exit where a mass flow rate of .123 kg/sec is used. The five separate tests run on this channel all had similar heat fluxes. The calculated heat fluxes at an inlet plasma temperature of 2500°K ranged from 96 watts/cm^2 at the inlet electrode to 86 watt/cm^2 at the exit electrode where a 75°K plasma temperature drop was predicted over the 17 cm long test duct. These heat fluxes compare with experimental values of 130-110 watts/cm^2 measured by calorimetry. The higher experimental values confirms the postulate that not all the heat absorbed by the water is coming through a path normal to the electrode surface, as the heat flux calculation assumes.

The thermocouples measurements in the copper electrodes were not a good measure of the copper temperature leading to the postulate that contact between the thermocouple bead and the copper was poor; temperatures as high as 800°C were indicated at one point, however, water calorimetry clearly indicated that such a condition did not exist. The measured temperature was therefore influenced to a great extent by the ceramic interelectrode insulator which ran much hotter than the copper.

3.5.2.2 Test No. 36 ($LaCrO_3$ Hot Electrodes)

Test No. 36 was the first hot test, $LaCrO_3$ electrodes, conducted in the facility. The purpose of the test was to test $LaCrO_3$ electrodes at a surface temperature of 1700°C and at a current load of 1 A/cm^2 for ten hours. A description of this test assembly is presented in Section 3.4.1.

Heat transfer coefficients of .065 watt/cm^2K and .052 watt/cm^2°K were predicted at the first and last electrode respectively where a mass flow rate of .146 kg/sec was used.

The calculated heat fluxes at an inlet plasma temperature of 2500°K ranged from 34 watt/cm^2 at the inlet electrode to 26 watt/cm^2 at the exit electrode where a 20°K plasma temperature drop was predicted over the 17 cm long test duct. These heat fluxes compare with experimental values of 35 to 50 watt/cm^2 measured by calorimetry.

The thermocouples in the materials were in better agreement with the heat fluxes measured by calorimetry than was the case in the cold copper duct. Their readings indicated that the surface temperature of the electrodes was about 1900°C.

3.5.3 Electrical Testing

Electrodes are electrically tested in WESTF by impressing the voltage required to produce the desired loading across each electrode-pair of the test channel. The ability of a given electrode design to stand up under the required loading is determined by monitoring the electrical performance of the test channel continuously during the test, and by observing the physical condition of the channel after completion of the test.

In testing electrodes it is necessary to evaluate whether they are able to stand up under the conditions of MHD loading, and whether the integrity of the inter-electrode insulation is being adversely affected. The quality of the insulation between electrodes is assessed by measuring the changes in the electrical leakage resistance with time. The presence of two separate leakage paths, one through the plasma and one through the solid insulation, complicates the evaluation of duct insulation. However, during a life test in which plasma temperature and conductivity are held constant, any increases in leakage currents observed are attributable to decreases in electrical resistance.

The circuit shown in Figure 12 is used to evaluate the performance of electrodes in terms of their capability of handling the required current, and the quality of the interelectrode insulation. The same circuit is employed for each electrode-pair being tested. The switch shown in the circuit permits the option of operating with the electrodes floating, or with either the anode or cathode electrodes grounded. When the floating mode of operation is used, the anode and cathode electrode currents are identical. When either the anode or the cathode electrode is grounded, the non-grounded electrode usually operates at a significantly higher current. The increase in current represents the leakage current to ground from the ungrounded electrode. If the leakage current to ground is zero, the current leaving the ungrounded electrode is equal to the current leaving the grounded electrode.

The interface between the MHD test curcuit and the data acquisition system is also shown in Figure 12. The wiring work for connecting the data acquisition system to the circuit had not been completed when the tests described in the present quarterly report were conducted. The use of paper punch tape at the output the DAS will permit use of the mini-computer for tabulation of data, necessary computations, and for plotting experimental results.

3.5.3.1 Copper Channel Results (Test No. 35)

Initial Tests

The resistance between opposing electrodes of the copper channel originally was the order of 1000 megohms before the channel was connected to the water lines. This resistance dropped to the order of 10^5 ohms when the water lines were connected. The lower conductivity was due to electrical conduction in both the water and the rubber hose. The leakage resistances between the electrodes and ground and between adjacent electrodes had the same order of magnitude as the leakage resistance between opposing electrodes.

An insulation test conducted on the electrodes upon installation in WESTF established that in most cases in which voltage was applied between opposing electrodes, between the electrodes and ground, and between adjacent electrodes, 1000 volts could be applied without a breakdown being experienced. Tests

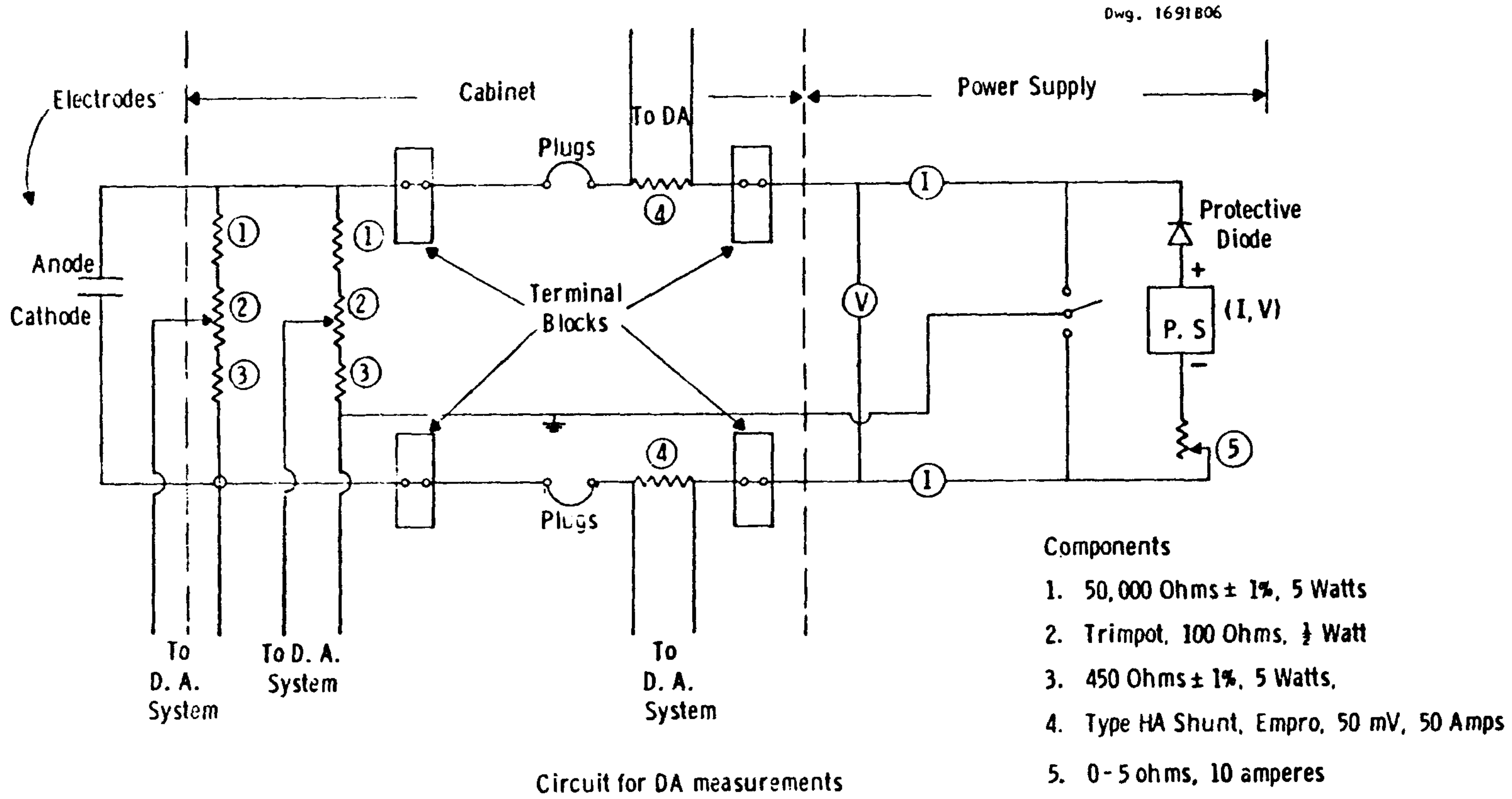

Figure 12. Circuit

involving the upstream electrodes, and the last 2 downstream electrodes, however, showed breakdowns between 100 and 1000 volts. No breakdown tests were conducted on the different constituents of the wall insulation of the copper channel.

<u>Test No. 35-1</u>

The channel was brought up in temperature in test 35-1 on 6/30/77 but no seed was introduced. Electrode leakage currents were monitored by imposing dc potentials between the electrodes of interest, and observing the resulting currents. The calculated magnitude of leakage resistances are indicated in Tables 5, 6 and 7 as taken at various intervals during the test run. Table 5 indicates leakage resistance across opposing electrodes, Table 6 between the electrodes and ground and Table 7 between adjacent electrodes.

The room temperature leakage resistances before and after Test No. 35-1 are given for purposes of reference in the second and last columns of Tables 5, 6 and 7.

The performance pattern exhibited by the copper channel during Test No. 35-1 in many respects was similar to those exhibited in tests on experimental channels at Waltz Mill. As heating of the channel proceeded the upstream electrode leakage resistances dropped from the order of 10^5 ohms to the order of 10^3 ohms. The resistances at the downstream end of the channel were about a factor of 10 higher than of the upstream electrodes throughout the test, apparently due to the lower temperatures.

It was interesting to note in Tables 5, 6 and 7 that the lateral leakage between adjacent electrodes was somewhat lower than the leakage resistance between opposing electrodes, and the leakage resistance to ground. The leakage resistance between adjacent electrodes is one of the more critical areas in MHD channel design. Since interelectrode insulation in an actual generator is subject to the very high electric fields in the MHD generator due to the Hall effect, it is mandatory that good quality insulation be utilized.

TABLE 5

LEAKAGE RESISTANCE BETWEEN OPPOSING ELECTRODES IN OHMS FOR COPPER ELECTRODES, TEST 35-1

Electrode-Pair No. / Approx. Temperature	6/29/77 Water Hoses Connected, No Water / Room Temperature	Test Run of 6/30/77 (#35-1): Water-Cooling On / Room Temperature	Test Run of 6/30/77 (#35-1): Preheat Only 11:30 AM / 630°C Preheat Air	Test Run of 6/30/77 (#35-1): 1:25 PM / ~1400°C	Test Run of 6/30/77 (#35-1): 2:42 PM / ~1950°C	7/7/77 Room Temperature
1	6.3×10^{6}	8.0×10^{5}	6.7×10^{5}	9.1×10^{4}	1.2×10^{4}	3.6×10^{3}
2	11.5×10^{6}	1.0×10^{6}	6.5×10^{5}	3.3×10^{5}	2.9×10^{4}	4.0×10^{3}
3	1.3×10^{8}	1.1×10^{6}	6.3×10^{5}	2.4×10^{5}	2.6×10^{4}	4.0×10^{3}
4	1.5×10^{8}	1.1×10^{6}	7.7×10^{5}	3.3×10^{5}	3.3×10^{4}	4.2×10^{3}
5	1.0×10^{8}	9.1×10^{6}	4.0×10^{5}	2.0×10^{5}	6.7×10^{4}	5.0×10^{3}
6	1.0×10^{8}	1.0×10^{6}	3.6×10^{5}	1.8×10^{5}	5.0×10^{4}	7.1×10^{3}
7	1.1×10^{8}	1.2×10^{6}	5.0×10^{5}	2.0×10^{5}	4.8×10^{4}	7.1×10^{3}
8	1.1×10^{8}	1.3×10^{6}	5.7×10^{5}	3.3×10^{5}	5.0×10^{4}	2.9×10^{4}
9	8.3×10^{7}	1.1×10^{6}	6.7×10^{5}	2.5×10^{5}	7.7×10^{4}	9.1×10^{4}
10	7.7×10^{7}	1.1×10^{6}	4.4×10^{5}	1.7×10^{5}	7.1×10^{4}	3.2×10^{3}
11	2.6×10^{7}	5.4×10^{5}	3.8×10^{5}	2.0×10^{5}	8.3×10^{4}	2.4×10^{4}
12	5.0×10^{7}	7.7×10^{5}	6.5×10^{5}	1.4×10^{5}	8.7×10^{4}	1.7×10^{4}
Column	1	2	3	4	5	6

TABLE 6

LEAKAGE RESISTANCE BETWEEN ELECTRODES & GROUND IN OHMS FOR COPPER ELECTRODES
TEST 35-1

Electrode Number Temperature	6/29/77 Water Hoses Connected, No Water Room Temperature	Test Run of 6/30/77 (#35-1) Water-Cooling On Room Temperature	Preheat Only 11:30 AM 611°C	1:35 PM ~1400°C	2:35 PM 1950°C	3:15 PM ~2050°C	4:10 PM ~2100°C	5:15 PM ~1550°C Cooling	7/7/77 Room Temperature
101	7.4×10^6	3.7×10^5	3.0×10^5	5.0×10^4	1.0×10^4	7100	5900	1.7×10^5	3800
102	2.9×10^7	2.5×10^5	1.9×10^5	5.3×10^4	1.0×10^4	5300	4700	1.3×10^5	3300
103	2.7×10^7	3.2×10^5	2.0×10^5	1.3×10^5	1.0×10^4	4800	4200	8.3×10^4	2800
104	2.3×10^7	3.1×10^5	1.9×10^3	1.0×10^5	1.1×10^4	5900	4300	5.9×10^4	3100
105	2.3×10^7	2.1×10^5	1.5×10^5	5.9×10^4	1.7×10^4	1.0×10^4	5400	7.1×10^4	3300
106	1.8×10^7	1.9×10^5	1.1×10^5	5.6×10^4	1.4×10^4	9100	7100	4.5×10^4	3700
107	1.7×10^7	2.4×10^5	1.3×10^5	5.6×10^4	1.3×10^4	8700	7400	4.3×10^4	1.1×10^4
108	1.5×10^7	1.8×10^5	1.2×10^5	6.3×10^4	1.5×10^4	1.1×10^4	1.1×10^4	7.7×10^4	1.5×10^4
109	1.4×10^7	2.0×10^5	1.5×10^5	7.1×10^4	2.0×10^4	1.5×10^4	1.5×10^4	9.0×10^4	6.7×10^4
110	1.4×10^7	1.9×10^5	1.2×10^5	6.7×10^4	2.4×10^4	1.7×10^4	1.4×10^4	8.3×10^4	3.3×10^4
111	1.3×10^7	1.2×10^5	1.1×10^5	6.3×10^4	2.2×10^4	1.8×10^4	1.3×10^4	7.7×10^4	2.0×10^4
112	1.6×10^7	4.2×10^5	3.6×10^5	6.7×10^4	2.2×10^4	1.9×10^4	6300	1.7×10^5	1.3×10^4
201	6.7×10^6	3.3×10^5	2.5×10^5	5.0×10^4	8.3×10^3	5100	4000	1.3×10^5	400
202	5.9×10^7	6.7×10^5	3.8×10^5	8.3×10^4	1.4×10^4	7400	5000	8.3×10^4	2000
203	7.1×10^7	5.6×10^5	3.3×10^5	8.3×10^4	1.3×10^4	6300	3800	7.1×10^4	3300
204	1.0×10^8	6.9×10^5	4.5×10^5	1.3×10^5	1.5×10^4	9500	6700	1.1×10^5	3300
205	5.9×10^7	5.9×10^5	1.9×10^5	1.1×10^5	1.4×10^4	8900	6100	5.6×10^4	3800
206	6.3×10^7	5.0×10^5	1.9×10^5	1.0×10^5	1.7×10^4	1.1×10^4	9500	9.1×10^4	6300
207	6.7×10^7	7.1×10^5	2.6×10^5	1.3×10^5	1.6×10^5	1.1×10^4	1.1×10^4	1.3×10^5	1.7×10^4
208	5.9×10^7	7.1×10^5	3.2×10^5	1.7×10^5	1.4×10^4	1.3×10^4	1.2×10^4	1.7×10^5	1.7×10^4
209	5.3×10^7	6.3×10^5	4.2×10^5	1.4×10^5	1.8×10^4	1.7×10^4	1.5×10^4	1.3×10^5	1.7×10^4
210	4.5×10^7	7.1×10^5	2.5×10^5	1.0×10^5	2.0×10^4	1.7×10^4	1.3×10^4	7.7×10^4	2.0×10^4
211	1.4×10^7	3.3×10^5	2.3×10^5	1.1×10^5	2.0×10^4	1.7×10^4	1.5×10^4	7.1×10^4	1.3×10^4
212	2.5×10^7	2.5×10^5	2.1×10^5	7.7×10^4	1.9×10^4	1.7×10^4	1.5×10^4	7.1×10^4	1.4×10^4
Column	1	2	3	4	5	6	7	8	9

NOTE: 100 Series of Electrodes are Cathodes
200 Series of Electrodes are Anodes

TABLE 7

LEAKAGE RESISTANCE BETWEEN ADJACENT ELECTRODES IN OHMS FOR COPPER ELECTRODE, TEST 35-1

Electrodes / Temperature	6/29/77 Water Hoses Connected, No Water / Room Temperature	Test Run of 6/30/77 (#35-1) Water-Cooling On / Room Temperature	11:36 AM / -	1:15 PM / ~1400°C	2:30 PM / ~1950°C	7/7/77 / Room Temperature
101 - 102	4.0×10^{7}	6.3×10^{5}	5.7×10^{5}	2.0×10^{5}	2.0×10^{4}	2300
102 - 103	1.4×10^{7}	5.7×10^{5}	4.2×10^{5}	2.9×10^{5}	1.5×10^{4}	2200
103 - 104	1.2×10^{7}	6.3×10^{5}	2.5×10^{5}	1.2×10^{5}	1.7×10^{4}	1500
104 - 105	5.6×10^{6}	5.3×10^{5}	3.4×10^{5}	2.2×10^{5}	4.0×10^{4}	1500
105 - 106	5.3×10^{6}	3.7×10^{5}	1.5×10^{5}	8.3×10^{4}	5.0×10^{4}	1850
106 - 107	2.4×10^{6}	4.2×10^{5}	1.3×10^{5}	5.1×10^{5}	2.0×10^{4}	11000
107 - 108	2.4×10^{6}	4.0×10^{5}	2.6×10^{5}	1.4×10^{5}	4.0×10^{4}	4300
108 - 109	2.8×10^{6}	3.1×10^{5}	1.8×10^{5}	5.0×10^{4}	4.0×10^{4}	6.7×10^{4}
109 - 110	1.2×10^{6}	3.0×10^{5}	1.5×10^{5}	4.5×10^{4}	5.0×10^{4}	8.3×10^{4}
110 - 111	1.5×10^{6}	2.2×10^{5}	1.1×10^{5}	5.0×10^{4}	5.0×10^{4}	2.9×10^{4}
111 - 112	1.1×10^{7}	4.5×10^{5}	3.8×10^{5}	1.3×10^{5}	9.1×10^{4}	5.0×10^{4}
201 - 202	7.1×10^{7}	1.1×10^{6}	5.9×10^{5}	1.4×10^{5}	2.9×10^{4}	2200
202 - 203	1.1×10^{8}	1.3×10^{6}	5.6×10^{5}	1.3×10^{5}	6.7×10^{4}	2100
203 - 204	1.2×10^{8}	1.3×10^{6}	8.2×10^{5}	4.0×10^{5}	9.1×10^{4}	2000
204 - 205	2.0×10^{8}	1.3×10^{6}	6.7×10^{5}	5.0×10^{5}	1.0×10^{5}	2200
205 - 206	1.0×10^{8}	1.1×10^{6}	2.0×10^{5}	1.4×10^{5}	8.3×10^{4}	3800
206 - 207	1.1×10^{8}	1.3×10^{6}	5.1×10^{5}	1.2×10^{5}	1.0×10^{5}	2000
207 - 208	5.3×10^{7}	1.4×10^{6}	4.0×10^{5}	2.9×10^{5}	9.1×10^{4}	1.7×10^{4}
208 - 209	4.0×10^{7}	1.4×10^{6}	7.7×10^{5}	2.9×10^{5}	9.1×10^{4}	1.2×10^{4}
209 - 210	2.8×10^{7}	1.4×10^{6}	7.1×10^{5}	5.0×10^{4}	1.1×10^{5}	1.2×10^{4}
210 - 211	5.9×10^{7}	1.1×10^{6}	2.7×10^{5}	9.1×10^{4}	8.3×10^{4}	1.2×10^{4}
211 - 212	4.5×10^{7}	3.8×10^{5}	3.3×10^{5}	1.3×10^{5}	1.0×10^{5}	4300

A noteworthy feature of Tables 5, 6 and 7 is the failure of the leakage resistance to recover after the test. Some recovery in leakage resistance would normally be expected in the absence of seed. It is surmized that the low leakage resistance later at room temperature was due to a combination of moisture and combustion products in the channel.

Test No. 35-2

This test was the first one in which seed was introduced. Tables 8, 9 and 10 give the characteristic electrode resistance values obtained at various intervals during the test obtained by applying voltages and measuring the magnitudes of the resulting currents.

By comparing the last columns of Tables 5, 6 and 7, which are the room temperature leakage resistances of the electrodes prior to Test 32, with the first columns of Tables 8, 9 and 10, which are the leakage resistances after the channel has been subject to modest amounts of heat, it is clear that the moisture responsible for the low room temperature leakages resistances observed after Test 31, was eliminated as the result of the modest temperatures incurred as the channel was heating up during Test 35-2.

Perhaps the most important criterion of good electrical channel performances is the ratio of leakage conductance in the plasma to the leakage conductance of the solid insulation on the channel walls. A high ratio is desired since it is important that the generator loading be confined to the plasma. Leakage currents along the insulating sections of the generator, represent power losses and interfere with the proper operation of the generator. Unfortunately, as mentioned previously, the ratio of plasma conduction to insulation leakage conductance is difficult to determine because the electrical paths are in parallel. Once seed is introduced it is difficult to separate these two currents. However, a comparison between leakage currents experienced immediately before and after the introduction of seed can be useful.

Such a comparison is afforded by comparing the columns of Tables 8, 9 and 10 taken immediately before and immediately after the introduction of seed. (Seed was introduced at 1340 hrs.)

TABLE 8

LEAKAGE RESISTANCE IN OHMS BETWEEN OPPOSING ELECTRODES FOR COPPER ELECTRODE, TEST 35-2 BEFORE AND AFTER INTRODUCTION OF SEED

Electrode-Pair No. / Temperature	Test Run of 7/11/77: 8:35 AM	10:30 AM	13:35 PM	13:40 PM	14:05 PM	16:30 PM	17:35 PM	18:15 PM	21:25 PM	7/12/77
	~600°C			Seed Introduced	~2000°C					Room Temperature
1	1.0×10^6	9.1×10^4	1.9×10^4		71.4	41.7	38.5	41.7	33.3	833
2	2.0×10^5	7.1×10^4	1.3×10^4		100	71.4	62.5	62.5	71.4	667
3	2.5×10^5	5.3×10^4	1.1×10^4		125	71.4	62.5	71.4	167	333
4	3.3×10^5	5.3×10^9	3100		167	111.1	83.3	100	143	181
5	2.5×10^5	4.5×10^4	8700		222	156	167	250	200	161
6	5.0×10^5	4.0×10^4	1.8×10^4		250	227	250	333	278	133
7	2.0×10^5	3.4×10^4	1.4×10^4		200	200	143	333	200	143
8	2.0×10^5	5.0×10^4	2.1×10^4		667	417	500	500	417	154
9	1.7×10^5	5.0×10^4	3.1×10^4		1000	500	500	500	500	222
10	1.4×10^5	4.8×10^4	3.1×10^4		1000	500	500	263	500	200
11	2.0×10^5	5.3×10^4	2.6×10^4		1000	556	500	200	500	250
12	1.0×10^6	5.0×10^4	3.1×10^4		1250	500	500	500	500	192

NOTE: Seed Introduced 13:40

TABLE 9

LEAKAGE RESISTANCE IN OHMS BETWEEN ELECTRODES AND GROUND FOR COPPER ELECTRODE, TEST 35-2 BEFORE AND AFTER INTRODUCTION OF SEED

Electrode-Pair No.	Test Run of 7/11/77									
	8:15	10:25	13:20	13:40	13:50	13:59	16:15	18:05	21:06	
Temperature	580°C Preheat			Seed Introduced	~2000°C					7/12/77 Room Temperature
101	1.6×10^5	3.5×10^4	2.5×10^4		100		38.5	40	25	5000
102	5.9×10^4	3.6×10^4	8000		111		45.5	55.6	26.3	667
103	7.7×10^4	2.9×10^4	8300		143		55.6	55.6	23.7	455
104	6.7×10^4	2.4×10^4	9500		192.3		62.5	71.4	14.7	250
105	5.3×10^4	2.0×10^4	1.0×10^4		256		71.4	125	15.6	200
106	4.8×10^4	1.8×10^4	1.1×10^4		263		83.3	167	15.6	182
107	4.0×10^4	1.6×10^4	1.6×10^4		333		100	143	15.6	400
108	3.7×10^4	1.5×10^4	1.4×10^4		400		100	500	16.7	333
109	1.0×10^5	1.4×10^4	1.7×10^4		476		125	500	16.7	400
110	3.8×10^4	1.7×10^4	2.2×10^4		400		100	500	17.9	400
111	3.4×10^4	1.7×10^4	2.2×10^4		250		111	500	125	500
112	5.0×10^5	2.4×10^4	4.0×10^4		118		62.5	500	100	500
201	2.0×10^5	2.0×10^4	2.0×10^4		Short	56	31.0	33.3	20.8	143
202	8.3×10^4	2.0×10^4	1.0×10^4		Short	125	50	41.7	15.6	222
203	8.3×10^4	2.2×10^4	9.1×10^4		56	167	55.6	50	62.5	222
204	1.1×10^5	2.6×10^4	Short		Short	182	62.5	125	83.3	238
205	1.0×10^5	2.2×10^4	6700			192	71.4	143	111.1	238
206	1.1×10^5	2.2×10^4	1.7×10^4			200	83.3	250	125	238
207	9.1×10^5	2.9×10^4	1.4×10^4			200	111	625	200	1110
208	1.0×10^5	2.5×10^4	2.0×10^4			250	111	500	333.3	238
209	5.0×10^4	2.5×10^4	2.5×10^4			291	125	500	500	286
210	1.1×10^5	2.5×10^4	2.5×10^4			250	111	500	286	286
211	1.1×10^5	2.5×10^4	2.0×10^4			250	111	167	500	286
212	3.3×10^5	2.2×10^4	2.5×10^4			111	66.7	500	500	313

NOTE: Seed Introduced 13:40

TABLE 10

LEAKAGE RESISTANCE IN OHMS BETWEEN ADJACENT ELECTRODES FOR COPPER ELECTRODES, TEST 35-2 BEFORE AND AFTER INTRODUCTION OF SEED

Electrodes	Run of 7/11/77								
	8:45 AM Preheat	10:30 AM	13:25 AM	13:40 AM	14:00 PM	16:25 PM	18:10 PM	21:15 PM	
Temperature	~600°C Preheat			Seed Introduced	~2000°C				7/12/77 Room Temperature
101 - 102	1.0×10^6	3.5×10^4	1.0×10^4		59	29	28	31	830
102 - 103	5.0×10^5	6.7×10^4	7100		71	28	42	42	560
103 - 104	1.3×10^5	2.9×10^4	1.0×10^4		67	43	67	28	220
104 - 105	1.1×10^5	2.9×10^4	9500		140	163	170	Short	200
105 - 106	1.1×10^5	1.0×10^4	1.1×10^4		140	140	250	8.3	130
106 - 107	1.0×10^5	2.0×10^4	1.1×10^4		110	170	200	11	190
107 - 108	8.3×10^4	1.2×10^4	1.7×10^4		140	160	500	Short	130
108 - 109	1.0×10^5	9300	2.2×10^4		670	500	500	4.0	120
109 - 110	9.1×10^4	9500	2.0×10^4		670	500	500	Short	110
110 - 111	9.1×10^4	2.0×10^4	2.5×10^4		1000	500	500	500	290
111 - 112	1.0×10^6	2.0×10^4	4.0×10^4		500	500	500	500	170
201 - 202	5.0×10^5	2.0×10^4	1.25×10^4		60	50	33	28	110
202 - 203	9.1×10^4	1.2×10^4	3400		60	38	36	125	710
203 - 204	2.0×10^5	2.2×10^4	3100		60	63	50	111	770
204 - 205	2.0×10^5	2.6×10^4	6100		60	83	180	250	53
205 - 206	5.0×10^5	2.6×10^4	1.7×10^4		110	200	250	250	53
206 - 207	5.0×10^5	2.9×10^4	1.1×10^4		200	330	250	170	51
207 - 208	5.0×10^5	3.2×10^4	1.5×10^4		125	330	500	330	51
208 - 209	1.7×10^5	1.5×10^4	1.1×10^4		200	420	500	500	77
209 - 210	2.0×10^5	2.9×10^4	2.5×10^4		1000	500	500	500	91
210 - 211	2.0×10^5	2.6×10^4	2.0×10^4		500	500	500	560	51
211 - 212	1.0×10^6	2.5×10^4	2.2×10^4		300	500	500	560	51

In general the ratio of the measured resistances without seed to the resistance with seed is 40 or greater. The ratio appears to be high enough to provide for satisfactory operation of an MHD generator. Unfortunately after seed is introduced, an increase in leakage along the surface and through the volume of the solid insulation would be expected. The comparison between the operation with and withcut seed would be more meaningful if the channel had previously been subject to seed and then, operated under conditions where seed would have impregnated the solid insulation at a time when little or no seed was present in the gas.

Once seed reached the vicinity of the electrodes in Test 35-2 the electrode resistances dropped to the order of 30 or 40 ohms across the upstream electrodes of the channel. (See times between 1600 hrs to 2115 hrs in the Tables 8, 9 and 10.) If the current observed across the channel were entirely through the plasma, a resistance of 40 ohms across the plasma would correspond to a plasma conductivities of 1.25 mhos/m. Evidently, the plasma conductivity present in the downstream section of the channel, where resistances of the order of 500 ohms were observed, is considerably higher.

It is interesting to note that the leakage resistances observed in Tables 8, 9 and 10 decreased the longer seed was injected into the system. In Test 35-2 there was no electrical evidence of an extensive deposition of seed on the electrodes. (In Test 35-5 extensive deposition of seed and Al_2O_3 and seed reaction product on the electrodes provided a very significant increase in the resistance between opposing electrodes).

Test No. 35-4

In this test the plasma was brought to the neighborhood of 2050°C prior to seed being introduced. The fact that seed and already once been in the channel permits evaluating the leakage resistance in the solid insulation when it is contaminated by seed, and there is relatively little conductivity in the plasma. Tables 11 and 12 give the leakage resistances measured with an ohmeter at different times during the run. The temperatures observed on the 2-color pyrometer at the downstream end of the mixer have also been included in the tables when available.

TABLE 11

LEAKAGE RESISTANCES IN OHMS BETWEEN ANODE AND CATHODE, BETWEEN ANODE & GROUND, AND CATHODE AND GROUND AS TEMPERATURE OF CHANNEL IS INCREASED WITHOUT SEED, TEST 35-4

Time	10:35 AM			11:35 AM			12:20 PM		
Electrode-Pair	A-C	A-G	C-G	A-C	A-G	C-G	A-C	A-G	C-G
3	290	180	115	230	115	110	190	60	90
4	260	160	120	240	115	120	210	82	95
5	240	110	160	180	120	140	190	100	110
6	230	160	80	260	182	85	270	185	90
7	900	750	55	320	260	56	370	290	60
8	3500	2700	600	780	550	330	600	500	210
9	4200	1650	1700	1500	970	700	1300	1100	550
10	6000	5000	1450	2200	1700	1050	1950	1900	1100
Temperature On 2 - Color Pyrometer	-			1960°C			2020°C		

NOTE: A-C Anode to Cathode
A-G Anode to Ground
C-G Cathode to Ground

TABLE 12

LATERAL LEAKAGE RESISTANCES IN OHMS BETWEEN ADJACENT ELECTRODES AS TEMPERATURE IS INCREASED WITHOUT SEED
TEST 35-4

Time	10:40 AM		11:42 AM		12:23 PM	
Electrodes	Anodes	Cathodes	Anodes	Cathodes	Anodes	Cathodes
3 - 4	130	100	120	180	110	180
4 - 5	220	240	190	170	175	180
5 - 6	240	220	190	200	175	190
6 - 7	850	90	340	110	400	110
7 - 8	2800	460	460	200	480	180
8 - 9	3600	2000	1100	700	950	550
9 - 10	6000	3000	1800	1000	1800	150
Temperature On 2-Color Pyrometer	-		1970°C		2050°C	

In run 35-4 the first 2 and the last 2 of the 12 electrodes in the channel were used as guard electrodes. In the numbering of electrode-pairs in Tables 11 and 12 the numbering of electrode-pairs is maintained, i.e., one through twelve for the full channel.

Since seed had been introduced in this channel in an earlier run, the leakage resistances observed may be considered to represent maximum values of the insulation leakage resistance, i.e., the leakage resistance caused by the presence of seed in the insulation of the channel with very little leakage currents traversing the plasma. It is important to recognize that if seed had been introduced during Test 35-4, the leakage through the solid insulation would probably have increased somewhat, in addition to the substantial increase in leakage which would be expected from the ionization of the plasma and conduction through it.

If the values indicated in the tables are taken as the leakage resistance of the insulation, then the plasma resistance, if seed were introduced, should be less than roughly 5% of the values measured in the table. Thus for electrode-pair #3, which had an insulation leakage of 190 ohms, a plasma resistance of roughly 10 ohms, or a plasma conductivity of more than 5 mhos/meter would have been necessary for reasonable MHD performance.

Test 35-4 was characterized by a very substantial increase in resistance in going from electrode 1 upstream to electrode 12 downstream which indicates substantially lower temperatures at the downstream electrodes and perhaps significants lower depositions of seed on the walls of the duct. The downstream electrodes, and hence the plasma separating them were apparently too low in temperature to provide reasonable MHD performance. Later tests with hot electrodes did not exhibit such large changes in performance from the upstream to the downstream region of the channel.

In general the resistances on the anode side of channel tended to be higher than the resistances on the cathode side, particularly at the downstream region of channel. This result would indicate that operation of the channel in the previous test resulted in the deposition of greater quantities of seed on the cathode side.

Test No. 35-5

A rather unexpected result was obtained when an attempt was made to compare interelectrode resistances before and after introduction of seed in Table 13. The electrode resistance between opposing electrodes, as measured with an ohmeter increased by a significant factor despite an increase in temperature of about 100°C. See columns 1 and 2 of Table 13. It is interesting to note that the resistance between the anode electrodes and ground did not change significantly. See columns 3 and 4 of Table 13. However, the resistance between the cathode electrodes and ground, see columns 5 and 6, increased after the introduction of seed.

The resistance between adjacent electrodes tended to decrease on the anode side, when seed was introduced. See Table 14. The resistances between electrodes on the cathode side showed some increase in resistance and some shorting when seed was introduced. Further investigation of the shorting effect indicated it was sensitive to the polarity of the ohmmeter. This effect which has also been observed at Waltz Mill is probably related to the presence of barrier layers in the materials comprising the electrical circuits being energized. This effect is always accompanied by a battery action in which voltages as high as 0.5 volts have been observed. When the ohmeter levels are reversed, readings on the ohmmeter which previously indicated short, are now readable on the ohmeter scale.

After Test 35-5 was completed and the channel cooled to room temperature and opened, it was observed that significant condensation of seed and seed-Al_2O_3 reaction product had taken place on the upstream electrodes. Apparently the increased resistance bwtween opposing electrodes was due to the substantial deposits of seed and Al_2O_3 over the surface of the electrodes exposed to the plasma. The small change observed in the electrodes to ground resistance

TABLE 13

LEAKAGE RESISTANCE BEFORE AND AFTER INTRODUCTION OF SEED
ALL VALVES IN OHMS, TEST 35-5

Electrode - Pair	Anode to Cathode		Anode to Ground		Cathode to Ground		Anode to Ground		Cathode to Ground	
	(After Seed)	(After Seed)	(After Seed)	(After Seed)	(After Seed)	(After Seed)	(After Seed)	(After Seed)	(After Seed)	
Time	11:06 AM	12:09 PM	11:06 AM	12:09 PM	11:06 AM	12:09 PM	3:05 PM	3:05 PM	3:05 PM	
									Normal Polarity	Reverse Polarity
3	260	1000	120	130	130	1600	700	140	Short	240
4	320	850	150	150	130	1400	400	Short	Short	400
5	380	3400	190	210	220	3000	100	80	Short	90
6	360	1800	250	150	180	1400	1200	260	Short	410
7	500	1100	400	130	135	800	1900	170	Short	750
8	1000	1500	740	400	360	850	1600	170	Short	820
9	2000	5000	1500	1200	750	1900	4000	400	Short	720
10	2200	6000	1750	1300	950	850	8000	600	Short	650
Estimated Temp. (2 - Color)	1970°C	2070°C	1970°C	2070°C	1970°C	2070°C				
Column	1	2	3	4	5	6	7	8	9	10

NOTE: Seed Introduced at 11:50 PM

TABLE 14

LATERAL LEAKAGE RESISTANCE BEFORE AND AFTER INTRODUCTION OF SEED (OHMS), TEST 35-5

Electrode-Pairs	Anode Side		Cathode Side		Anode Side		Cathode Side	
	Before Seed	After Seed	Before Seed	After Seed	After Seed		After Seed	
Time	11:08 AM	12:09 PM	11:08 AM	12:09 PM	3:10 PM Normal Polarity	3:10 PM	3:10 PM Normal Polarity	3:10 PM Reverse Polarity
3 - 4	180	40	270	300	150	Short	90	Short
4 - 5	300	110	360	900	Short	30	Short	120
5 - 6	320	100	340	Short	Short	140	110	10
6 - 7	500	200	200	Short	100	10	155	Short
7 - 8	800	450	360	160	60	50	60	70
8 - 9	2000	1300	950	1300	50	230	100	120
9 - 10	2700	3000	1450	2100	210	280	90	180
Approx. Temp.	~1950°C	2070°C	~1950°C	2070°C				

indicates that this leakage, as expected, is along the internal solid insulation of the electrode assembly and not through the plasma. From the performance of the generator with seed, it could appear that the temperatures of the copper electrodes in this test were too low for use in MHD operation when slag is present.

The channel was operated for about 4 hours under moderate load conditions. Tables 15, 16 and 17 summarize the voltages employed and the currents observed. I_2 represents the current obtained on the anode side of the current, and I_1 the current read on the cathode side. See Figure 12. In general when the circuit was operated with both electrodes operating, the two currents were equal.

Cathode grounded operation was generally marked by higher anode currents since the I_2 meter will read the anode leakage current to ground, in addition to the plasma current. Anode grounded operation was similarly characterized by higher cathode currents for the same reason.

Exceptions to the above rules probably indicate that the leakage path from a given grounded electrode to the opposite member of the electrode-pair had lower impedance for charge carries travelling through the plasma by way of neighboring adjacent grounded electrodes.

Conductivity readings were taken by impressing a voltage in the axial direction along the channel between downstream electrodes which are shorted together and upstream electrodes also shorted together. The electric field E present in the plasma is determined by using the intervening electrodes as voltage probes according to the equation $E = V/d$, where d is the distance between the observed electrode. The current density J traversing the plasma is determined by measuring the plasma current I and substituting in the equation $J = \frac{I}{A}$ where A is the cross-sectional area of the channel.

The average conductivity for the region of the channel on which the measurements were made is given by $\sigma = \frac{J}{E}$. The conductivity observed when the measurements were made between electrode-pairs 3 and 4, and between electrode pairs 7 and 8 was about 0.8 mhos/meter.

TABLE 15

INITIAL ELECTRICAL LOADING
TEST 35-5

Time	11:31 AM			11:53 AM			12:03 PM			12:22 PM			12:29 PM		
Electrode-Pair	V	I_2	I_1	V	I_2	I_1	V	I_2	I_1	V	I_2	I_1	V	I_2	I_1
3	49	.19	.08	49	0.6	0.55	50	.95	0.9	44	1.1	1.0	26	0.9	0.4
4	49	.18	.1	49	0.4	.35	50	0.9	0.85	41	1.2	1.0	18	2.2	1.0
5	49	0.2	0.18	49	0.6	0.55	50	1.3	1.3	39	2.0	2.0	22	2.4	1.6
6	48	0.1	0.08	48	0.4	.35	50	0.6	0.6	45	0.7	0.7	28	0.4	0.5
7	50	0.1	0.04	50	0.35	0.3	50	0.5	0.4	49	0.7	0.7	30	0.4	0.2
8	49	0.1	0.01	49	0.2	0.9	50	.25	0.2	48	0.2	0.2	32	0.2	0.1
9	52	0.1	0.05	52	0.1	.05	50	.1	0.5	51	0.1	0.1	30	0.1	0.1
10	51	.1	.02	51	0.1	.05	50	.1	0.2	52	0.1	0.1	32	0.1	0.1
Mode of Operation	Floating			Floating			Floating						Cathode Ground		

TABLE 16

ELECTRICAL LOADING (Continued)
TEST 35-5

Time	12:45 PM			1:08 PM			1:10 PM			1:25 PM			1:27 PM		
Electrode-Pair	V	I_2	I_1	V	I_2	I_1	V	I_2	I_1	V	I_2	I_1	V	I_2	I_1
3	26	.55	0.8	26	.8	.7	25	1.0	0.4	43	1.5	1.4	42	1.8	0.9
4	26	1.0	5.5	24	1.25	1.25	18	2.2	0.5	33	2.6	2.6	27	3.8	1.0
5	16	1.4	3.0	22	1.5	1.7	25	2.8	1.0	32	3.4	3.4	36	4.8	2.0
6	27	0.1	.75	29	.25	.2	30	0.2	0.55	43	1.2	1.2	46	0.6	2.6
7	29	0.25	0.6	30	.35	0.3	30	0.4	.2	47	0.7	0.7	47	0.8	0.3
8	30	0.3	--	30	.2	0.1	30	.15	.05	48	0.2	.15	48	0.2	0.15
9	32	.15	0.35	32	0.1	0.1	32	0.1	0.1	52	0.1	0.1	52	0.1	0.1
10	30	.1	0.3	30	0.1	.05	30	.08	.05	50	0.05	.05	50	.05	.05
Mode of Operation	Anode Grounded			Floating			Cathode Ground			Floating			Cathode Ground		

TABLE 17

ANODE TO CATHODE LEAKAGE RESISTANCE IN OHMS, TEST 36

Time	6:11 PM	7:33 PM	8:00 PM	9:08 PM	10:18 PM	10:30 PM	10:57 PM	10:56 PM	7:50 AM	7:53 AM	8:00 AM
Electrode-Pair				Seed On	Power Off		Seed Reapplied			Seed Off	
1	3900	230	270	-	-	1500	-	85	2.6	-	4.0
2	3600	150	180	-	-	2200	-	4	27	-	32
3	10,500	480	350	-	-	2600	-	13	2.7	-	4.5
4	1350	550	560	-	-	3900	-	18	2.3	-	3.8
5	1320	650	670	-	-	3100	-	4000	3.7	-	7.6
6	8100	320	350	-	-	2900	-	22	4.9	-	6.5
7	8600	380	420	-	-	2900	-	26	5.0	-	18
8	4500	280	305	-	-	2500	-	14	4.0	-	8.0
9	4000	310	330	-	-	3100	-	10	4.2	-	8.5
10	5100	310	330	-	-	2800	-	8	9.0	-	15
11	15,000	525	500	-	-	1300	-	25	12	-	15
12	23,000	1100	960	-	-	1400	-	60	28	-	45

3.5.3.2 Test No. 36 - Hot ($LaCrO_3$) Channel

Room Temperature Tests

The electrode walls of the test channel consisted of ceramic electrodes which were mounted on separately insulated water-cooled copper blocks. The insulation between adjacent electrodes was tested by applying and progressively increasing the applied voltage until 2000 volts was reached, and checking for stability of operation and low leakage current. The insulation between all sets of electrodes was satisfactory except for the insulation between electrodes 2 and 3 on the side of channel which was designated to be the cathode and between 3 and 4 on the side which was designated to be the anode.

Similar tests were conducted between the electrodes and the nearest channel mounting flange, with satisfactory results being noted to 2000 volts.

The insulation between the water-cooled copper plates which back the insulating wall ceramic blocks mounted on the top and bottom of the test duct, was also given the same test. About 30% of these intermediate insulating sections broke down at voltages lower than 2000 volts. The test pointed to the necessity of increasing the quality of insulation between the copper plates which back the insulating walls of the channel.

Operational Tests on the Hot Channel

Seed was injected into the channel at 9:08 PM on 9/28/77 after the channel was brought to operating temperature. The channel was operated under different load schedules for the next 11 hours until roughly 8:00 AM the following day, except for roughly a 1/2 hour period during which the system had to be shut down because of a power outage.

As the channel temperature was increased during the test run the leakage resistance between various electrodes as read on an ohmeter exhibited its usual decrease with temperature. The initial readings at modest temperatures corresponded to the values of the electrical resistances present in the circuit of Figure 12, indicating that the electrode resistance between the different electrodes was very high compared to 50,000 ohms.

The values of leakage resistance between the cathode and anode electrodes taken at different time intervals during the run is shown in Table 17. Similar leakage resistance values between the anode and cathode electrodes and ground potential, and between adjacent electrodes are shown in Tables 18 and 19 respectively. The ohmeter readings were taken rather infrequently since it was necessary to interrupt the electrical loading tests temporarily to make these measurements.

It is interesting to note that the leakage resistances between opposing and adjacent electrodes without seed, which were observed as the channel was coming up to temperature, are roughly a factor of two lower than the leakage resistance between the electrodes and ground. Once seed was introduced, the measurements of leakage resistance in the different electrode circuits tended to have the same order of magnitudes.

When the injection of seed was discontinued, the system was held at constant temperature for about 10 minutes. During this time the resistance between opposing electrodes and between the electrodes and ground increased by roughly a factor of 1.5 or 2. The resistance between adjacent electrodes exhibited a somewhat smaller increase in resistance during the same time interval. The indications are that the amount of seed in the gas drops very slowly once the injection of seed is terminated.

An abbreviated summary of the test operation is given in Tables 20, 21 and 22. The voltage V in the table refers to the voltage applied across the electrodes. I_2 and I_1 represent the currents read in the positive and negative legs of the circuit shown in Figure 12. For the most part the electrodes were loaded continuously in the cathode grounded mode, with occasional tests being made under anode-grounded and floating electrode conditions.

As noted earlier when the cathodes are grounded, it is anticipated that the I_2 currents to the anodes would be somewhat higher than the I_1 currents because the anode meter reads both plasma current and leakage current, whereas the

TABLE 18

LEAKAGE RESISTANCE IN OHMS, ELECTRODES TO GROUND, TEST 36

Time	6:11 PM		8:00 PM		9:08 PM	10:18 PM	10:30 PM		10:52 PM	10:56 PM		7:50 AM		7:53 AM	8:00 AM	
Electrode-Pair	A-G	C-G	A-G	C-G	Seed On	Power Off	A-G	C-G	Seed Reapplied	A-G	C-G	A-G	C-G	Seed Off	A-G	C-G
1	5000	7200	850	980	-	-	3000	5000	-	110	180	1.2	27	-	1.2	6.5
2	3000	5200	540	760	-	-	2200	10,000	-	70	1100	14	24	-	17	30
3	9000	9000	840	1050	-	-	4000	6000	-	100	100	10	5.5	-	30	11.5
4	9000	9500	1000	1020	-	-	5000	6100	-	100	100	14	5.2	-	30	10.5
5	11,000	13,000	1550	1480	-	-	6000	7700	-	200	400	42	5.3	-	75	11.5
6	6000	8000	850	1000	-	-	4200	3000	-	90	80	16	5.7	-	32	13.5
7	5000	5400	720	740	-	-	2800	3400	-	70	65	16	3.0	-	26	220
8	4900	4700	760	880	-	-	2200	4000	-	70	65	7.0	7.0	-	20	18
9	9000	8800	1300	1200	-	-	3100	5200	-	120	110	high	high	-	high	high
10	6200	9000	1050	1250	-	-	2400	4400	-	90	100	19	11	-	35	24
11	11,000	19,000	1450	1500	-	-	2400	1300	-	130	110	35	10	-	55	18.5
12	29,000	28,000	2100	1750	-	-	2600	4000	-	180	130	25	32	-	60	85

TABLE 19

LATERAL LEAKAGE RESISTANCE IN OHMS BETWEEN ADJACENT ELECTRODES, TEST 36

Time	6:13 PM		8:02 PM		9:08 PM	10:18 PM	10:36 PM		10:52 PM	11:05 PM		7:52 AM		7:53 AM	8:02 AM	
Electrode-Pair					Seed	Power Off			Seed Reapplied					Seed Off		
1-2	3800	9500	410	510	-	-	2500	1400	-	60	72	11	50	-	17	40
2-3	8000	7400	28	295	-	-	260	1000	-	10	15	9	14	-	37	8.5
3-4	12,000	14,000	290	500	-	-	75	730	-	10		5.5	1.0	-	6	1.3
4-5	12,500	13,000	205	355	-	-	1800	800	-	60	180	13	0.8	-	30	3.7
5-6	16,000	18,000	1200	800	-	-	2000	2500	-	110	250	22	1.2	-	14	5.2
6-7	8800	9500	400	580	-	-	3500	500	-	50	33	22	8.0	-	14	13.5
7-8	8000	6000	440	290	-	-	1300	850	-	21	10	13	7.0	-	17	11.5
8-9	1300	1000	140	92	-	-	8	400	-	6.0	55	55	0.8	-	5.5	8.0
9-10	3600	6700	250	460	-	-	2000	1000	-	22	15	11	6.5	-	16.0	17.0
10-11	2000	14,000	78	310	-	-	1000	1000	-	6.0	8.0	18	4.0	-	40	80
11-12	15,000	20,000	660	590	-	-	800	270	-	62	10	35	4.6	-	45	30

TABLE 20

INITIAL ELECTRICAL OPERATION OF TEST 36

Time	E-P	1	2	3	4	5	6	7	8	9	10	11	12	Remarks	Circuit
8:47 PM	V	50	50	50	50	50	52	50	52	53	46	52	40	Without	C.G.
	I_2	.10	.15	.10	.10	0	.15	.10	0	.10	0	.1	0	Seed	
	I_1	.10	.10	.10	.15	0	.05	.10	0	0	0	0	0		
8:53	V	50	50	50	50	50	51	50	53	49	46	54	50	Without	A.G.
	I_2	.10	.10	.09	.1	0	.10	.10	0	.10	0	.05	0	Seed	
	I_1	.15	.15	.10	.1	0	.08	.10	0	.10	0	.05	0		
9:14	V	38	41	40	39	49	41	42	41	46	42	41	39	Seed On	C.G.
	I_2	2.2	1.8	2.1	2.2	0.4	2.1	1.6	2.0	0.4	3.5	1.9	1.2	at 9:08	
	I_1	1.4	2.3	2.0	1.9	0.9	1.8	1.6	0.0	3.0	1.9	1.5	1.7		
9:20	V	42	40	40	40	44	42	40	53	26	43	41	40		A.G.
	I_2	2.4	1.6	2.0	2.4	.1	2.0	1.2	1.3	2.3	2.0	1.6	1.0		
	I_1	1.9	2.2	2.0	1.9	1.2	2.0	2.0	0	0.4	2.9	1.6	2.0		
9:36	V	38	41	39.5	38.5	49	40	42	40	44	43	42	39		C.G.
	I_2	2.3	1.8	2.1	2.2	.39	2.0	1.6	2.0	.4	3.1	1.6	0.9		
	I_1	1.6	2.1	2.0	1.9	1.2	1.7	1.8	0.0	2.7	1.6	1.5	1.9		
9:42	V	62	65	63	63	75	75	69	65	62	45	51	40		C.G.
	I_2	3.6	3.0	3.5	3.6	1.2	3.3	2.5	3.0	5.4	0.5	2.5	0.6		
	I_1	2.6	3.0	3.2	3.0	2.3	2.8	2.8	0	4.9	2.4	2.0	2.5		
9:47	V	64	63	76	76	88	79	71	77	64	46	52	39		C.G.
	I_2	5.0	3.0	5.0	4.5	2.0	4.0	3.6	4.3	5.4	0.3	2.3	0.8		
	I_1	2.9	3.4	3.5	3.6	3.0	3.3	2.6	0	5.4	2.4	2.1	2.5		
9:55	V	64	75	93	93	107	98	100	93	70	47	63	39		C.G.
	I_2	5.3	2.6	6.4	5.8	3.3	5.3	5.0	6.4	5.1	2	2.2	0.5		
	I_1	3.0	3.8	4.1	4.5	3.9	4.3	4.6	0	5.4	2.6	2.3	2.6		

10:14 At 10:14 PM Main Circuit Breaker Opened when Voltages were Increased by a 25 Volt Increment.

NOTE: C.G. is Cathode Ground
A.G. is Anode Ground
F.L. is Floating
E.P. is Electrode-Pair

TABLE 21

ELECTRICAL OPERATION OF TEST 36

Time		1	2	3	4	5	6	7	8	9	10	11	Remarks	Circuit
12:00 MID	V	36	37	39	45	95	90	45	44	42	52	38	Seed	F.L.
	I_2	2.8	2.6	2.4	1.1	6.0	6.8	1.0	1.6	3.0	2.9	2.0		
	I_1	2.8	2.6	2.3	1.1	6.0	6.8	1.0	1.6	3.0	2.9	2.0		
12:10 AM	V	39	41	44	62	70	70	46	46	43	49	40	1% Seed	A.G.
	I_2	2.5	1.7	4.0	4.0	1.6	3.6	1.8	2.2	4.0	2.2	2.3		
	I_1	2.2	1.7	1.2	0	7.9	8.2	0.7	1.4	2.0	3.2	2.1		
12:30	V	40	43	46	50	55	56	46	48	42	46	40		A.G.
	I_2	2.9	2.0	3.4	3.7	1.5	3.3	1.9	3.0	2.4	2.9	2.9		
	I_1	1.9	1.4	1.0	0.2	86	8.5	0.7	0.9	2.2	3.7	0.6		
12:42	V	37	38	38	38	74	69	46	44	41	48	49	$\sum I_1$ = 28.9A	C.G.
	I_2	2.6	2.0	2.5	2.0	5.2	6.0	0.8	1.7	3.0	3.5	2.1	$\sum I_2$ = 31.4A	
	I_1	2.0	2.0	2.5	3.0	3.2	4.9	1.8	1.0	3.2	3.0	2.3		
1:55	V	14	23	16	29	67	72	45	43	40	49	41		C.G.
	I_2	7.0	4.5	6.7	4.0	6.5	5.5	0.7	1.7	6.3	3.2	1.7		
	I_1	0.4	0.7	0.9	6.3	3.4	4.5	1.3	2.9	2.4	2.2	1.7		
2:00	V	40	42	40	38	44	44	43	42	42	46	41	$\sum I_2$ = 35.0A	A.G.
	I_2	1.9	2.7	7.3	5.1	1.5	2.6	1.3	1.9	6.5	1.8	2.4	$\sum I_1$ = 39.4A	
	I_1	2.0	1.7	1.9	2.4	10.5	9.6	1.2	2.1	2.7	4.2	1.1		
4:36	V	38	20	12	25	62	62	33	27	-	40	41	$\sum I_2$ = 52.5A	C.G.
	I_2	2.3	5.7	7.1	4.5	7.2	7.2	3.4	4.5	-	7.0	3.6	$\sum I_1$ = 38.6A	
	I_1	0.3	0.8	1.3	10.5	8.2	6.8	1.6	3.7	-	1.8	3.0		
4:43	V	43	34	23	24	62	63	35	29	-	43	41		F.L.
	I_2	1.4	2.9	5.1	5.1	7.3	7.2	2.8	4.3	-	5.0	2.4		
	I_1	1.4	2.9	5.0	5.0	6.9	7.0	2.8	4.4	-	5.0	2.4		
4:45 AM	V	36	37	33	21	55	30	35	31	-	42	41		A.G.
	I_2	2.1	1.6	8.4	4.6	8.4	1.0	2.9	5.2	-	3.5	2.1		
	I_1	2.9	2.5	3.6	5.6	8.4	9.6	2.6	3.9	-	5.5	3.0		

TABLE 22

ELECTRICAL OPERATION OF TEST 36

Time		1	2	3	4	5	6	7	8	9	10	11	Remarks	Circuit
6:17 AM	V	50	19	29	42	55	54	31	31	20	40	41		C.G.
	I_2	8.4	6.0	4.2	1.6	8.4	7.0	1.8	4.0	-	6.5	3.0		
	I_1	6.5	1.0	1.7	4.2	4.4	4.7	2.1	4.4	-	3.8	5.5		
6:27	V	33	39	39	46	62	65	40	30	19	42	41		F.L.
	I_2	3.4	2.3	2.5	0.5	7.3	6.7	1.9	4.2	-	5.9	2.9		
	I_1	3.4	2.3	2.4	0.5	7.3	6.7	1.9	4.3	-	5.9	2.9		
6:30	V	19	36	37	38	43	43	41	41	39	41	40		A.G.
	I_2	2	1.3	2.4	2.9	1.3	3.1	1.9	2.8	8.5	3.3	4.0		
	I_1	-	2.9	2.5	2.1	11	9.6	1.6	2.3	0	4.9	6.8		
7:30	V	17	27	33	42	64	60	39	32	17	41	40		C.G.
	I_2	6.5	4.3	3.4	1.4	6.8	7.5	1.9	3.7	0	5.8	5.8		
	I_1	6.9	1.1	2.7	3.2	3.6	4.4	2.4	2.4	2.2	3.2	7.6		
7:32	V	29	37	28	45	64	60	39	32	16	41	40		F.L.
	I_2	4.2	2.5	2.4	0.9	6.8	7.3	2.0	3.6	-	5.7	5.8		
	I_1	4.2	2.5	2.3	0.9	6.8	7.3	2.1	3.7	0	5.7	5.8		

I_1 current reads only the pressure current. Similarly, when the anode was grounded, higher I_1 cathode currents are anticipated. With the electrodes were in the floating mode, $I_1 = I_2$.

Prior to the introduction of seed, the values of I_2 and I_1 observed conformed to expectations. After seed was introduced the non-grounded electrodes did not always have higher magnitudes of current than their grounded counterparts. The discrepancies were apparently due to preferred paths through the plasma which can occur when the potentials applied to the different electrodes are not uniform, as when there are lower potential drops between certain electrodes and the plasma. For example an anode electrode when at a higher potential than its neighbors can attract an electrical current from the grounded cathodes of adjacent electrode-pairs as well as from its own cathode. Similarly electrodes which have lower ohmic losses or lower cathode or anode falls because of higher operational temperatures or lower work functions tend to take more than their share of load current.

If the total anode and cathode currents are summed, See Table 21 under remarks, it is evident that the total anode current is greater than the total cathode current when the measurements are made under cathode grounded conditions. Similarly the sum of all the cathode currents is greater than the sum of all the cathode currents when the measurements are made under grounded anode conditions.

On the basis of the observation that the better electrodes tend to be loaded more heavily than from electrodes under anode or cathode grounded conditions, the decision was made that future tests would be conducted with electrodes floating.

Conductivity Measurements

During Test 36 conductivity measurements were taken between 11:10 and 11:30 PM on 10/28/77. As indicated previously they were made by applying an axial voltage between a group of electrodes tied together on the upstream side of the channel and a similar group of electrodes tied together on the downstream side of the channel. The plasma currents and the potentials of the intermediate electrodes were observed using the DAS.

The voltage profiles observed during four sets of measurements are shown in Figure 13.

It is evident that there is only slight evidence of anode or cathode falls in the 4 checks. The low anode and cathode falls are apparently the result of relatively high electrode surface temperatures. Data taken in earlier tests where the electrode temperatures were lower exhibited higher anode and cathode falls than are present in Figure 13.

The plasma conductivities observed during the four measurements varied between 3.2 and 4.2 mhos/meter.

4.0 TASK 4 - TECHNICAL SUPPORT FOR THE COOPERATIVE US/USSR PROGRAM ON MHD

4.1 U-02 Phase III Program

4.1.1 Electrode Development

There are two general classes of materials that can be considered for hot (surface temperatures exceedubg 1700^oC) electrodes under "clean" fuel MHD conditions: 1) refractory oxides based on either ZrO_2 or HfO_2, and 2) somewhat less refractory but electronically conducting oxides of either the perovskite or spinel structure. ZrO_2 (or HfO_2) based compositions are very resistive to hot plasma; however, these materials are ionic conductors, thus, are subject to electrolysis and are electrically too resistive below 1400^oC, thus requiring means for current lead-out at very high temperatures. On the other hand, the perovskites and, to a somewhat lesser extent, the spinels have good electrical properties over a wide temperature range, but suffer from high vaporization rates, poor erosion resistance and poor compatibility with other channel materials at temperatures above 1700^oC. Much effort has been made to improve the performance of ZrO_2-based electrodes by the search for

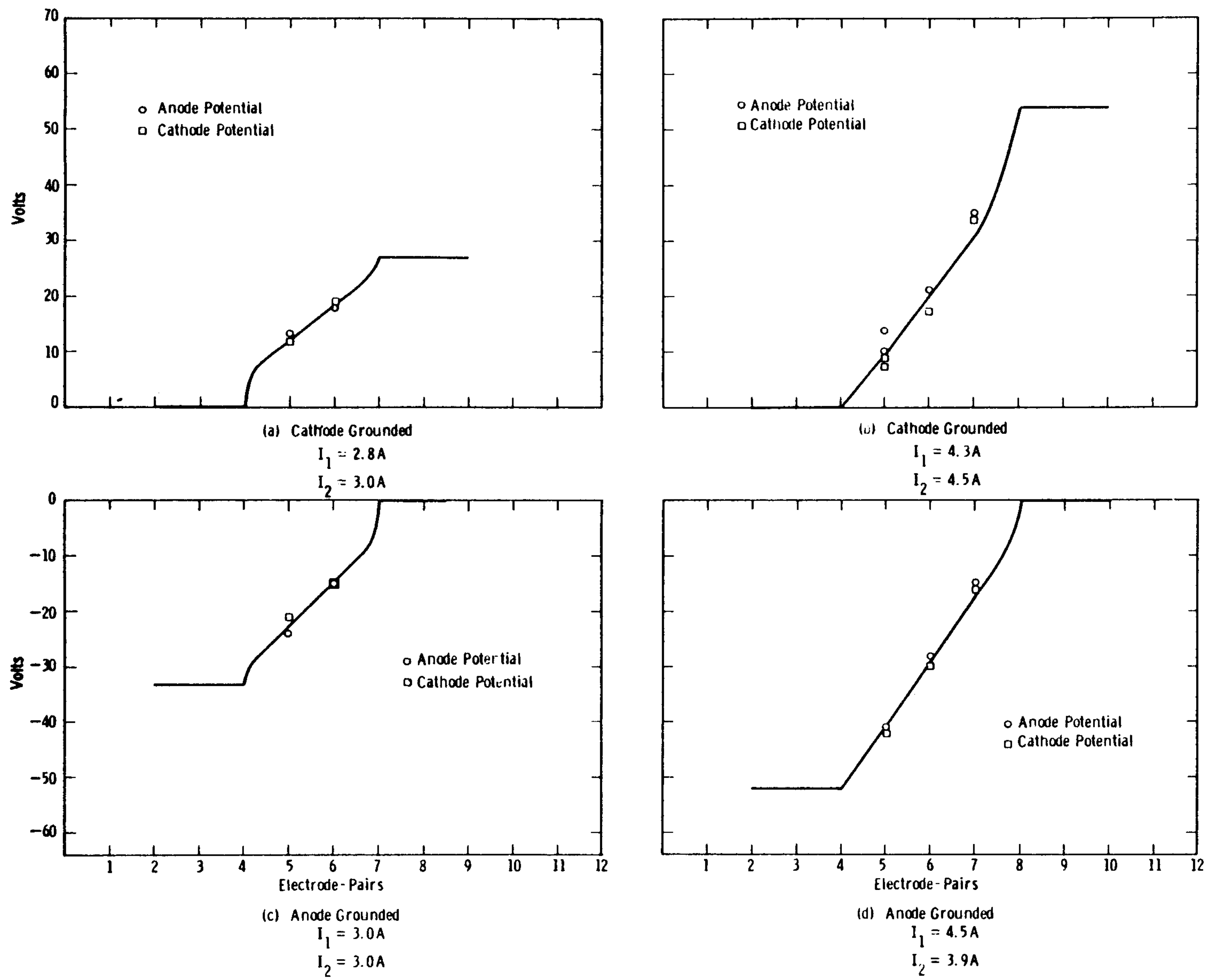

Figure 13. Voltage profiles taken during conductivity measurements, Run 36

compositions with more attractive electrical characteristics and by the development of various current lead-out structures and materials; while relatively little effort has been placed upon realizing the full potential of perovskite and spinel electrode compositions.

The initial selection of candidate electrode materials for the Phase III test included a spinel, magnesium aluminate ferrous ferrite (MAFF)[2], a perovskite, magnesia doped lanthanum chromite[3], and HfO_2 based composition. Several modifications of $LaCrO_3$ with improved refractory and erosion resistant properties were also included.

Magnesium oxide, MgO, and magensium aluminate spinel, $MgAl_2O_4$, were included in the proof tests as interelectrode insulators. Strontium zirconate was eliminated as a possible insulator on the basis of poor high temperature resistivity. Both sintered (or hot pressed) monolithic and arc-plasma sprayed electrode and insulator materials will be tested.

The 11 electrode/insulator structures that have been selected for proof tests are shown in Table 23. Seven of these electrodes are based upon $LaCrO_3$, three upon $MgAlO_4 \cdot Fe_3O_4$ (MAFF) and one upon a HfO_2-metal composite. The $LaCrO_3$ compositions are based upon several concepts. First, solid solutions of $LaCrO_3$-$LaAlO_3$ have shown promise in laboratory tests to reduce vaporization losses while maintaining refractoriness and electrical properies[4]. Secondly, mixtures of $LaCrO_3$ with either ZrO_2[5] or $SrZrO_3$[6] have also been reported to improve erosion resistance and lower vaporization losses. Finally, the concept of "capping" moderately refractory oxides with very refractory (ZrO_2-or-HfO_2-based) oxides has been advocated[7]. The refractory cap composition selected was 85 m/o ZrO_2-12 CeO_2-3Y_2O_3 which has been reported to be 40-60% electronically conducting at temperatures above 1500^oC[8].

Pre-test property measurements and material characterization were used to provide design information and to establish a base for comparison of post-test results. Pre-test examination included measurements of: thermal conductivity, thermal expansion, electrical conductivity, elastic modulus, fracture strength,

TABLE 23

U-02 PHASE III MODULE CANDIDATE ELECTRODE/INSULATORS

Supplier	Fab.* Tech.	Attachment	Electrode	Insulator	Proof Test No.
GE	M	Flexbed	$MgAl_2O_4$ (Fe_3O_4)	$MgAl_2O_4$	1
W/Technetics	PS	Mesh	$MgAl_2O_4$ (Fe_3O_4)	$MgAl_2O_4$	1
ANL	M	HfO_2 - Metal Composite		$MgAl_2O_4$	1
W/EP	M	Compliant	$LaCrO_3/ZrO_2$ Cap	MgO	2
W/APS	PS	Cermet	$LaCrO_3/ZrO_2$ Cap	$MgAl_2O_4$ (PS)	2
W	M	Compliant	$LaCrO_3$ - ZrO_2 Composite	$MgAl_2O_4$	2
W/Technetics	M	Mesh	$LaCrO_3$	$MgAl_2O_4$	2
W	M	Compliant	$LaCrO_3$ - $LaAlO_3$	MgO	3
W	M	Compliant	LaCrO - $SrZrO_3$	MgO	3
GE	M	Flexbed	$LaCrO_3$	$MgAl_2O_4$	3
W/APS	PS	Cermet or $FeAl_2O_4$	$MgAl_2O_4$ (Fe_3O_4)	$MgAl_2O_4$ (PS)	3

*PS - Plasma Spray
M - Monolithic (Sintered or Hot Pressed)

chemical composition, phase composition, microstructure and porosity. Purchase orders have been placed with several subcontractors to produce powders, ceramic blocks and electrode structures; these supporting activities are summarized in Table 24. In addition, General Electric and Argonne National Laboratories will each submit an additional set of electrodes for proof tests.

The first three sets of electrodes have been received and are in the process of being assembled into electrode walls for the first proof test. General Electric submitted three pairs of electrodes consisting of $4MgAl_2O_4 \cdot 1Fe_3O_4$ ceramic electrodes on a metal "FLEXBED" structure with sintered spinel inter-electrode insulators. Argonne also has submitted three pairs of electrodes; these consist of an integral wire-mesh electrical leadout/attachment system that is co-fabricated with the ceramic electrode body. Argonne submitted two variations of this electrode: a) 9.7 m/o Y_2O_3-16.3 m/o CeO_2 - 74 m/o HfO_2 with nichrome wire and b) 18 m/o CeO_2-82 m/o HfO_2 with Hoskins 875 wire. $MgAl_2O_4$ inter-electrode insulation was applied by arc plasma spray deposition. The third set of electrodes was arc plasma spray deposited $3MgAl_2O_4 \cdot 1Fe_3O_4$ on the Hoskins 875 BRUNSBOND mesh. Three anodes were prepared by Technetics and the three cathodes were sprayed by APS materials. Sintered $MgAl_2O_4$ insulators from Transtech provided the inter-electrode insulation. Specific details on the development of these electrodes will be provided in the next quarterly.

The remaining eight sets of electrodes are in various stages of development or fabrication. Their status is as follows:

Hot Pressed ZrO_2 Capped $LaCrO_3$ Electrodes (Eagle-Picher Industries, Miami, Okla)

Twenty-seven ceramic blocks (2.1 cm x 2.1 cm x 0.9 cm) were received from Eagle Picher. These ZrO_2 capped $LaCrO_3$ ceramics will be fabricated into three electrode pairs. The development effort of Eagle-Picher will be documented in the next quarterly. In summary, this effort identified powders from which dense, crack-free electrode blocks could be made. The reduction of $LaCrO_3$ to form Cr metal complicated the processing of these pieces, requiring use of ceramic hot pressing linings and lower pressing temperatures. Bodies which were totally crack-free could not be produced in the framework of time and budget. However, cap attach-

TABLE 24

ELECTRODE/INSULATOR MATERIAL VENDORS

Vendor	Product
APS Materials, Inc. (Dayton, Ohio)	Plasma sprayed electrode/insulator structures
Technectics Div., Brunswick Corp. (Milford, Conn.; LeGrande, Fla.)	Plasma sprayed and sintered ceramic attached BRUNSBOND™ compliant metal mesh layer (electrode structures) - W supplies monolithic insulator
Eagle-Picher Co. (Miami, Okla.)	Hot pressed graded (ZrO_2 to $LaCrO_3$) blocks
General Refractories (Philadelphia, Pa.)	$LaCrO_3$ ceramic blocks and powders
A-T Research (Vichy, Mo.)	$LaCrO_3$ based powders and sintered blocks, ZrO_2 powders
Trans-Tech Co. (Gaithersburg, Md.)	$MgAl_2O_4$ and MgO insulators, MAFF and $LaCrO_3$ powders
Norton Co. (Worchester, Mass.)	MgO (90% dense) insulators
Cerac Co. (Milwaukee, Wis.)	Various ceramic powders

ment appeared to be good (from torch-type thermal tests). Conductivity measurements conducted at NBS showed that the conductivity of the $85ZrO_2$-$12CeO_2$-$3Y_2O_3$ composition to be 0.1 $ohm^{-1}cm^{-1}$ at 1280°C. Therefore the temperature of the interface between the two $ZrO_2/LaCrO_3$ layers must be greater than 1280°C to avoid Joule heating.

$LaCrO_3$-ZrO_2 Composite

Several samples consisting of mechanical mixtures of a fine reactive $La_{.95}Mg_{.05}CrO_3$ powder (General Refractories Company, Philadelphia, Pennsylvania) and coarse fused 88 m/oZrO_2-12 m/oU_2O_3 grains (Norton Company, Worchester, Massachusetts) were hot-pressed at 1620°C and 2000 psi. The addition of refractory ZrO_2 grains to $LaCrO_3$ should increase its erosion resistance and decrease its volatilization rate. Densities in the range of 92-94% of theoretical were achieved. Samples with 30% and 40% ZrO_2 were sent to NBS for measurement of high temperature conductivity. This data is shown in Figure 14 along with data for $La_{.95}Mg_{.05}CrO_3$. Lower temperature data shows the temperatures where the conductivity is 0.1 $ohm^{-1}cm^{-1}$ is 237°C for 30 v/o ZrO_2 and 390°C for 40 v/o ZrO_2. On the basis of maximizing ZrO_2 content without producing large amounts of joule heating due to poor low temperature conductivity at electrode/attachment interface temperatures (200-250°C), 30 v/o ZrO_2-70 v/o $La_{.95}Mg_{.05}CrO_3$ appeared as optimal. Billets of this materials are now being pressed for proof test #2 electrodes.

$LaCrO_3$ Electrodes

$La_{.95}Mg_{.05}CrO_3$ blocks were received from General Refractories Company. Brazing trials were conducted at Technetics Division, Burnswick Corporation in LeGrade, Florida to bond these blocks to the BRUNSBOND nickel mesh. A Western Gold and Plantinum Company (WESCO) brazing alloy "Ticusil" containing 4.5% Ti, 67% Ag, 28.5% Cu was found to produce an adequate bond between $LaCrO_3$ and nickel mesh. Technetics will be shipping these brazed assembies shortly for the second proof test.

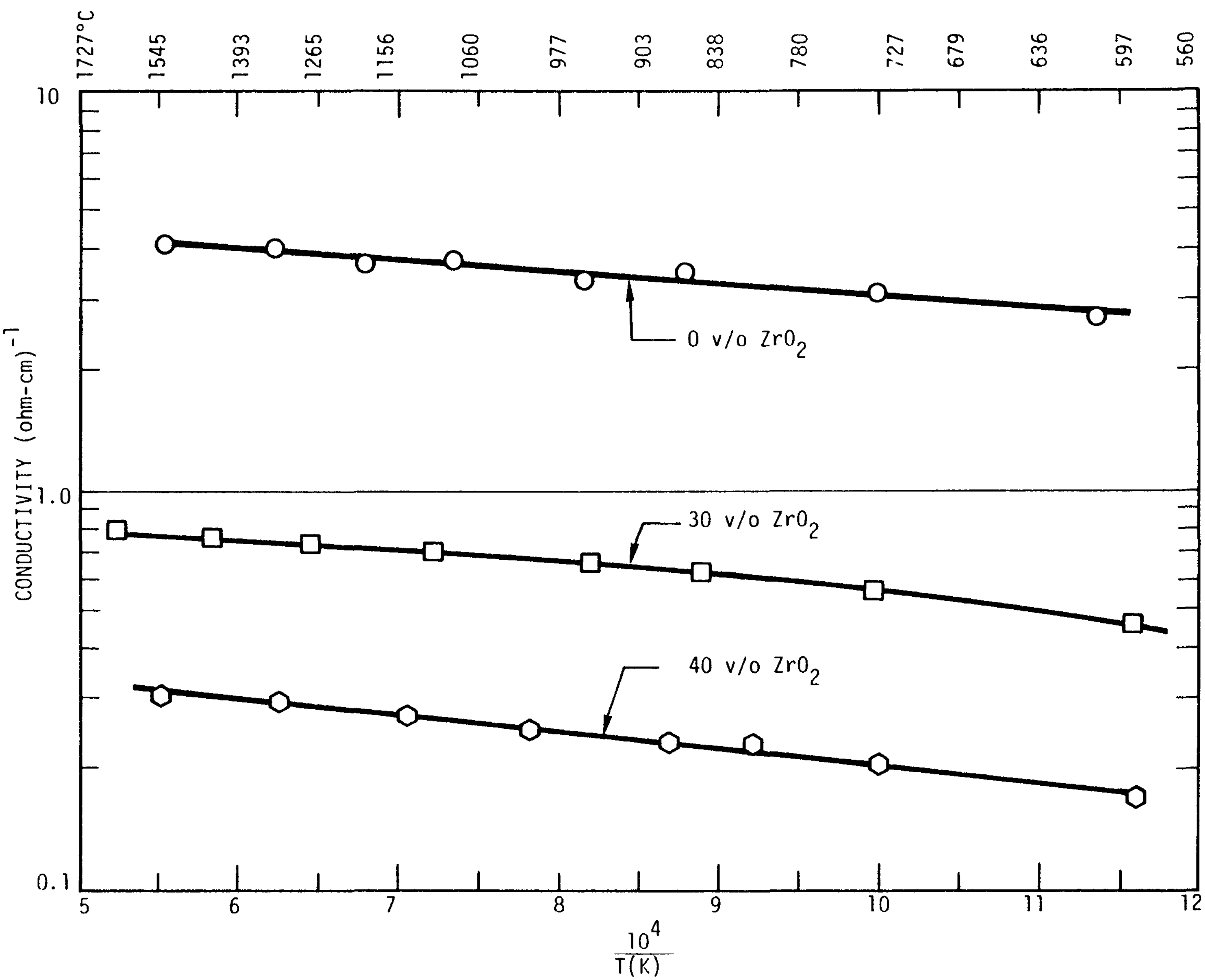

Figure 14. Electrical conductivity of hot pressed $La_{.95}Mg_{.05}CrO_3$ with Additions of 0, 30 and 40 volume percent Y_2O_3-Stabilized ZrO_2 - Measurements made at NBS (2.3) at $pO_2 = 10^{-3}$ atm.

$LaCrO_3$-$LaAlO_3$ Electrodes

Anderson et al[3] have demonstrated that substitution of Al for Cr in MgO doped $LaCrO_3$ significantly lowers the voliatization rates of this material. As shown in Figure 15 the substitution of Al on 10% of the Cr sites reduces the volatility of $La_{.95}(Mg_{.05}Cr)O_{2.83}$ by a factor of six. This could represent an increase in maximum operating temperature of $100^{o}C$. Further substitution of Al yields further improvement in high temperature weight changes. Compositions containing graded layers of $La(Mg,Cr,Al)O_3$ were produced by both hot pressing and sintering. The electrical conductivity of these layers were measured at NBS and are shown in Figure 16. This data shows, first, that hot pressing produces material with better electrical conductivity and secondly compositions should be limited to a maximum of 32% Al substitution on the basis of electrical conductivity. Therefore, graded electrode blocks were produced by hot pressing for proof test #3 with layers containing $La_{.95}Mg_{.05}Cr_{.68}Al_{.32}O_3$ (hot surface), $La_{.95}Mg_{.05}Cr_{.75}Al_{.25}O_3$, and $La_{.95}Mg_{.05}Cr_{.85}Al_{.25}O_3$ (cold surface).

$LaCrO_3$/$SrZrO_3$ Electrodes

Composition studies in the $LaCrO_3$/$SrZrO_3$ system are under way at A-T Research Company. Promising samples will be sent to NBS for resistivity measurements. These electrodes will be included in the third proof test.

Arc Plasma Spray Deposited Electrodes (APS Materials, Inc., Dayton, Ohio)

APS Materials, Inc. is currently conducting an effort to produce plasma spray deposit electrodes of sufficient thickness for U-02 tests. Attention is being given to graded attachments and production of crack-free, single phase $LaCrO_3$ and $3MgAl_2O_4 \cdot 1FeO_3$. Since this work is still in progress details will be reported in the next quarterly.

4.1.2. Characterization of Electrode/Insulator Materials

To fully evaluate and design the insulator/electrode assemblies to be used in the U-02 Phase III MHD test, a number of different properties of the selected channel materials must be determined. These properties include the bulk

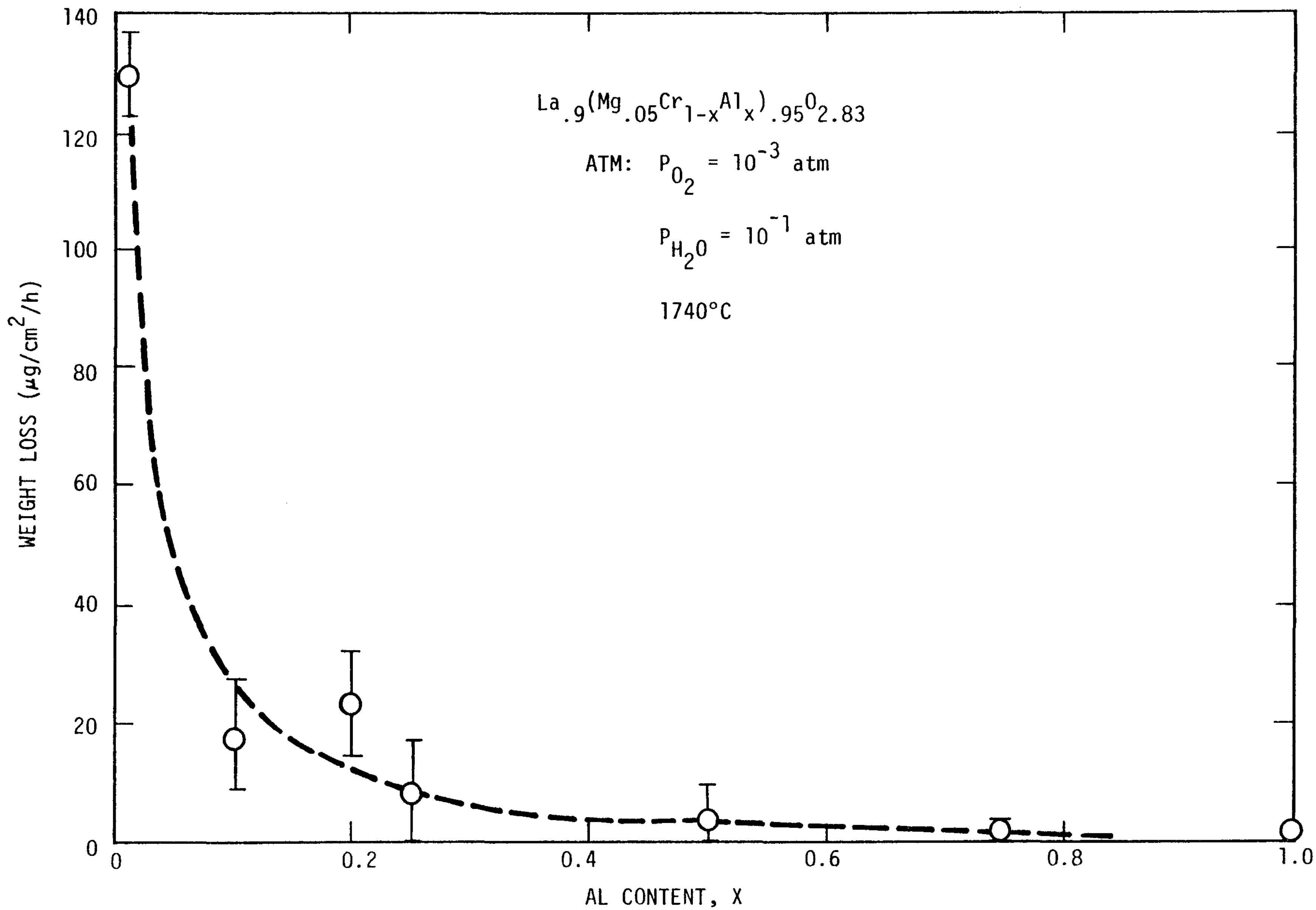

Figure 15. Weight Loss Rates of $La_{.9}(Mg_{.05}Cr_{t-x}Al_x)_{.95}O_{2.83}$ compositions as a function of Al content measurements made at University of Missouri (Reference 4)

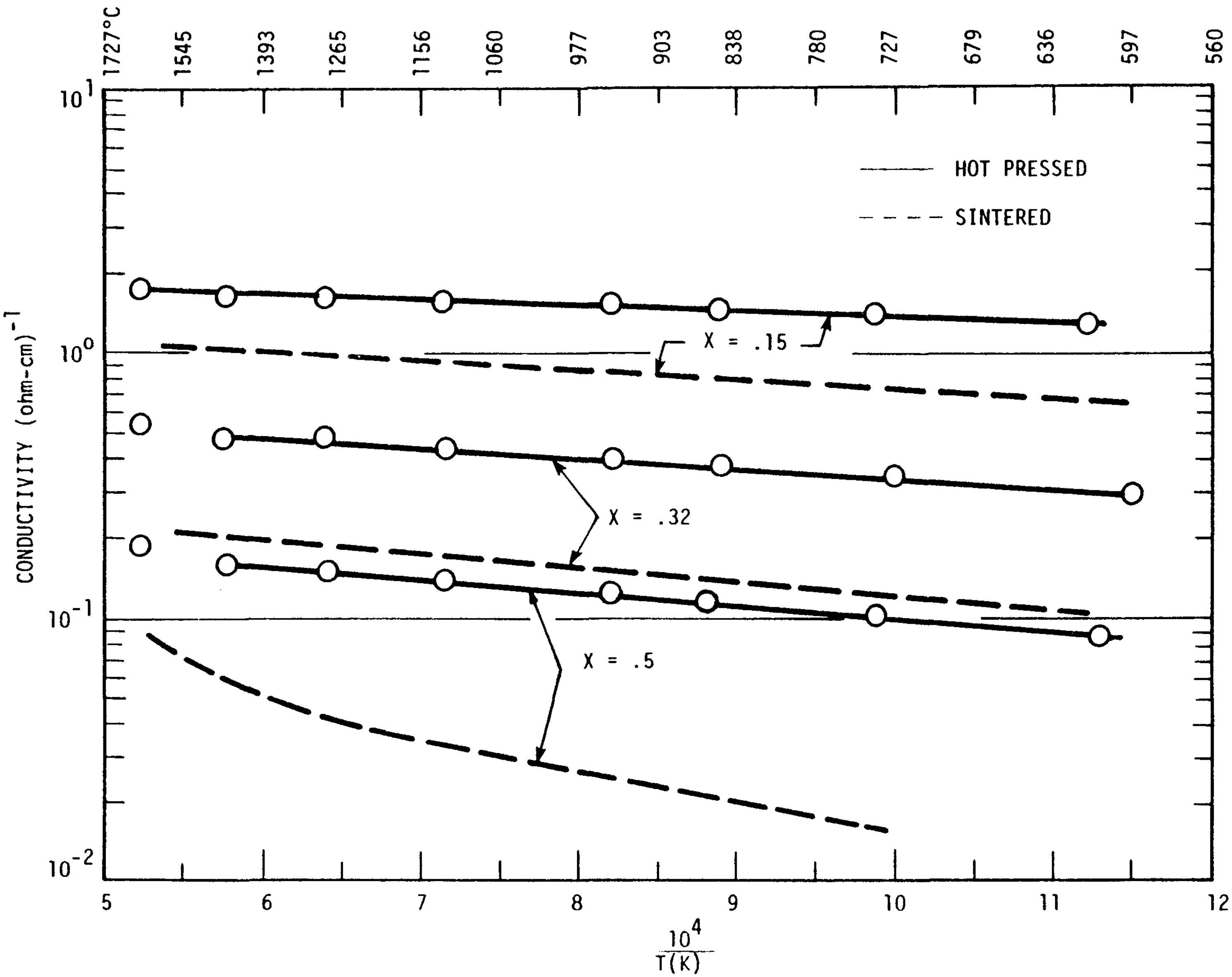

Figure 16. Electrical conductivity of hot pressed and sintered $La_{.95}Mg_{.05}Cr_{1-x}Al_xO_3$ compositions in air measurements made at NBS (Reference 2)

density, electrical and thermal conductivity, the elastic modulus and fracture strength, the thermal expansion, and the x-ray analysis and emission spectroscopy of both the starting powders and sintered/hot-pressed components. The following data is a continued compilation of these properties.

4.1.2.1 Thermal Conductivity/Diffusivity

Thermal conductivity/diffusivity measurements were made on a number of materials being tested in the U-02 Phase III Proof Tests. These tests were conducted at Battelle-Northwest* using a laser pulse technique.

$MgAl_2O_4$ (Plasma-Sprayed)

$MgAl_2O_4$ was processed by APS** by arc plasma spraying the material into a free-standing piece with a final density of 3.25 g/cc. From Figure 17 it is apparent that the thermal conductivity of the plasma sprayed material is much lower than $MgAl_2O_4$ that has been sintered. This material is being used as insulation around a set of electrodes being tested in Proof Test II.

Hoskins 875 Mesh

Hoskins 875 mesh was fabricated by Brunswick Corporation* to a density of 4.23 g/cc. This material is to be used as an attachment media between the electrode and copper cooling block in a number of assemblies in the upcoming Proof Tests. Figure 18 shows the thermal conductivity and diffusivity for the temperature range the mesh will be exposed.

Ni-205 Mesh

Ni-205 mesh was fabricated by Brunswick Corporation by pressure sintering to a density of 3.66 g/cc. This material is to be used as an attachment media for a set of lanthanum chromite electrodes to be run in the 2nd U-02 Proof Test. In Figure 19, note the break in the continuity of the thermal conductivity curve due to a phase change at 631°K

* Lambert Bates, Richland, Washington. 99352
** D. Harris, Dayton, Ohio 45401

Curve 693028-A

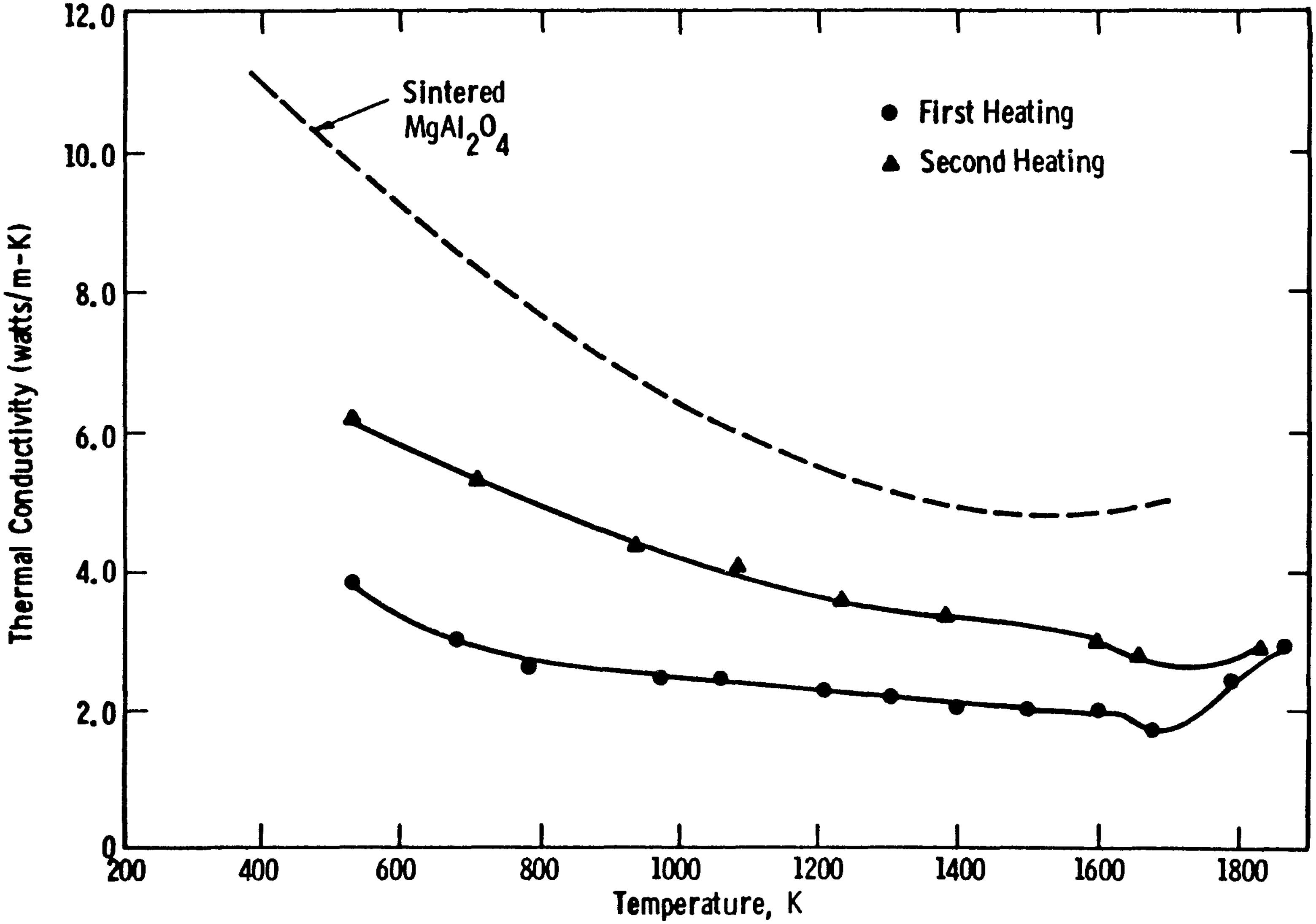

Figure 17. Thermal conductivity of plasma-sprayed $MgAl_2O_4$ (Measured by BNW)

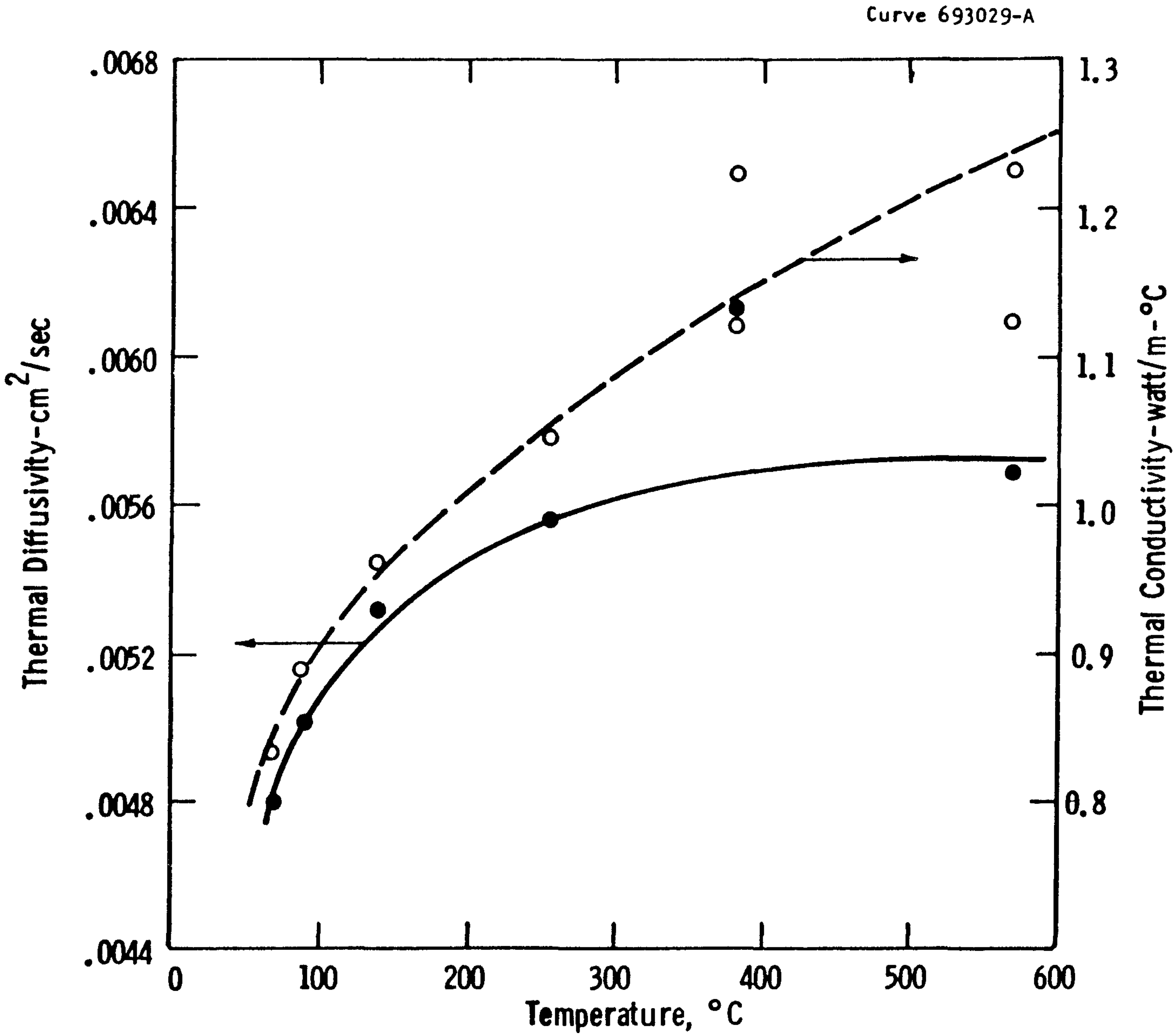

Figure 18. Thermal diffusivity/conductivity of Hoskins 875 Mesh (Measured by BNW)

Curve 693025-A

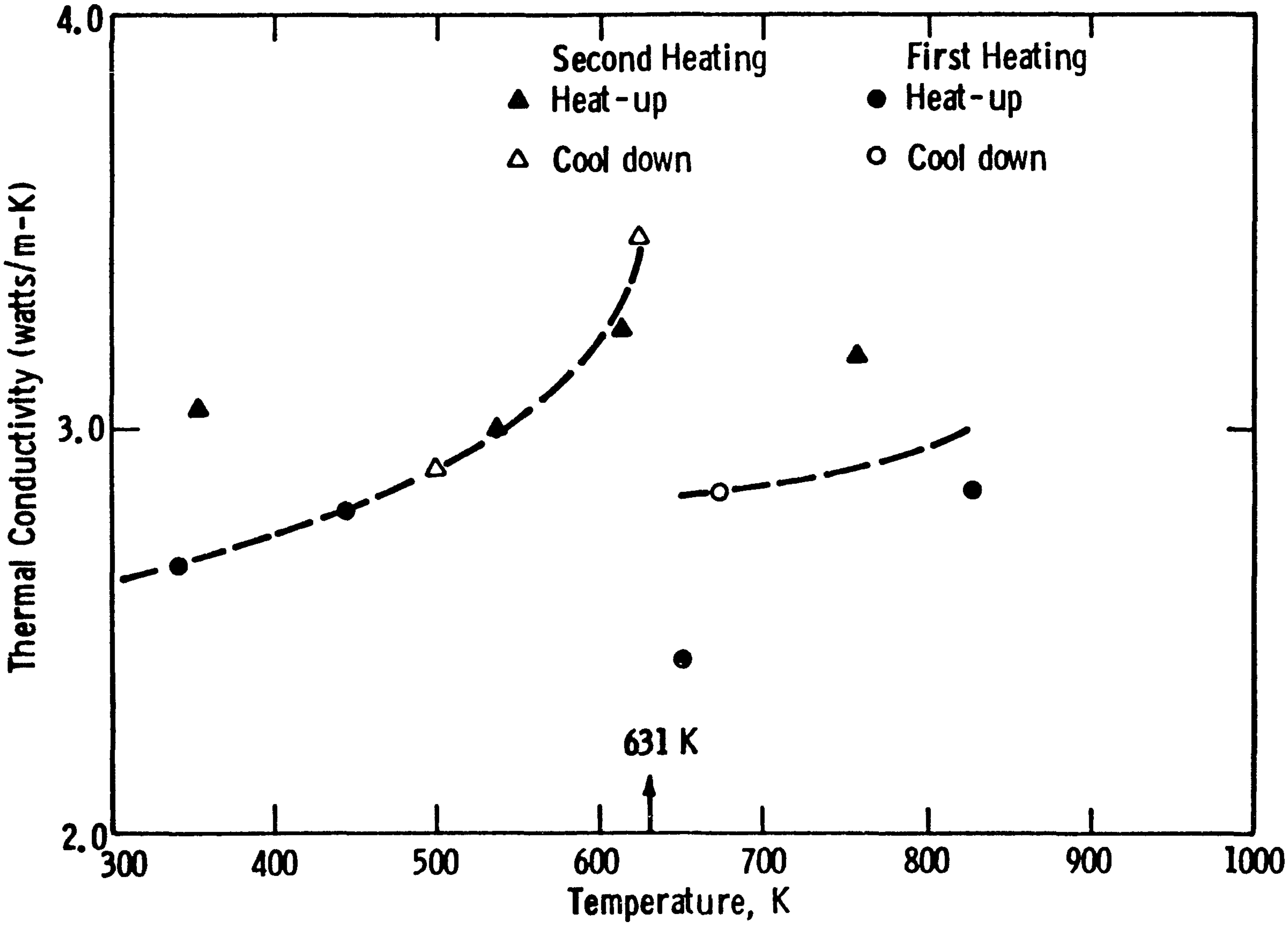

Figure 19. Thermal conductivity of Ni-205 mesh (Measured by BNW)

4.1.2.2 Electrical Conductivity

The electrical conductivity of electrode and insulator materials were determined by the National Bureau of Standards using a d.c. four probe technique. This method minimizes any measurement difficulties due to contact emf's or polarization effects.

$SrZrO_3$

$SrZrO_3$ was processed by cold pressing and sintering to a final density of 5.16 g/cc. It is a material which has potential as an interelectrode insulator. The electrical conductivity was measured from 800°C - 1650°C at various oxygen partial pressures. In Figure 20 note the comparatively high conductivity valves at the higher temperatures. Insulators in an MHD channel are targeted for a conductivity of at least 10^{-2} ohm-cm^{-1}, which is borderline for this case.

4.1.2.3 Elastic Modulus

The elastic modulus for various electrode/insulator materials were measured at Westinghouse by using a four point flexure fixture and measuring the radial deflection using a three rod deflectometer. The specimens were loaded at a strain rate of 0.005 to approximately 75% of its fracture strength at each of the desired temperatures.

Flame-Sprayed Electrode/Insulator Materials

Three plasma-sprayed insulator/electrode materials, $75MgAl_2O_4$-$25Fe_3O_4$, $La_{.95}Mg_{.05}CrO_3$, and $MgAl_2O_4$, were processed at Westinghouse and the elastic modulus measured. Figure 21 shows the valves obtained from room temperature to 1400°C.

* Technetics Div.

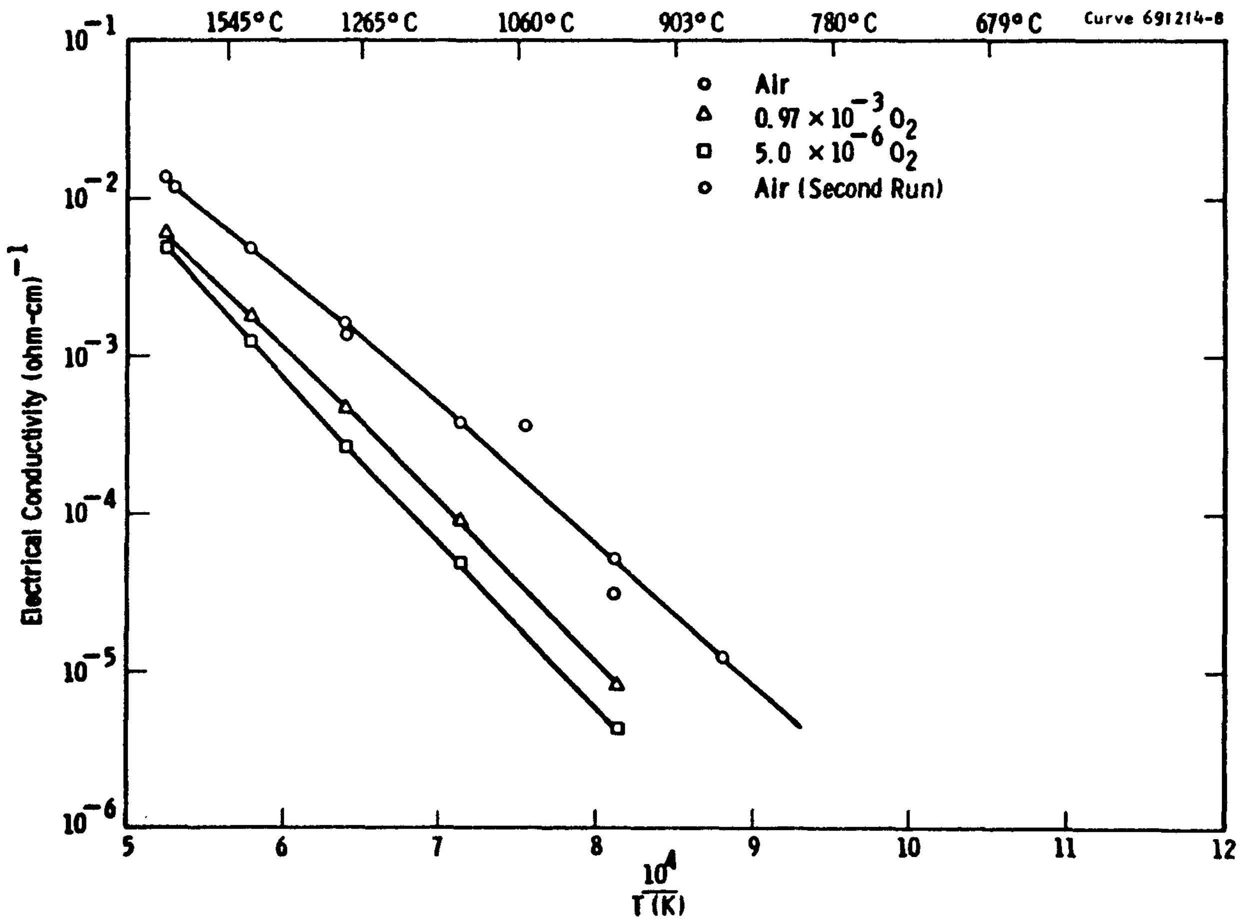

Figure 20. Electrical conductivity of sintered strontium zirconate insulator material at elevated temperatures and various oxygen partial pressures (Measured by NBS)

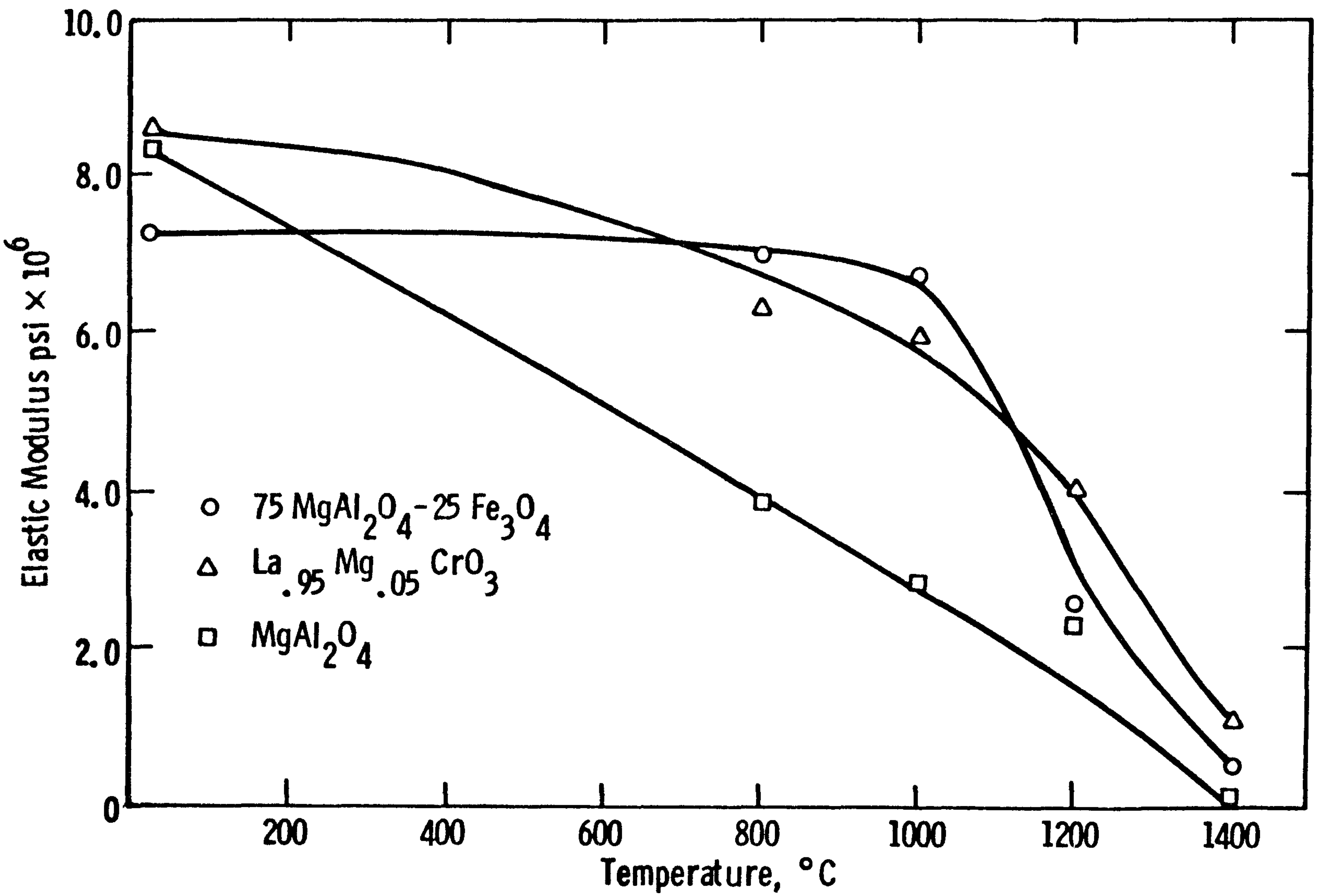

Figure 21. Elastic modulus versus temperature for three plasma-sprayed electrode/insulator materials

All three materials exhibited the largest elastic modulus at room temperature, with a steady decrease in their value as the temperature was raised. Quite a bit of plasticity was evident above 1000°C from the deformation versus load curves for both $MgAl_2O_4$ and $La_{.95}Mg_{.05}CrO_3$. $75MgAl_2O_4 \cdot 25Fe_3O_4$ showed even earlier indications of plastic flow at around 800°C. All three plasma-sprayed materials showed markedly lower elastic modulus values than their counterparts which had been sintered. This is a clear indication that the crystalline bonds for plasma-sprayed material are of a different nature than sintered pieces, and evidently, are much weaker.

4.1.2.4 Fracture Strength

The fracture strength of a number of electrodes/insulators that might possibly be used in the U-02 Phase III Proof Tests was measured by using a three point bend test on a rigid Instron testing machine. The fracture strength of these materials is very important for use in comparison with the thermal stresses achieved during actual MHD channel conditions. Obviously, an objective is to keep these thermal stresses below the fracture strength of the electrode/insulator assembly.

Spinel

Spinel which had been hot-pressed here at Westinghouse and that which had been hot-pressed at Transtech* were evaluated as shown in Figure 22. The Transtech spinel had overall greater strength values up to 1200°C where upon some plastic deformation was apparent. The Westinghouse spinel, in comparison, had a lower overall strength but maintained it through the temperature range investigated. The Westinghouse spinel was ~99% of theoretical density and the Transtech spinel was 97% of theoretical density.

---

* Mr. L. Domingus, Gaithersburg, Md.

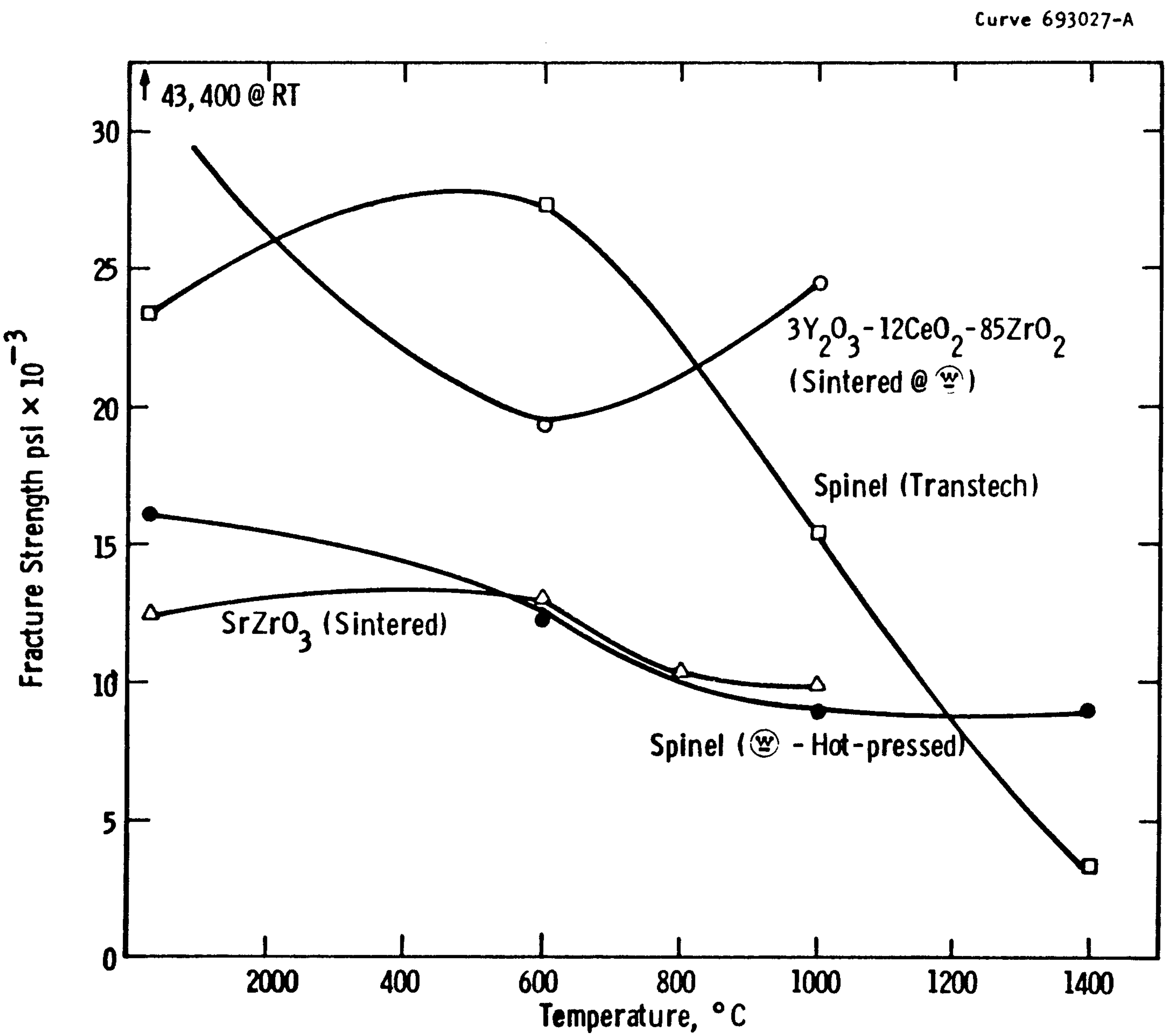

Figure 22. Fracture strength versus temperature for a number of electrode/insulator materials

$SrZrO_2$

$SrZrO_2$ was sintered here at Westinghouse to ~95% of theoretical density. The strengths obtained, as shown in Figure 22, were fairly low but were maintained from RT to 1000°C. Along with the spinels, $SrZrO_3$ is a candidate interelectrode insulator material.

$3Y_2O_3$-$12CeO_2$-$85ZrO_2$

$3Y_2O_3$-$12CeO_2$-$85ZrO_2$ was processed by sintering to a density of ~94% of theoretical. The material shows very good strengths from RT to 1000°C. Strengths at the higher temperatures are needed, though, due to its application as the "cap" section of an electrode, where temperatures of 1500-1800°C are maintained.

4.1.3 Electrode Wall Design-Proof Tests

4.1.3.1 Thermal Design

Thermal design analyses were completed to size selected electrode systems to establish the desired electrode surface temperatures for the U-02 Proof Tests, to be conducted in WESTF, and to generate the necessary temperature profiles to be used as input for stress analysis and subsequent structural design optimizations of the electrode system. This design effort used a finite element three-dimensional model which is schematically shown in Figure 23. The effect of Joule heating was included in the analysis.

Objectives of the thermal design analysis was to establish an electrode surface temperature of 1700^{o}C at an electrode heat flux of 16 W/cm^2 and a current loading of 9 amps.

Assumptions included in the thermal analysis are as follows:

1) Negligible current in interelectrode insulator.

2) Stagnant gas filled gap between interelectrode insulator and electrode.

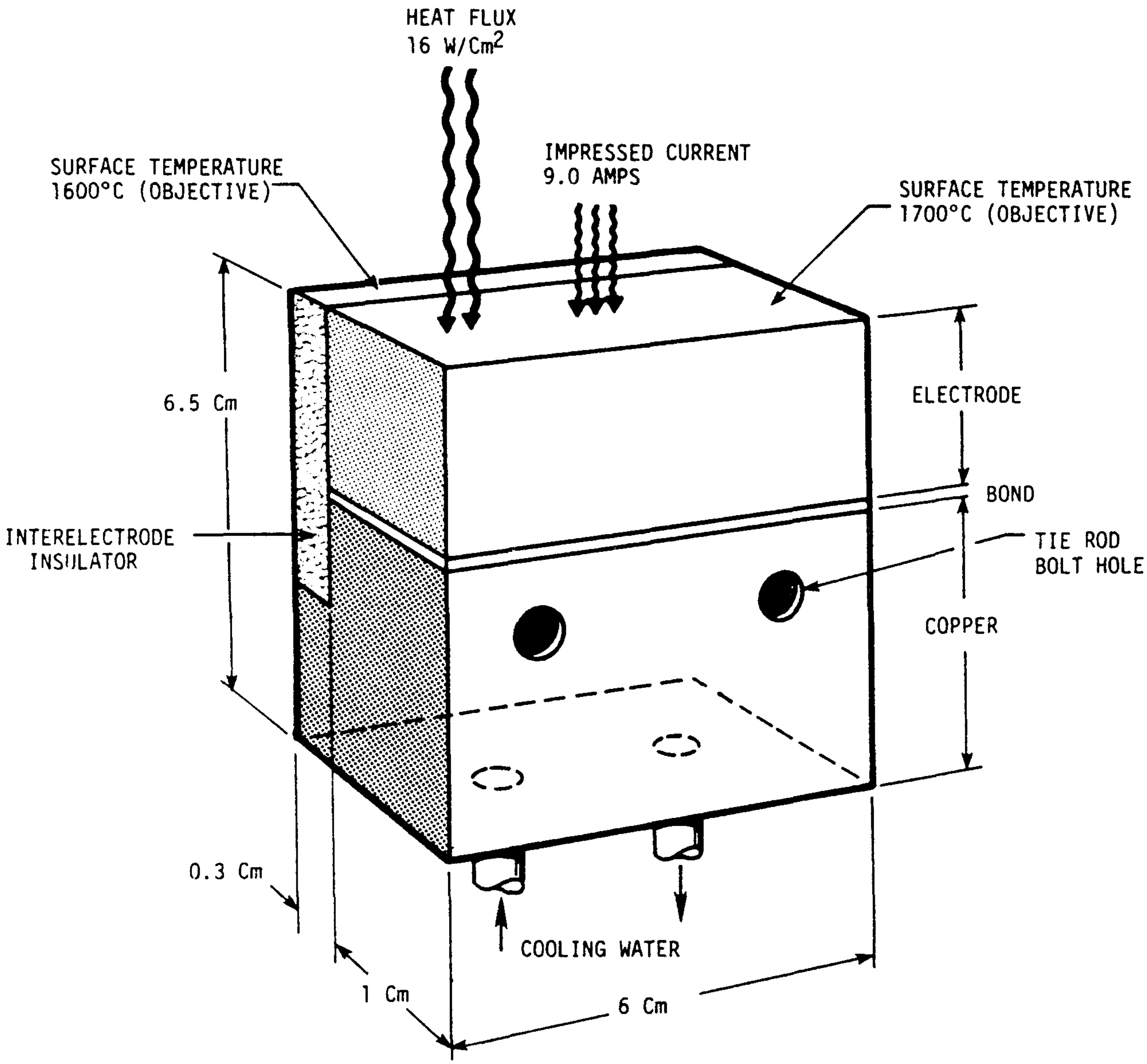

Figure 23. Electrode Design Schematic

3) Copper heat sink temperature of $30^{o}C$ at cooling channel (boundary condition).

4) Adiabatic electrode side walls (boundary condition).

5) Thermal boundary layer of the same magnitude as velocity boundary layer which varied according to the equation

$$\frac{U}{U_c} = \left(\frac{Y}{R}\right)^{1/7}$$

where: U = velocity at boundary layer

U_c = the centerline velocity

Y = boundary layer thickness

R = equivalent radius of channel

Analyses were completed for the following electrode systems:

Design 1 - $LaCrO_3$ electrode, silver-epoxy attachment, spinel insulator

Design 2 - $LaCrO_3$ electrode, nickel mesh attachment, spinel insulator

Design 3 - MAFF-31 electrode, Hoskins 875 mesh attachment, spinel insulator

The WESTF Test Assembly flow channel is approximately 5 cm (1.969 in) high by 2.5 cm (1 in) wide. Then the equivalent radius is:

$$R_e = 2\ (1.969)\ (1) / 2\ (1.969 + 1) = 0.663 \text{ inches}$$

Figure 24 shows the general electrode configurations and locations of reported temperatures while Figure 25 schematically shows the channel cross section and lines of constant velocity.

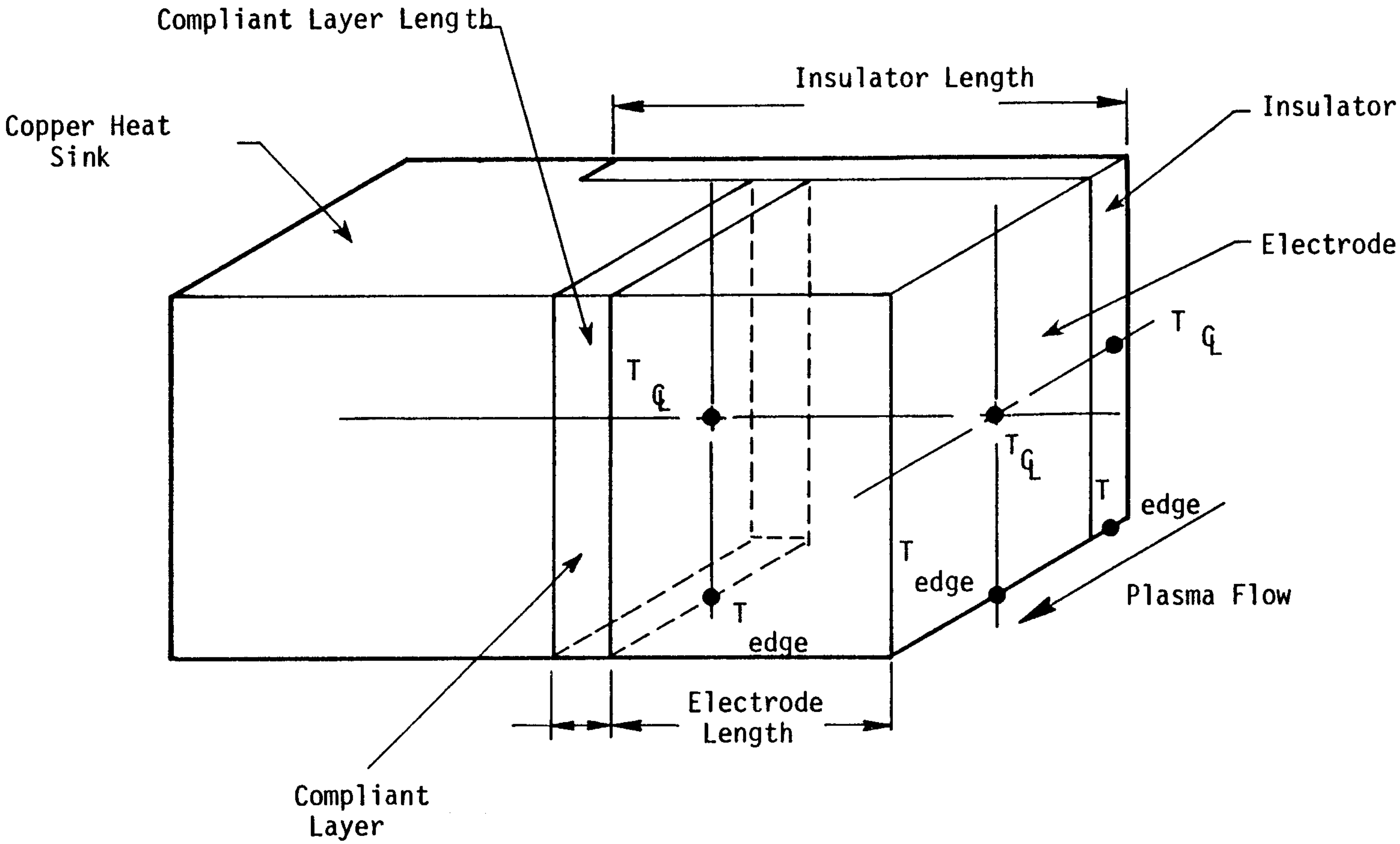

Figure 24. Electrode Configuration and Locations of Reported Temperatures

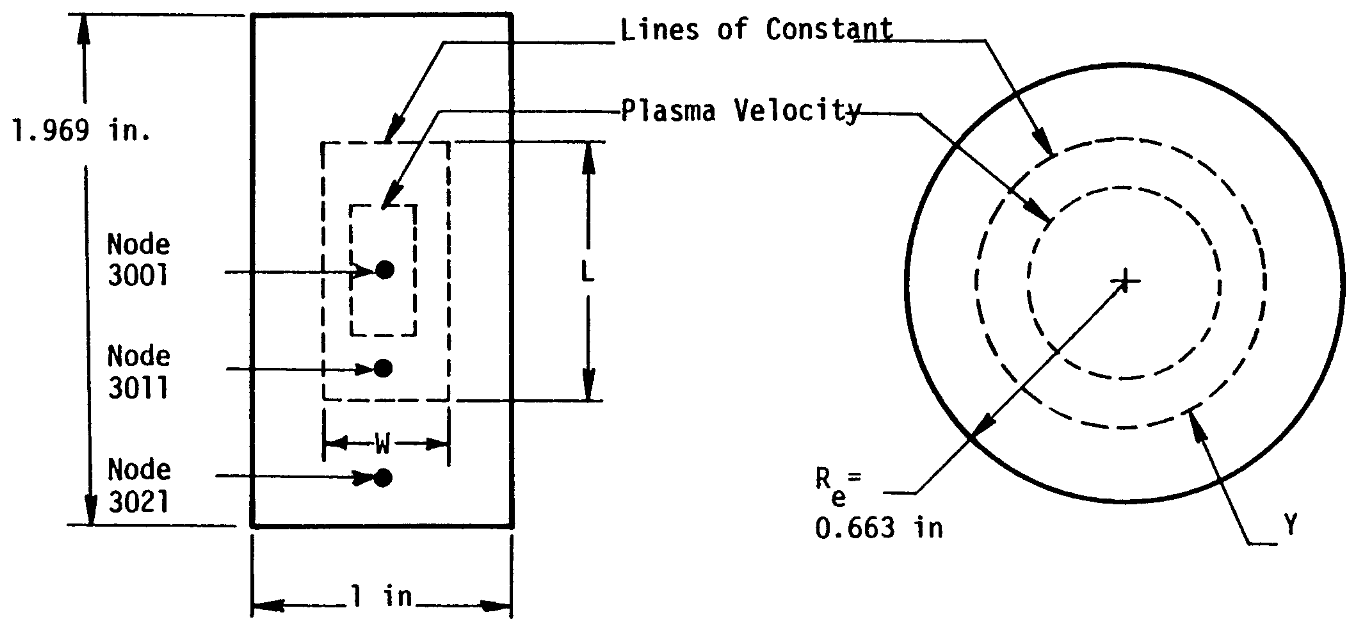

Convert rectangular cross section

Equivalent circular cross section

Figure 25. Channel Cross Section and Velocity Schematic

Let L = 1.969 x W, where L and W are the height and width of the channel cross section with a certain velocity ratio. Then:

$$0.663 - Y = \frac{2\ (1.969)\ W^2}{2\ (1.969\ W + W)}$$

$$W = (0.663 - Y)\ /\ 0.663$$

$$L = 1.969\ (0.663 - Y)\ /\ 0.663$$

The velocity profile in the channel was estimated as:

U/U_c	Y (inch)	W (inch)	L (inch)
1.0	0.663	0	0
0.95	0.463	0.302	0.594
0.90	0.317	0.522	1.028
0.75	0.089	0.866	1.130
0.50	0.0052	0.992	1.954

The temperature distribution across the face of the electrode was assumed to be symmetrical about the centerline, hence only one-half of the electrode was modeled. The electrode face had three vertical nodes and four horizontal nodes (1 for insulator, 1 for insulator-ceramic electrode gap, 2 for ceramic electrode). The velocity distribution across the face of the electrode was as follows:

Node 3011 (on centerline): U/U_c = 1.0

Node 3011 : U/U_c 0.94

Node 3021 : U/U_c 0.89

It was assumed that the thermal boundary layer was equal to the velocity boundary layer, i.e.:

$$(T_f - T_w) / (T_f - T_w)_c = U/U_c$$

T_f - fluid (plasma) temperature

T_w - wall temperature

With a given bulk plasma temperature at 4680^oR (2600 K) and a desired wall temperature of 3546^oR (1970 K), the plasma temperature at each node was:

Node 3001: $T_f = 4680^oR$
Node 3011: $T_f = 0.94\ (4680 - 3546) + 3546 = 4612^oR$
Node 3021: $T_f = 0.89\ (4680 - 3546) + 3546 = 4555^oR$

The heat transfer coefficient was then estimated from

$N_u = 0.023\ R_e^{0.8}\ P_r^{0.4}$, where at 2600^oK:

$N_u = hD/K$

$R_e = DV\rho/\mu$

$P_r = Cp\mu/K$

$\mu \sim 3.178 \times 10^{-5}$ lb/sec-ft
$K \sim 0.0799$ Btu/hr-ft-^oF
$D = 2\ (0.663) = 1.326$ inch
$\rho \sim 0.0408$ lb/ft^3
C_p 0.307 Btu/lb-^oF
$V \sim 1475.5$ ft/sec

Then: $\sim h$ 0.0653 Btu/sec-ft^2-°F

This is an estimate of the heat transfer coefficient at the centerline. Off the centerline, the coefficient was assumed to vary only with the velocity, i.e.

$$h = f\ ([U/U_c]^{0.8})$$

The design heat flux was 16 watts/cm^2, or 14.054 Btu/sec-ft^2. This was an average heat flux over the entire face of the electrode. To obtain this value, a multiplier was needed on the calculated heat transfer coefficient, since this calculated value was for the high heat flux zone at the center of the electrode face. In general:

$$q/A = k_o \cdot h \cdot \Delta T, \text{ where}$$

$$h = f\left(\left[(U/U_c \right]^{0.8} \right) = f\left([Y/R]^{0.8/7} \right)$$

$$\Delta T = f\left([Y/R]^{1/7} \right)$$

K_o = multiplier to obtain desired heat flux

$$q/A = K_o\ (0.0653)\ (Y/R)^{0.1143} \cdot (4680 - 3546)\ (Y/R)^{0.1428}$$

$$= 74.05\ K_o\ (Y/R)^{0.2571}$$

By integrating over the face of the electrode (Y/R goes from 0 to 1), and setting the result equal to 14.054 Btu/sec-ft^2, the value of K_o was determined:

$$\int_0^1 74.05\ K_o\ (Y/R)^{0.2571}\ d\,(Y/R) = 14.054$$

$$74.05\ K_o \cdot \frac{1}{1.2571} \cdot (Y/R)^{1.2571} \Big|_0^1 = 14.054$$

$$K_o = 0.2386$$

$$h = \frac{0.2386}{144} \times (0.0653) \times \left(\frac{U}{U_c}\right)^{0.8}$$

$$= 1.082 \times 10^{-4}\ (U/U_c)^{0.8}\ \text{Btu/sec-in}^2\text{-}^oF$$

The resulting heat transfer coefficient was as follows:

Node	Plasma Temp. (^{o}R)	H.T. Coefficient (Btu/sec-in^{2}-^{o}F)
3001	4680	1.082×10^{-4}
3011	4612	1.029×10^{-4}
3021	4555	9.857×10^{-5}

The following table summarizes the dimensions and temperatures for the three above-mentioned electrodes in S.I. units (cm, ^{o}C). The notation "C" and "edge" refer to the temperatures at the vertical center and at the edge of the electrode (interfacing with the insulating sidewall). For the insulator and electrode, the temperatures given are for the plasma-ceramic interface. For the compliant layer, the temperatures are for the compliant layer - electrode interface.

Design No.	Component	Lengths (cm)	Desired Temp. ^{o}C	Calculated Temp. ^{o}C ℄	Calculated Temp. ^{o}C Edge
	Electrode	2.286	~1700	1728	1650
1	Insulator	4.851	1400 - 1700	1522	1463
	Epoxy	0.0254	175	155	155
	Electrode	2.286	~1700	1761	1686
2	Insulator	5.062	1400 - 1700	1559	1502
	Nickel Mesh	0.236	200 - 300	285	285
	Electrode	1.27	~1700	1744	1677
3	Insulator	4.244	1400 - 1700	1576	1529
	Hoskins 875	0.434	600 - 1000	900	880

All of the above designs included the effect of Joule heating. This was a minor effect for designs No. 1 and 2 (the Lanthanum chromite electrode designs), but was fairly sizable for design No. 3 (the MAFF-31 electrode design). The Joule heating raised the temperatures approximately 10^{o}C for designs 1 and 2, but approximately 50^{o}C for design 3.

4.1.3.2 Structural Design

Structural analyses were completed to evaluate three different proof test electrode designs and to identify design optimizations to be incorporated into the hardware to be used in the proof test series.

Assumptions

Figure 23 provides a general sketch of the electrode. In addition to the thermal assumptions previously stated, the following assumptions were applicable to the structural analysis:

- Linear elastic stress analysis
- Two-dimensional plane stress state
- Steady state thermal stress case

The assumption which indicates that linear elastic stress analysis was used implies that the stress-strain relationship was assumed to be a linear one. For this type of analysis, stresses computed above the yield strength are inaccurate and cannot be used to qualify or disqualify a particular design. They can be used, however, to compare and evaluate the benefits of various design modifications. Such has been the focus of this investigation. It should be remembered that thermal stresses which exceed the material yield strength are often acceptable because of the self-limiting nature of thermal stresses in the plastic region. The ASME pressure vessel code recognizes this by permitting elastically computed thermal stresses to approach twice the yield strength.

The assumptions concerning the material properties are shown in Figures 26 through 30. The temperature dependency of Young's Modulus has been assumed in part for Spinel, MAFF-31, Hoskins 875 and Nickel 205.

All of the component materials analyzed were assumed to be homogeneous. Although the mesh bond materials were treated as being anisotropic, they were considered to be homogeneous so localized effects which distinguish the mesh braze from the filaments were not investigated.

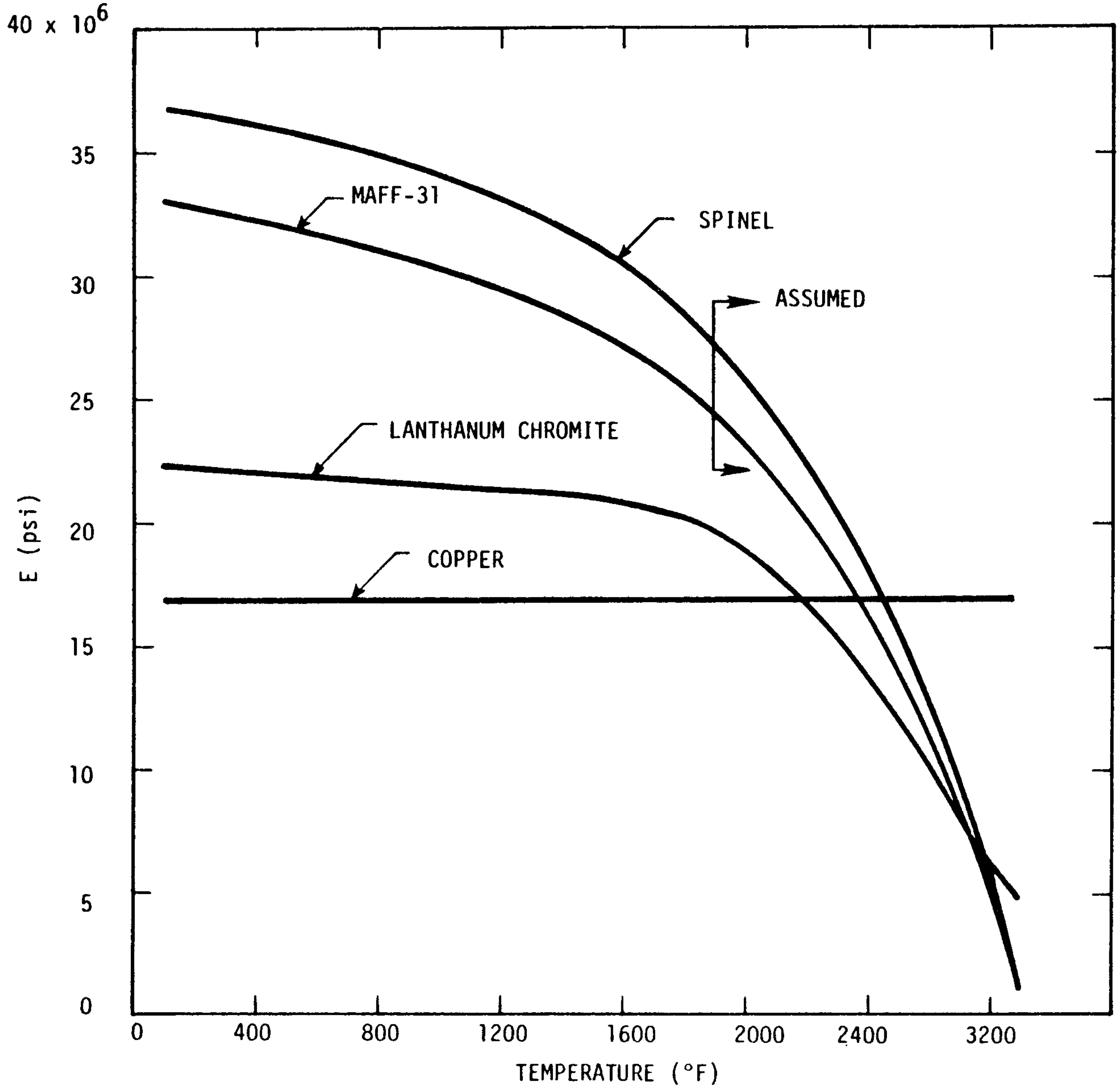

Figure 26. Young's Modulus for Electrodes and Insulator

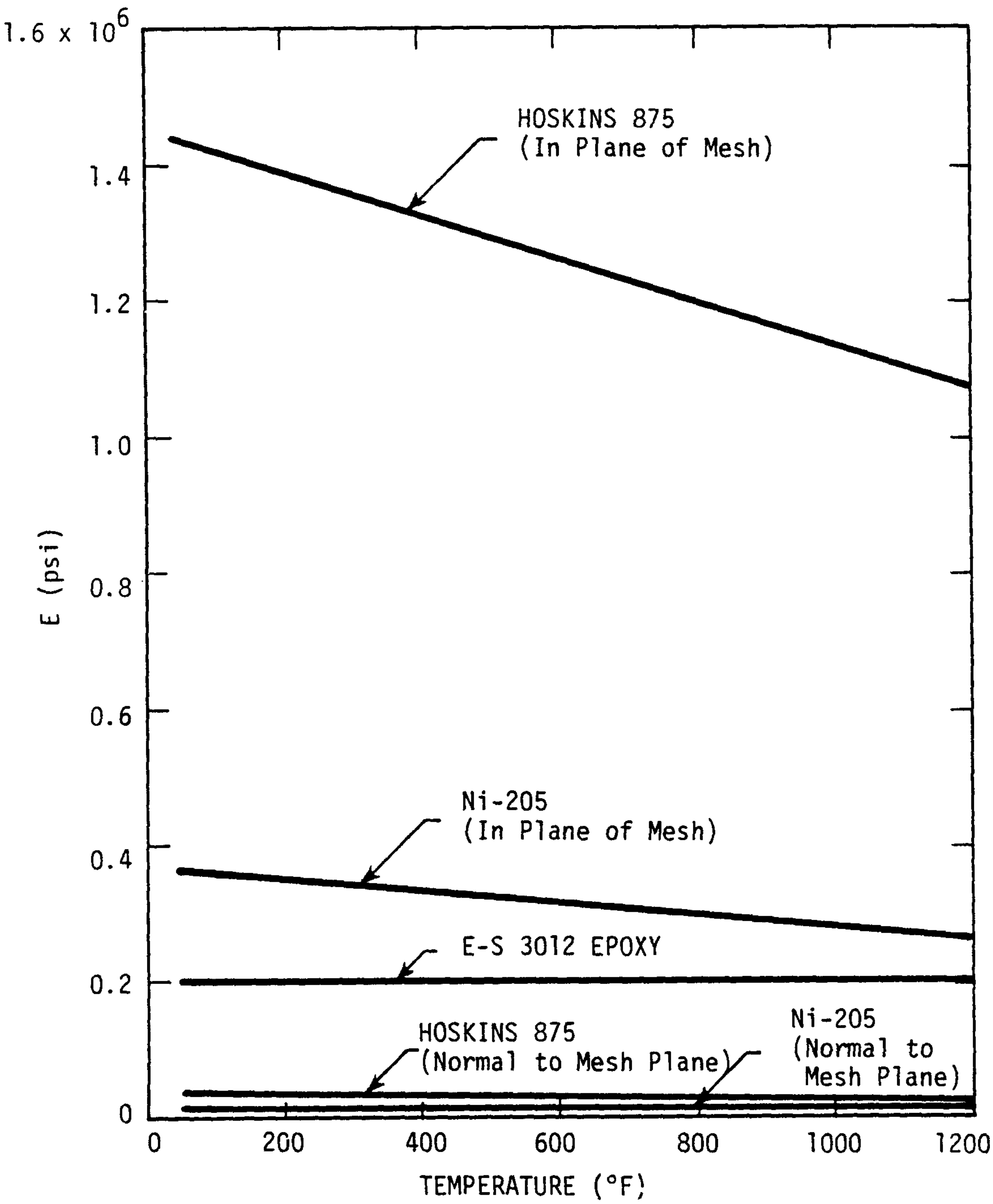

Figure 27. Young's Modulus for Compliant Bonds

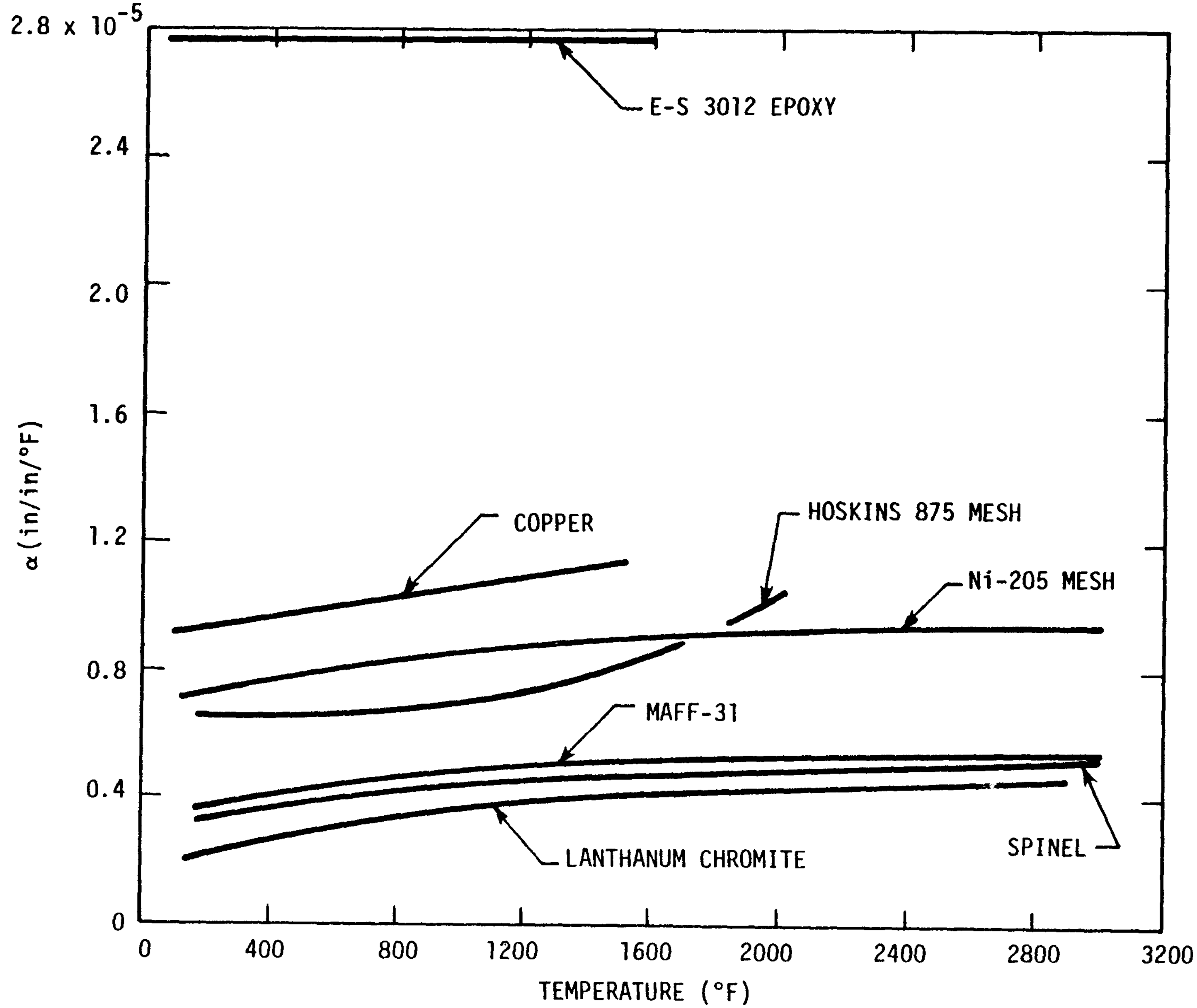

Figure 28. Coefficients of Thermal Expansion with the Stress Free Temperature Equal to 70°F

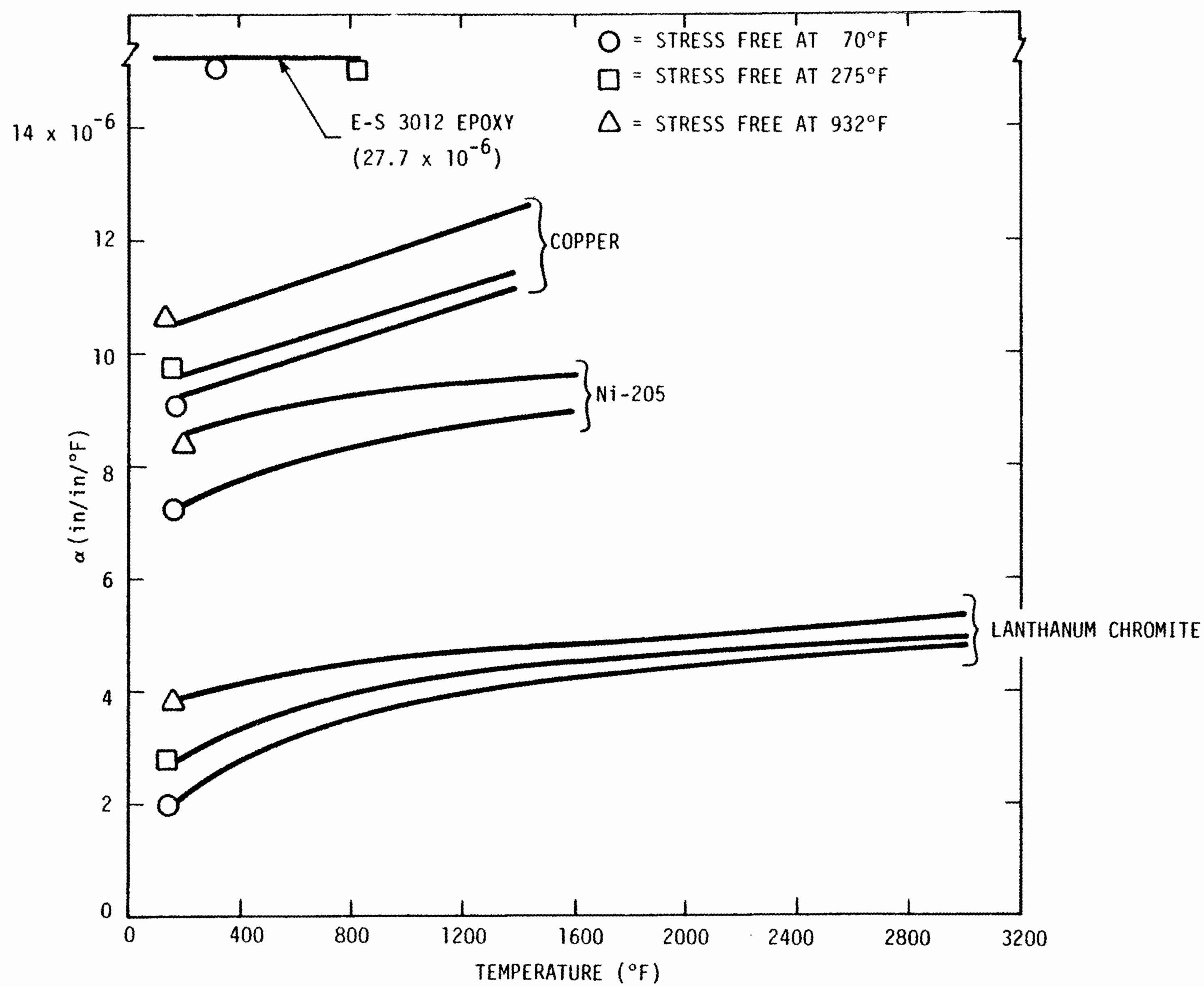

Figure 29. Coefficients of Thermal Expansion at Various Stress Free Temperatures

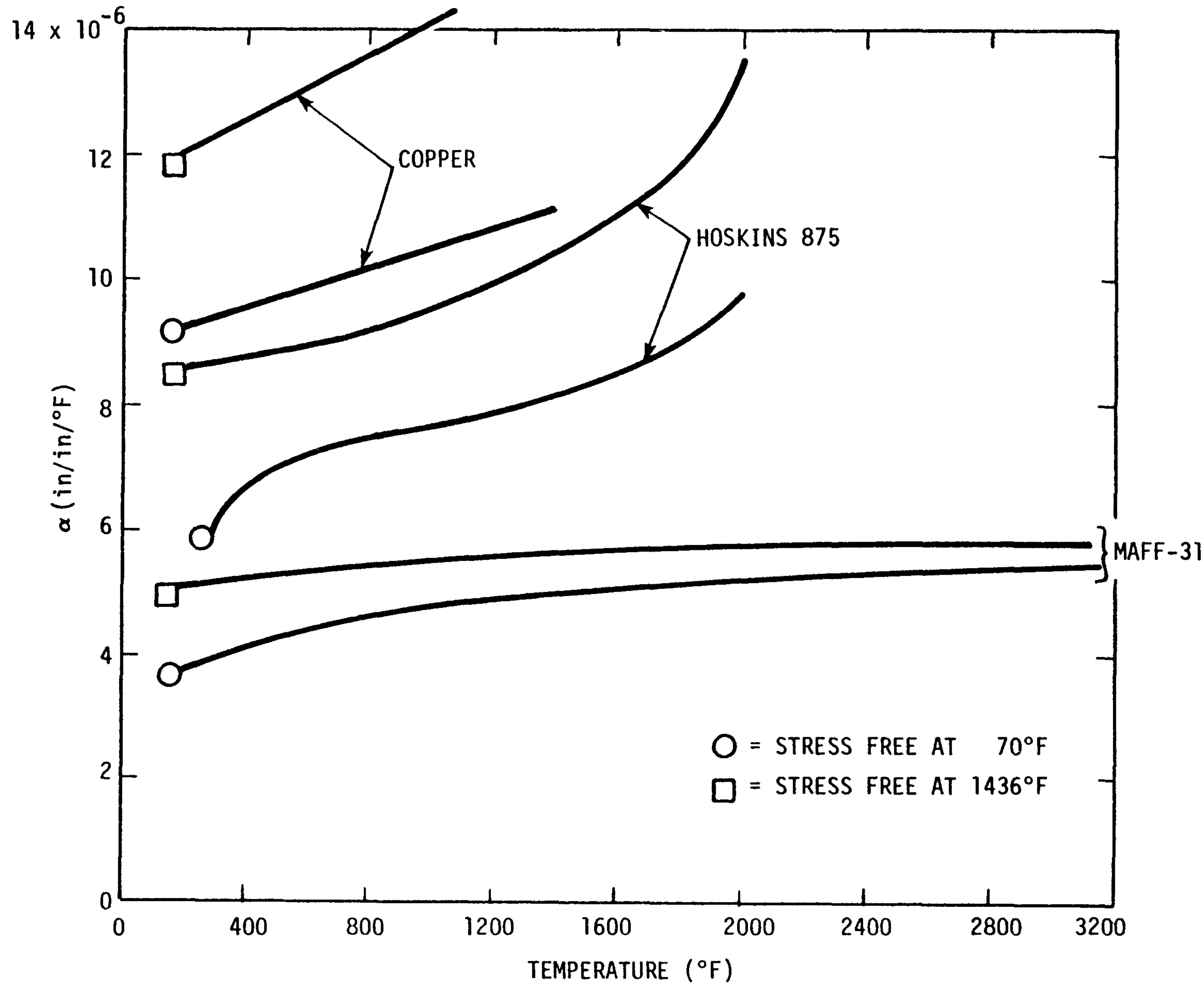

Figure 30. Coefficients of Thermal Expansion at Various Stress Free Temperatures

The coefficients of thermal expansion were derived for elevated stress free temperatures in order to investigate the effects of bond or braze temperature. The following formula was used for these computations:

$$\alpha_{T_0}(T) = \frac{\alpha_{RT}(T)\left[T - RT\right] - \alpha_{RT}(T_0)\left[T_0 - RT\right]}{T - T_0}$$

where

α_{T_0} (T) is the thermal expansion coefficient as a function of temperature T for reference temperature T_0

α_{RT} (T) is the thermal expansion coefficient as a function of temperature T for reference temperature RT (room temperature)

α_{RT} (T_0) is the thermal expansion coefficient at temperature T_0 for reference temperature RT (room temperature)

The material strength data for the component materials is shown in Table 25. Most yield strength data was not available.

Method of Analysis

The stress analysis was performed using a three dimensional finite element computer code. Finite element models were constructed for the three different electrode designs and for a Spinel insulator. An example of a typical two-dimensional model for the Lanthanum Chromite-Epoxy bonded electrode is shown in Figure 31. Symmetry of the electrode thermal gradients has been taken advantage of to reduce the model size in that only one-half of the electrode needed to be modeled. The nodes along the symmetric boundary were fixed in the x-direction to simulate this symmetry. The layer of Epoxy has a thickness comprised of five elements though they are not distinguishable in Figure 31. Finite element models for the Lanthanum Chromite-Ni 205 mesh bonded electrode, the MAFF 31 - Hoskins 875 mesh bonded electrode, and a Spinel insulator are shown in Figures 32 through 34.

Table 25 - MATERIAL STRENGTH

Material (Source)	Ultimate Strength (psi)	Yield Strength (psi)
$LaCrO_3$ (Westinghouse)	22,000 @ 70°F 19,700 @ 1832°F (1000°C) 17,700 @ 2552°F (1400°C)	--
MAFF-31 (Trans-Tech, Inc.)	17,700 @ 70°F 4,540 @ 1832°F (1000°C) 2,550 @ 2552°F (1400°C)	--
MAFF-31 (BNW)	7,520 @ 70°F 8,940 @ 1832°F (1000°C) 568 @ 2552°F (1400°C)	--
E-S 3012 Epoxy (Acme Chemical & Insulation Co.)	5,000 @ 77°F 2,000 @ 261°F (127°C)	--
Ni-205 Mesh (Rossing)	400 psi Normal to mesh	--
Hoskins 875 (Rossing) In plane of mesh	4400 @ 70°F 600 @ 1598°F (870°C)	4,300 @ 70°F 540 @ 1598°F (870°C)
Hoskins 875 (Rossing) Normal to plane of mesh	350 @ 70°F 280 @ 1598° (870°C)	320 @ 70°F 250 @ 1598°F (870°C)
Spinel (Rossing)	19,200 @ 70°F 15,600 @ 932°F (500°C) 4,300 @ 2192°F (1200°C)	--
OFHC (Rossing)	34,500 @ 70°F	7,900 @ 70°F

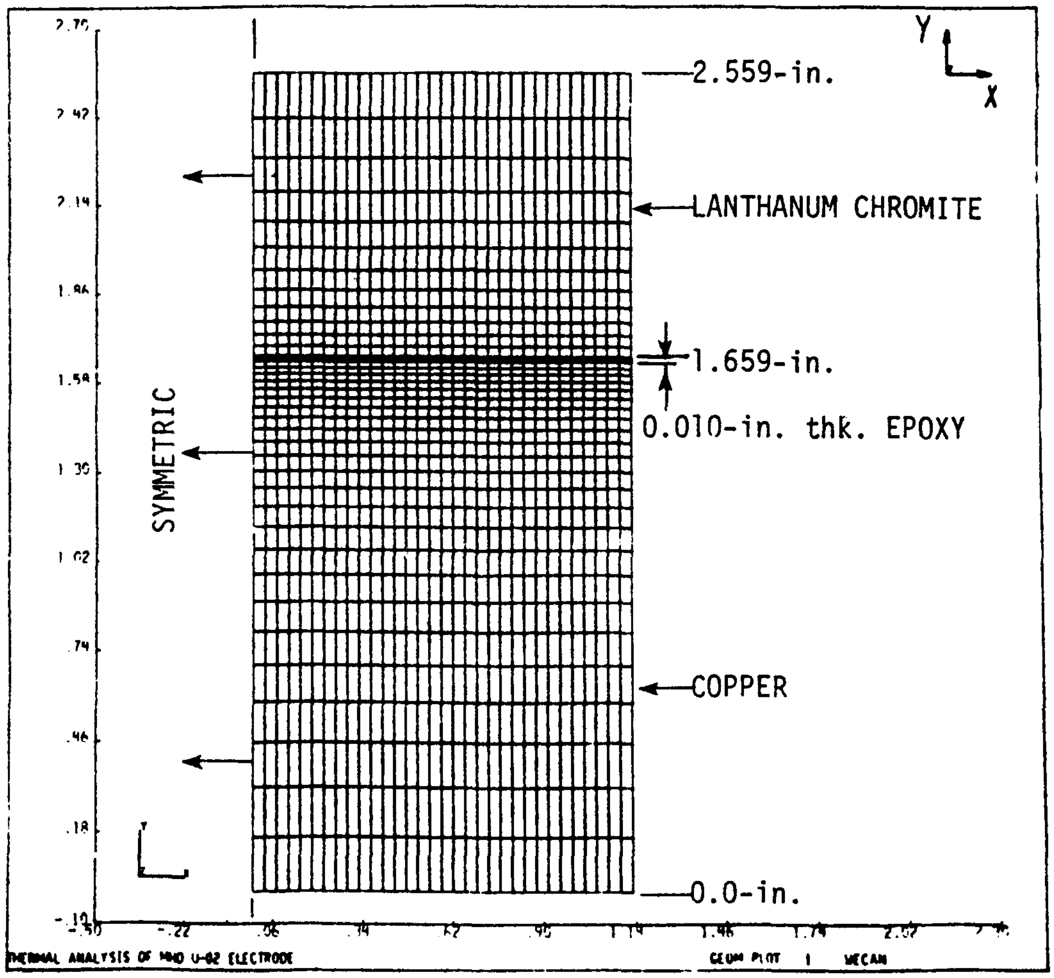

Figure 31. Finite Element Model of the Lanthanum Chromite - Epoxy Bonded Electrode

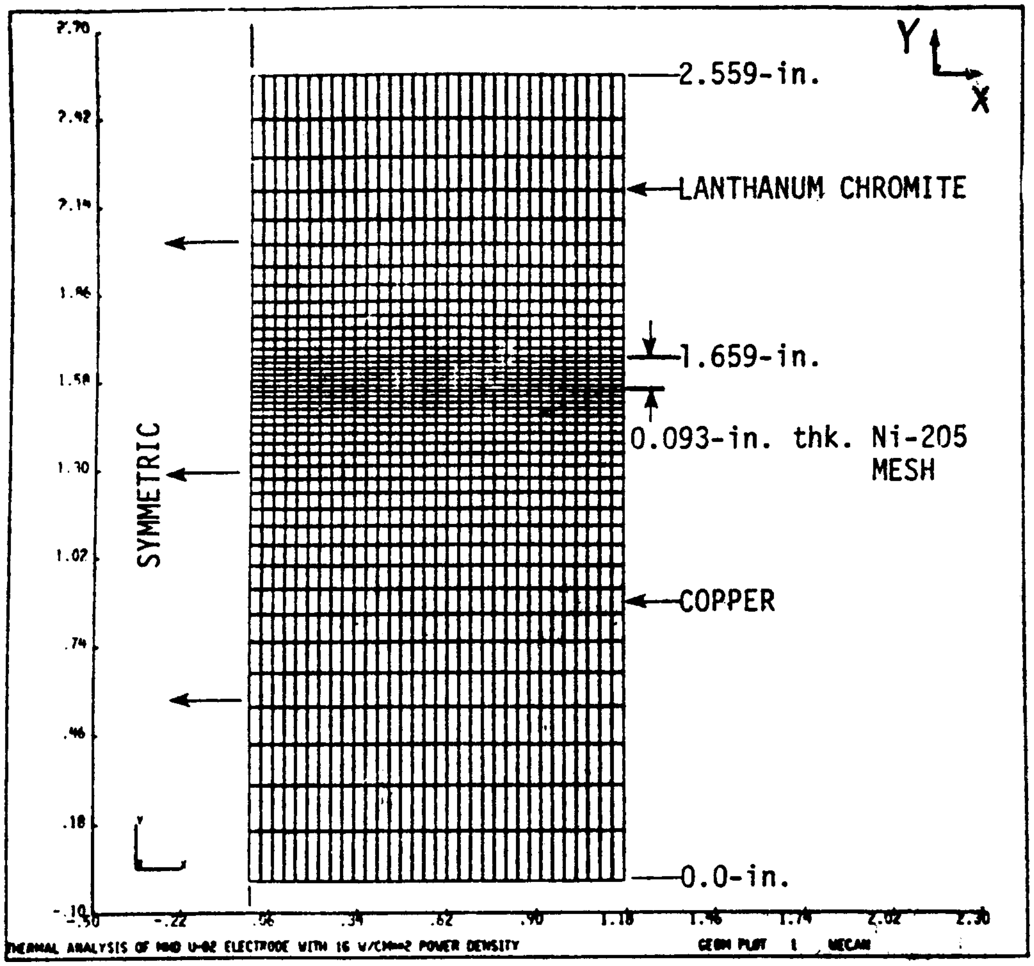

Figure 32. Finite Element Model of the Lanthanum Chromite - Ni-205 Electrode

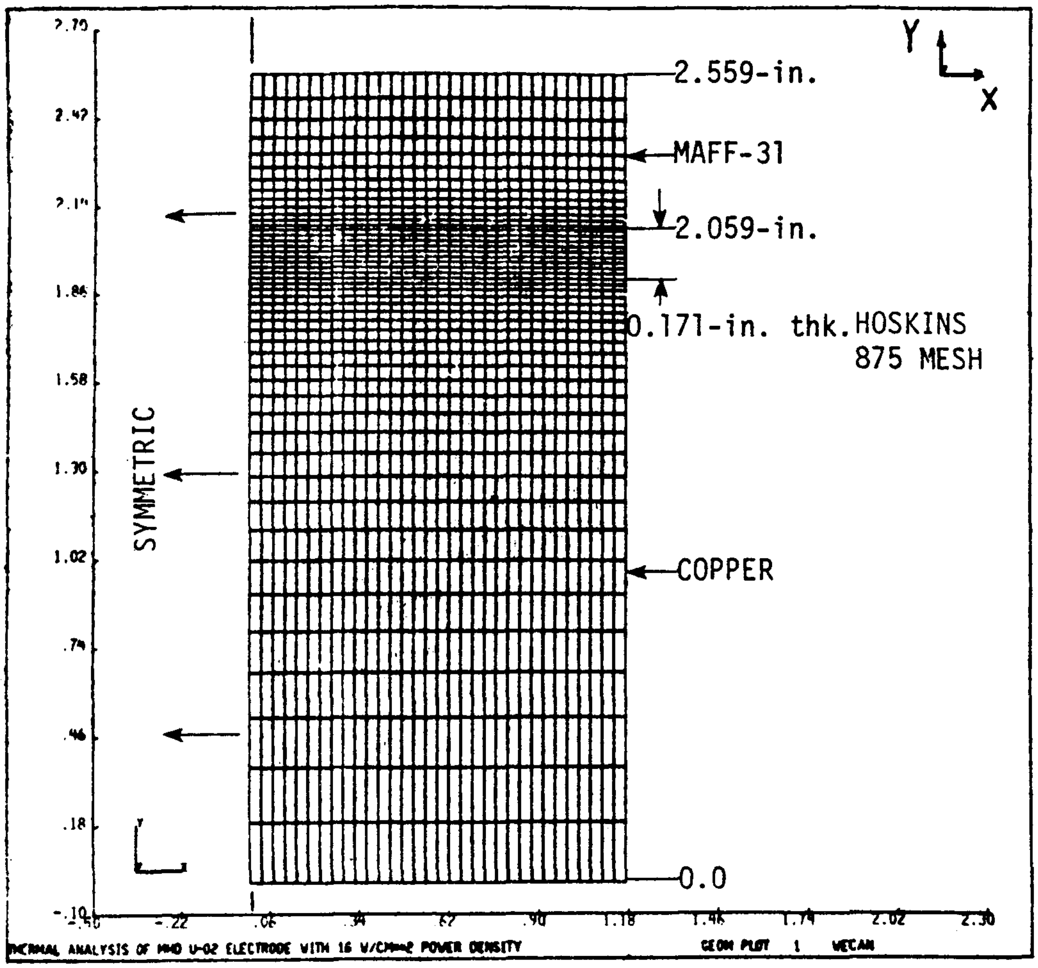

Figure 33. Finite Element Model of the MAFF-31 - Hoskins 875 Bonded Electrode

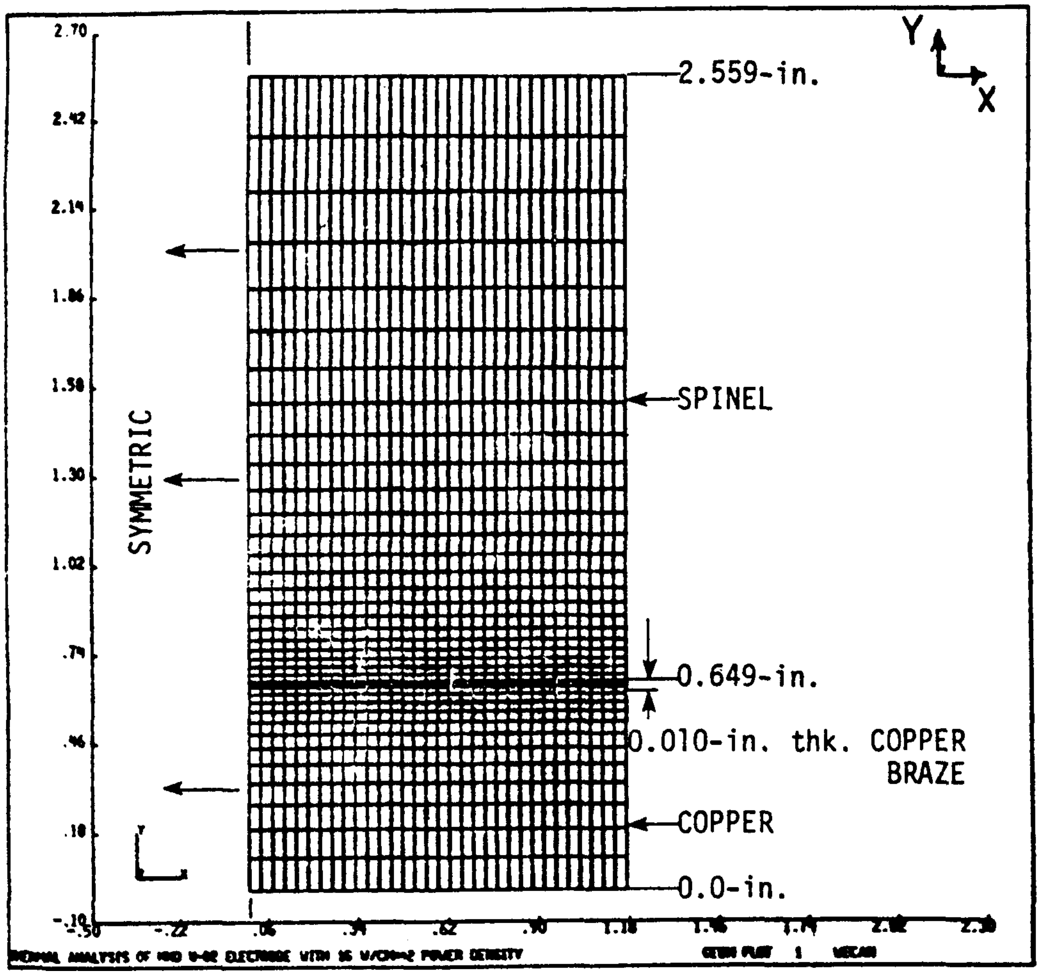

Figure 34. Finite Element Model of the Spinel Insulator Brazed to the Lanthanum Chromite - Epoxy Bonded Electrode

A number of variations of the basic electrode designs were evaluated in this study. One of these was to introduce cuts through the ceramic to relieve the thermal stress. For example, if the cuts were made through the Lanthanum Chromite and terminate at the surface of the Epoxy bond, the computer model for a three segmented electrode appeared as in Figure 35. If the cuts were made through the Epoxy and slightly into the copper cooling block, the computer model appeared as in Figure 36 for a six segmented design. For the analysis of this six segmented electrode design, the x-displacements on the symmetric boundary were only fixed for the cooling block nodes. An insulator design variation analyzed was that shown in Figure 37 where five vertical cuts were introduced at the base of a traction free electrode. A comparison of Figures 37 and 31 indicate that the insulator cuts terminate just below the Epoxy bond.

Summary of Results

A thermal analysis was conducted for each electrode design using a three-dimensional computer model with appropriate boundary conditions. Section 4.1.3.1 summarizes the thermal analysis and some of the results. These results were used as input for the thermal stress analysis in order to define the temperature gradients and to define the temperature dependent material properties. The four major cases examined here were:

(1) Lanthanum Chromite-Epoxy bonded electrode
(2) Lanthanum Chromite - Ni 205 mesh bonded electrode
(3) MAFF 31 - Hoskins 875 mesh bonded electrode
(4) Spinel insulator (Lanthanum Chromite-Epoxy bonded electrode)

The thermal gradients for the ceramics and insulator are shown in Figures 38 through 42. Joule heating was found to be a significant factor only for the MAFF-31 electrode as shown by comparing Figures 40 and 41. The only insulator analyzed in detail corresponded to that of the Lanthanum Chromite-Epoxy bonded electrode.

Some of the results from the stress analysis of the Lanthanum Chromite-Epoxy bonded electrode are shown in Figures 43 through 45 for the one segment design.

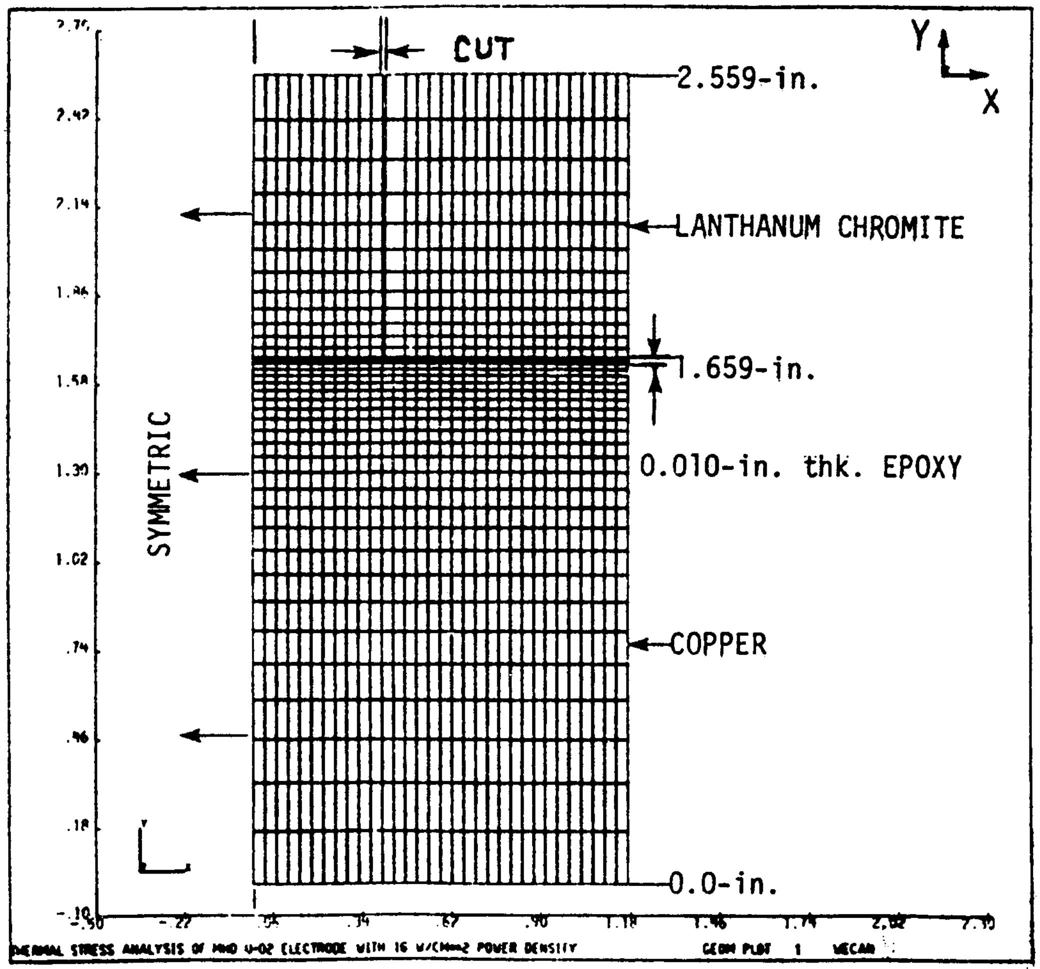

Figure 35. Finite Element Model of the Lanthanum Chromite - Epoxy Bonded Electrode (Three Segment Configuration)

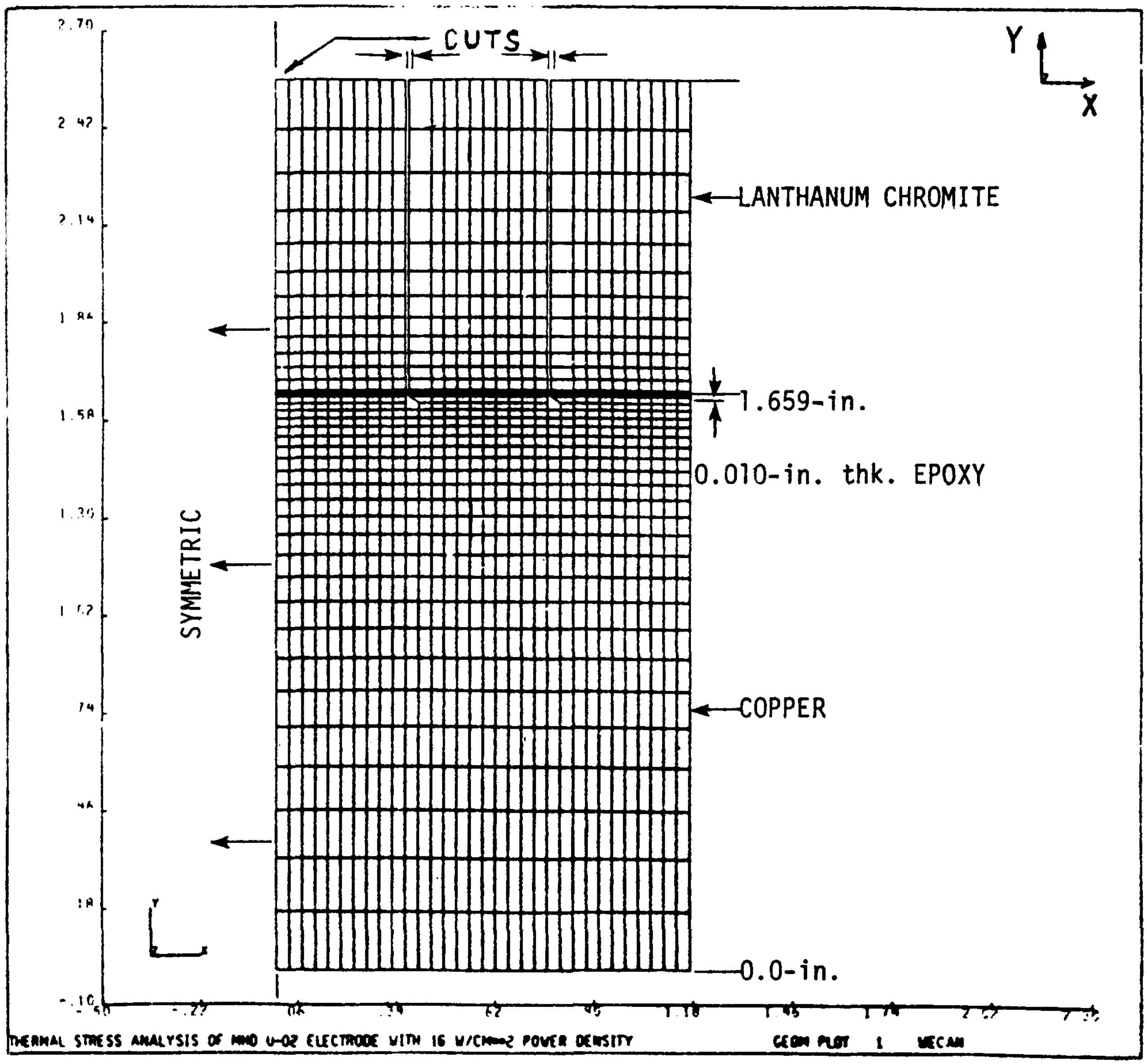

Figure 36. Finite Element Model of the Lanthanum Chromite - Epoxy Bonded Electrode (Six Segmented Configuration)

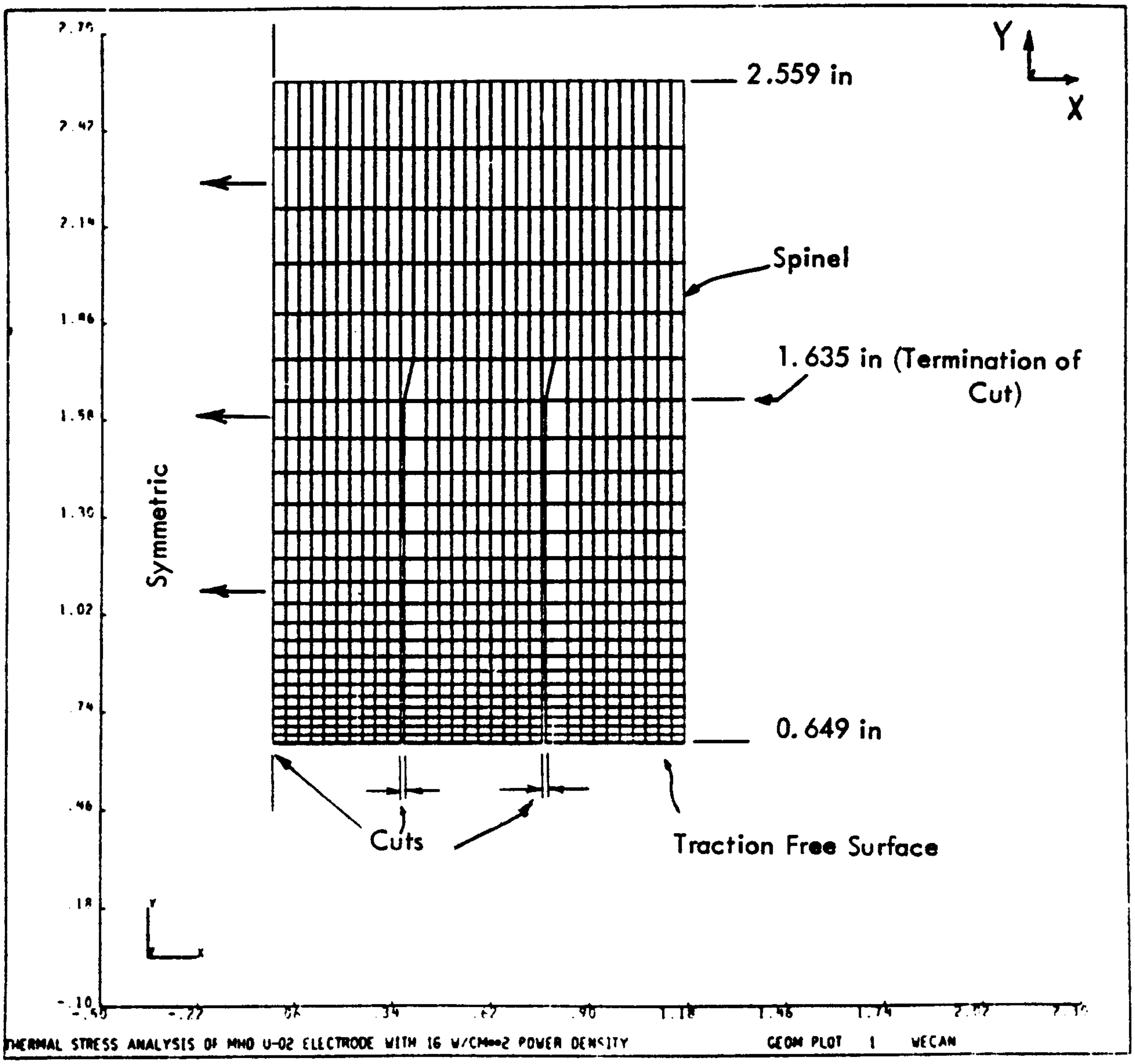

Figure 37. Finite Element Model of the Spinel Insulator in a Traction Free Condition with Five Cuts at the Base as Used with the Lanthanum Chromite - Epoxy Bonded Electrode.

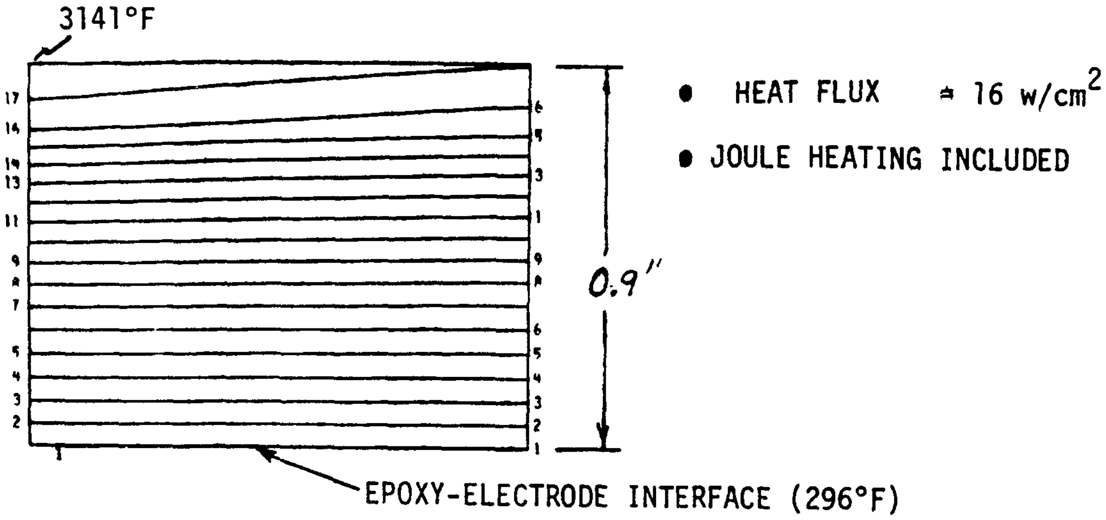

THERMAL PLOT FOR MHD U-O2 ELECTRODE TEMPERATURES PLOT 7 20CONPL

TEMPERATURES (°F) PLOT 7

1	300
2	450
3	600
4	750
5	900
6	1050
7	1200
8	1350
9	1500
10	1650
11	1800
12	1950
13	2100
14	2250
15	2400
16	2550
17	2700

Figure 38. Thermal Gradients for the Lanthanum Chromite - Epoxy Bonded Electrode

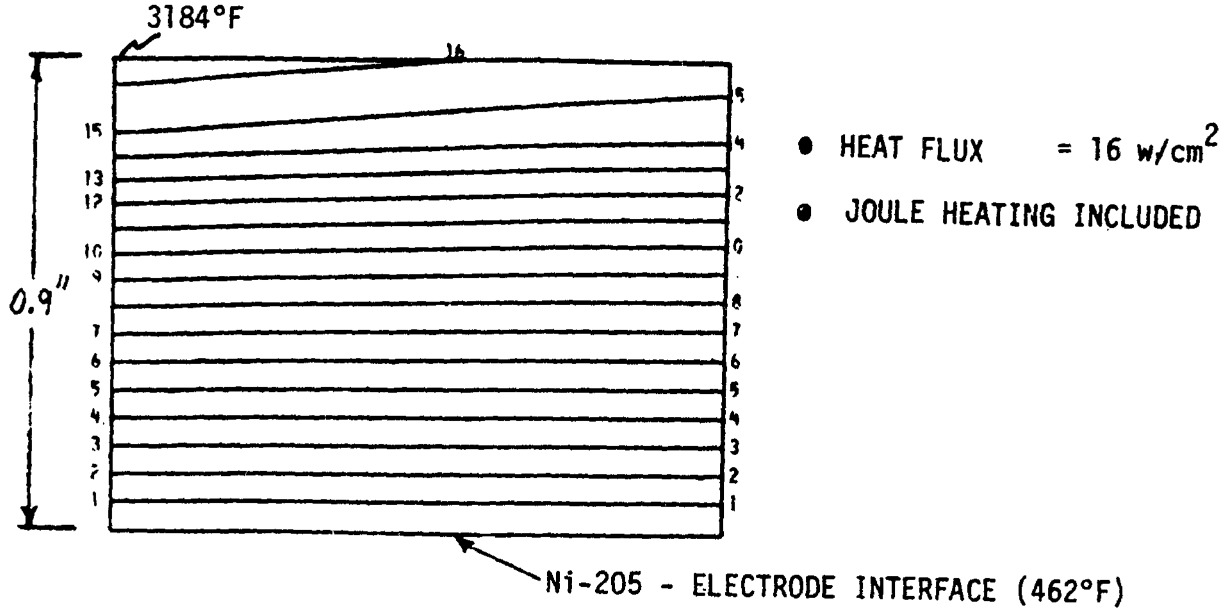

THERMAL PLOT FOR MHD U-02 ELECTRODE TEMPERATURES PLOT 8 20CONPL

TEMPERATURES (°F) PLOT 8

1	600
2	750
3	900
4	1050
5	1200
6	1350
7	1500
8	1650
9	1800
10	1950
11	2100
12	2250
13	2400
14	2550
15	2700
16	2850

Figure 39. Thermal Gradients for the Lanthanum Chromite - Ni-205 Bonded Electrode

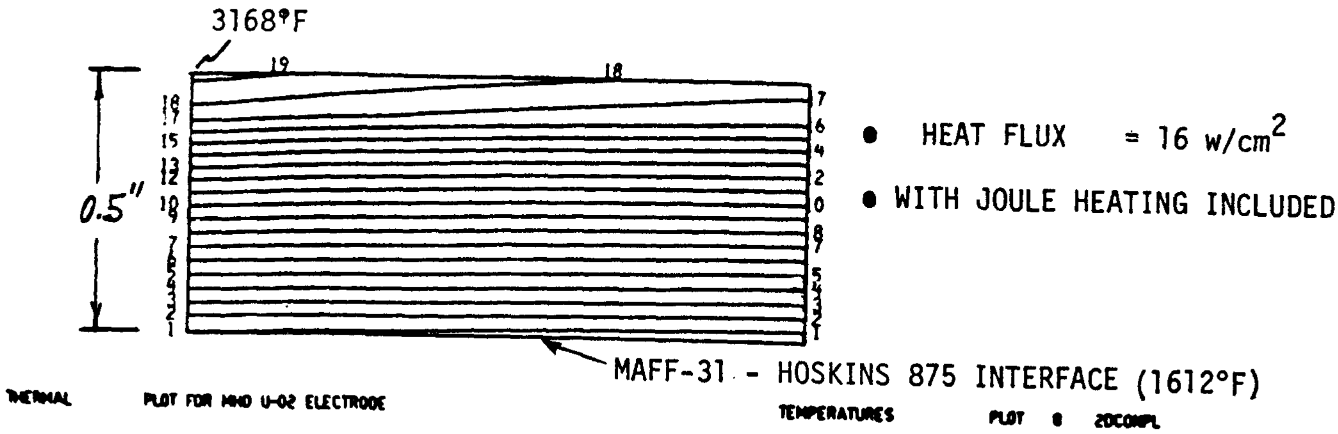

TEMPERATURES (°F) PLOT 8

1	1650
2	1725
3	1800
4	1875
5	1950
6	2025
7	2100
8	2175
9	2250
10	2325
11	2400
12	2475
13	2550
14	2625
15	2700
16	2775
17	2850
18	2925
19	3000

Figure 40. Thermal Gradients for the MAFF-31 - Hoskins 875 Bonded Electrode with Joule Heating

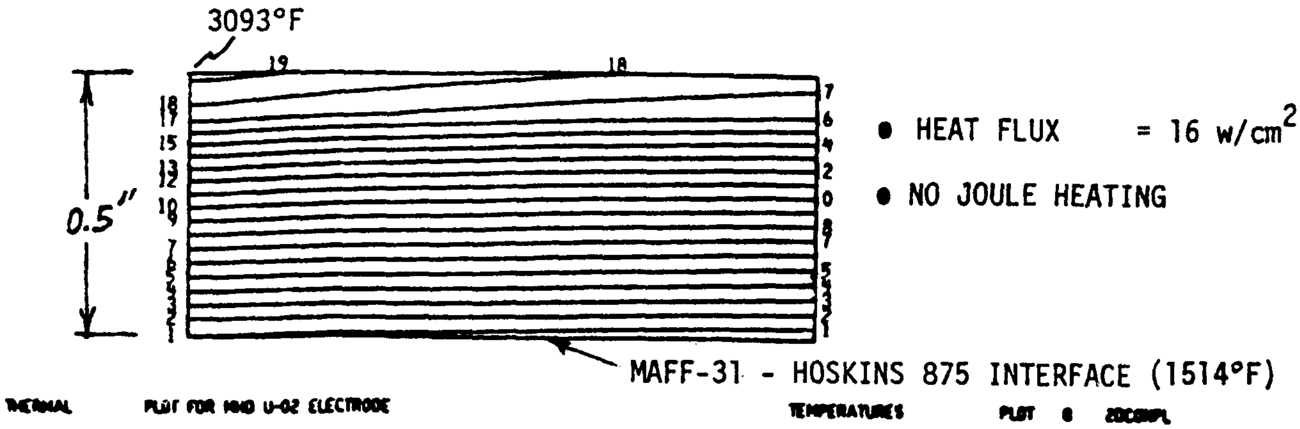

TEMPERATURES (°F) PLOT 8

1	1575
2	1650
3	1725
4	1800
5	1875
6	1950
7	2025
8	2100
9	2175
10	2250
11	2325
12	2400
13	2475
14	2550
15	2625
16	2700
17	2775
18	2850
19	2925

Figure 41. Thermal Gradients for the MAFF-31 - Hoskins 875 Bonded Electrode Without Joule Heating

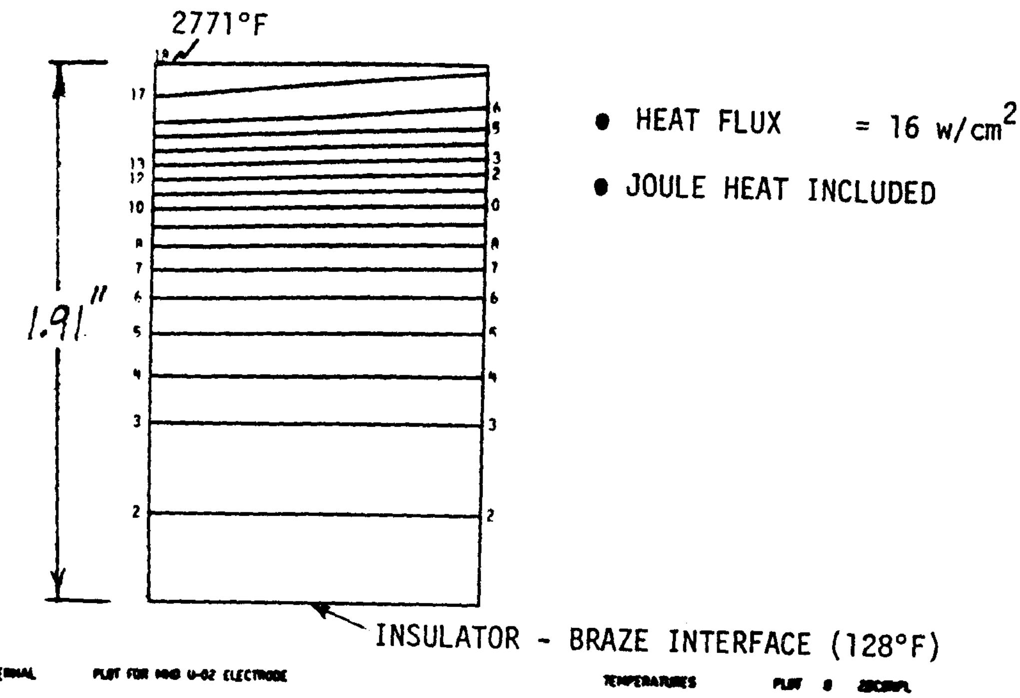

TEMPERATURES (°F) PLOT 8

1	0
2	150
3	300
4	450
5	600
6	750
7	900
8	1050
9	1200
10	1350
11	1500
12	1650
13	1800
14	1950
15	2100
16	2250
17	2400
18	2550

Figure 42. Thermal Gradients in the Spinel Insulator for the Lanthanum Chromite - Epoxy Bonded Electrode

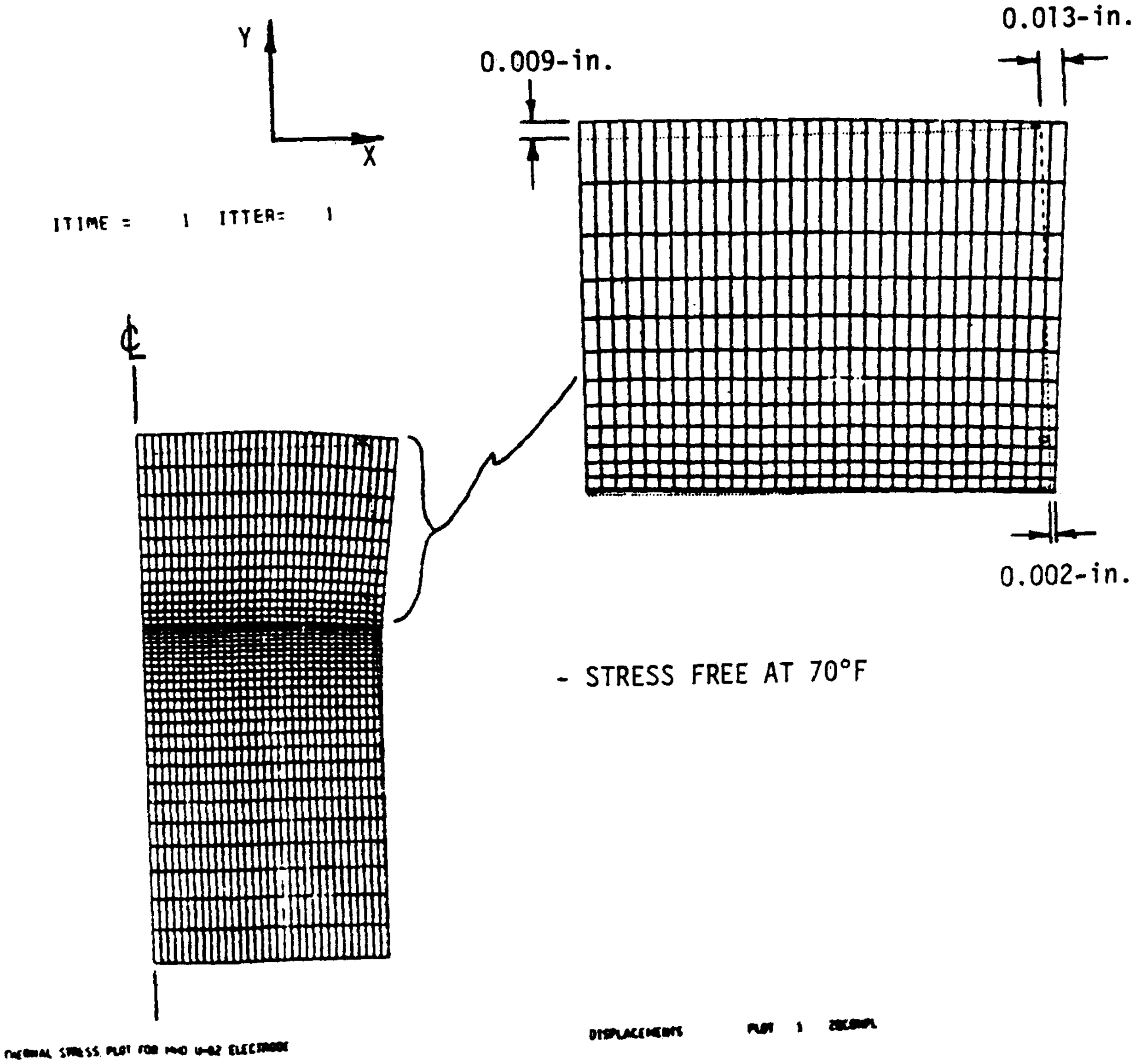

Figure 43. Lanthanum Chromite - Epoxy Bonded Electrode Displacement Plot (One Segment Design)

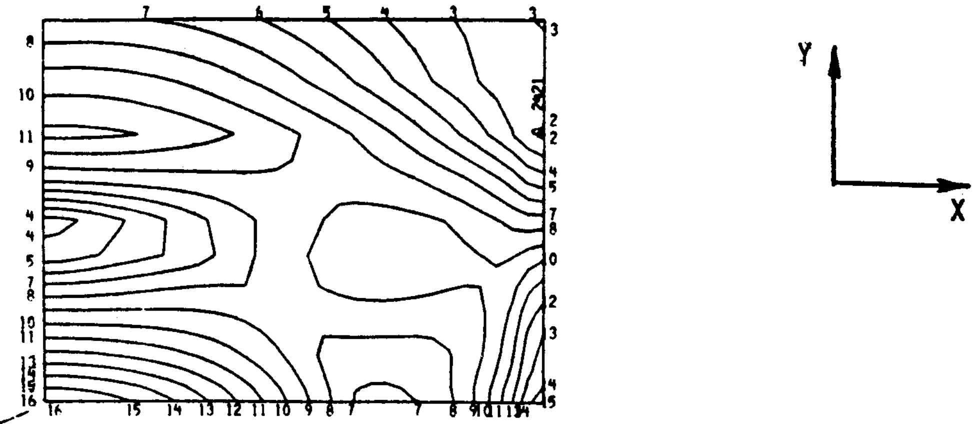

S_{int} (max) = 45,085 psi

THERMAL STRESS PLOT FOR MHD U-02 ELECTRODE   MAX STRESS INTNSY   PLOT 6   20COMPL

MAX STRESS INTNSY   PLOT 6

MINIMUM	2421 psi
1	0
2	3000
3	6000
4	9000
5	12000
6	15000
7	18000
8	21000
9	24000
10	27000
11	30000
12	33000
13	36000
14	39000
15	42000
16	45000
MAXIMUM	45085

- STRESS FREE AT 70°F

Figure 44. Lanthanum Chromite Maximum Stress Intensity of the Lanthanum Chromite - Epoxy Bonded Electrode (One Segment)

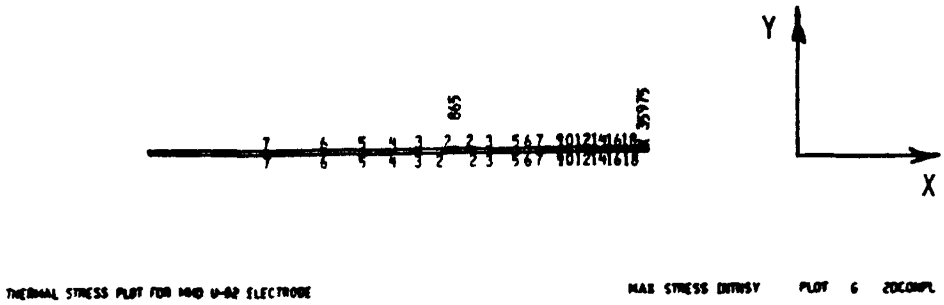

MAX STRESS INTNSY PLOT 6

MINIMUM	865 psi
1	0
2	2000
3	4000
4	6000
5	8000
6	10000
7	12000
8	14000
9	16000
10	18000
11	20000
12	22000
13	24000
14	26000
15	28000
16	30000
17	32000
18	34000
MAXIMUM	35975

- STRESS FREE AT 70°F

Figure 45. Epoxy Maximum Stress Intensity of the Lanthanum Chromite - Epoxy Bonded Electrode (One Segment Design)

Note that the electrode stress free temperature is 70^{O}F. The displacement plot of Figure 20 is not drawn to scale but is greatly magnified to show the distorted shape. The amount of distortion relative to the stress free shape is indicated at several points on the electrode. The maximum stress intensity shown in Figure 44 is defined as twice the magnitude of the maximum shearing stress. It represents a definition of stress which is frequently used to compare with an allowable level of normal stress in order to evaluate component structural integrity. The peak level of maximum stress intensity is shown to be about 45,100 psi in the ceramic. The temperature at this location is about 300^{O}F as indicated by Figure 38. The Epoxy maximum stress intensity was found to be about 36,000 psi as shown in Figure 45.

One attempt to lower the component stress levels of the one segment design was to investigate a three segmented ceramic (Figure 35). For this case the cuts terminate at the Lanthanum Chromite-Epoxy interface. The results of this analysis are shown in Figures 46 through 48. Also note that the stress free temperature here was 275^{O}F (135^{O}C) which represents the Epoxy bond cure temperature. The electrode deformation plot of Figure 46 indicates the relative displacement between adjacent electrode segments to be 0.010 inches. Although the distortion plot implies that segment interference would occur, in reality a 0.010 inch thick cut will accommodate the resulting relative displacement. The distortions as shown in the figure are again greatly magnified. The maximum stress intensity in the ceramic is shown to reach 22,000 psi in Figure 47. Figure 48 shows the maximum stress intensity of the Epoxy to be 9,560 psi.

A significant reductiion in ceramic stress level was obtained by extending the cuts through the Epoxy bond and slightly into the copper thereby reducing the stress concentration effect observed in Figure 47. For analysis purposes the cuts were assumed to penetrate the copper by about 0.04 inches though in reality the depth of penetration is probably not too important. Figures 49 and 50 indicate the resulting stress level in the ceramic and Epoxy. The most dramatic reduction in stress occurred in the ceramic which was lowered to 10,800 psi.

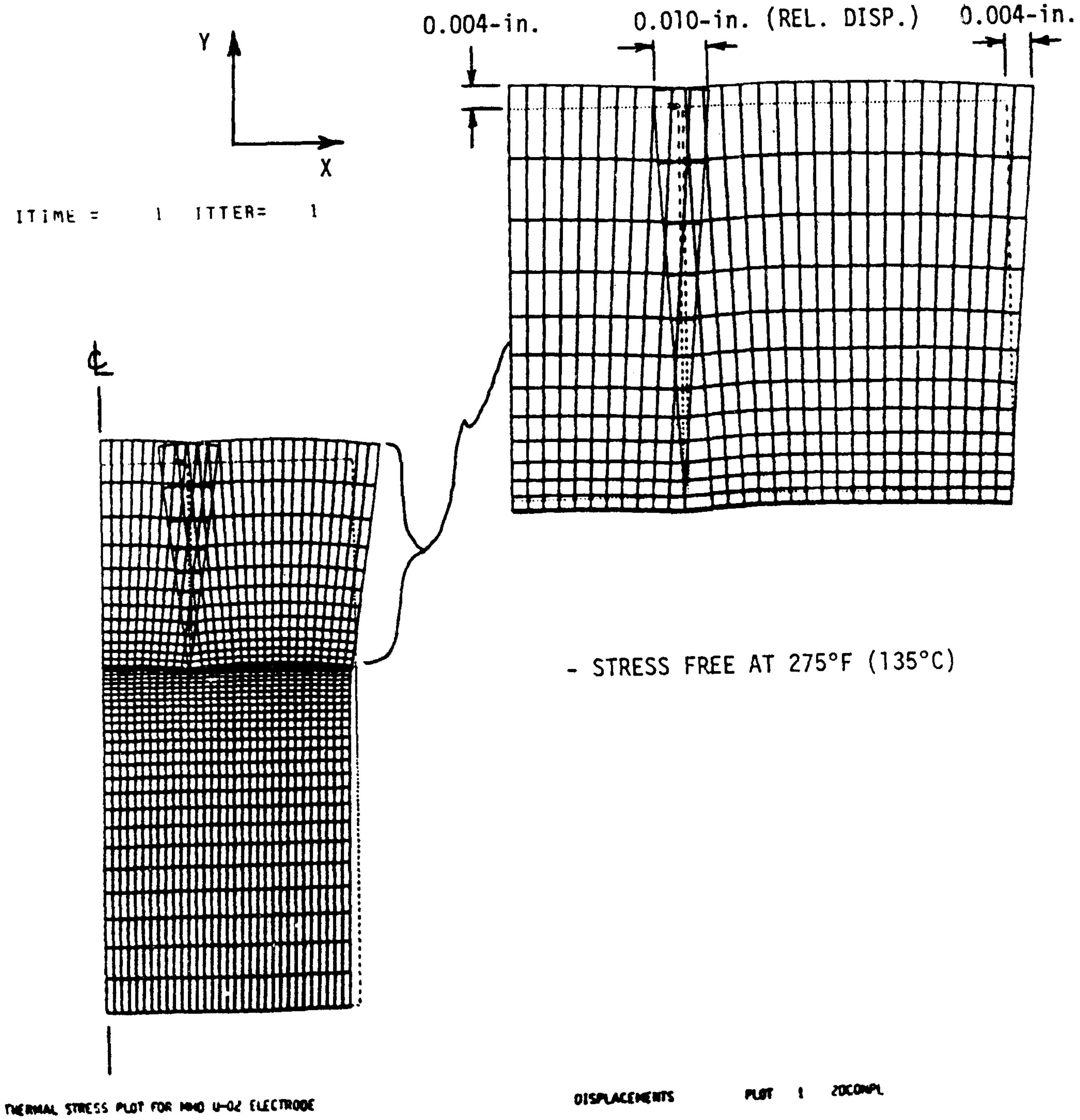

Figure 46. Lanthanum Chromite - Epoxy Bonded Electrode Displacement Plot (Three Segmented Design)

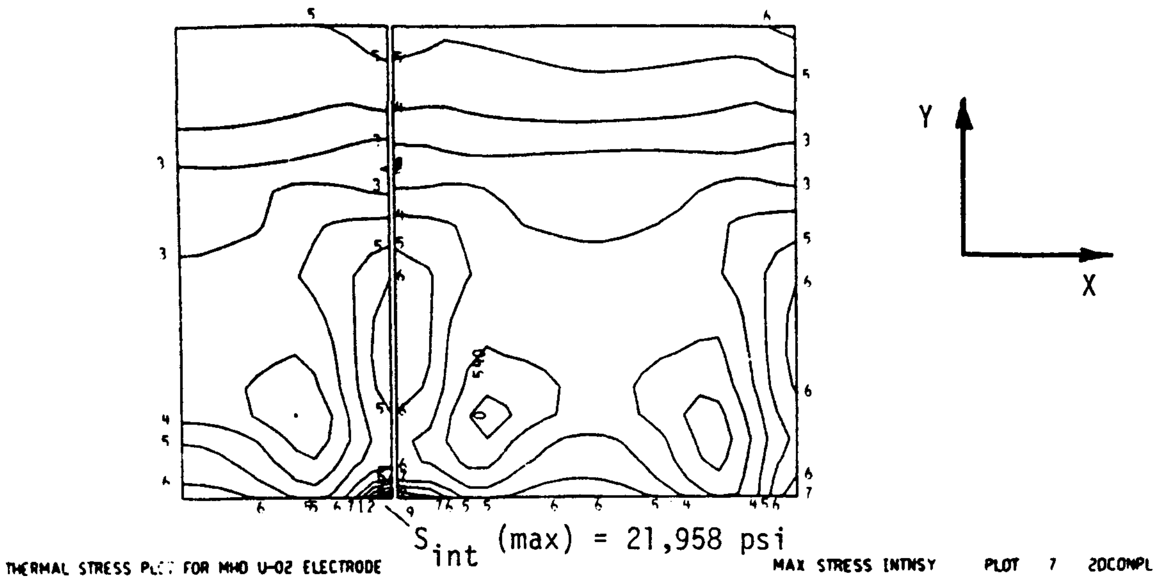

MAX STRESS INTNSY PLOT 7

MINIMUM	540 psi
1	0
2	1500
3	3000
4	4500
5	6000
6	7500
7	9000
8	10500
9	12000
10	13500
11	15000
12	16500
13	18000
14	19500
15	21000
MAXIMUM	21958

- STRESS FREE AT 275°F (135°C)

Figure 47. Lanthanum Chromite Maximum Stress Intensity of the Lanthanum Chromite - Epoxy Bonded Electrode (Three Segment Design)

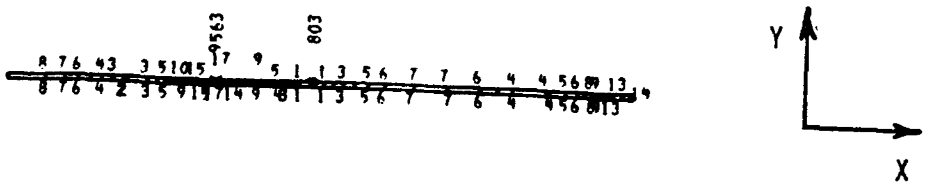

THERMAL STRESS PLOT FOR MHD U-02 ELECTRODE

MAX STRESS INTNSY PLOT 7 2DCONPL

MAX STRESS INTNSY PLOT 7

- STRESS FREE AT 275°F (135°C)

MINIMUM	803 psi
1	1000
2	1500
3	2000
4	2500
5	3000
6	3500
7	4000
8	4500
9	5000
10	5500
11	6000
12	6500
13	7000
14	7500
15	8000
16	8500
17	9000
18	9500
MAXIMUM	9563

Figure 48. Epoxy Maximum Stress Intensity for the Lanthanum Chromite - Epoxy Bonded Electrode (Three Segmented Design)

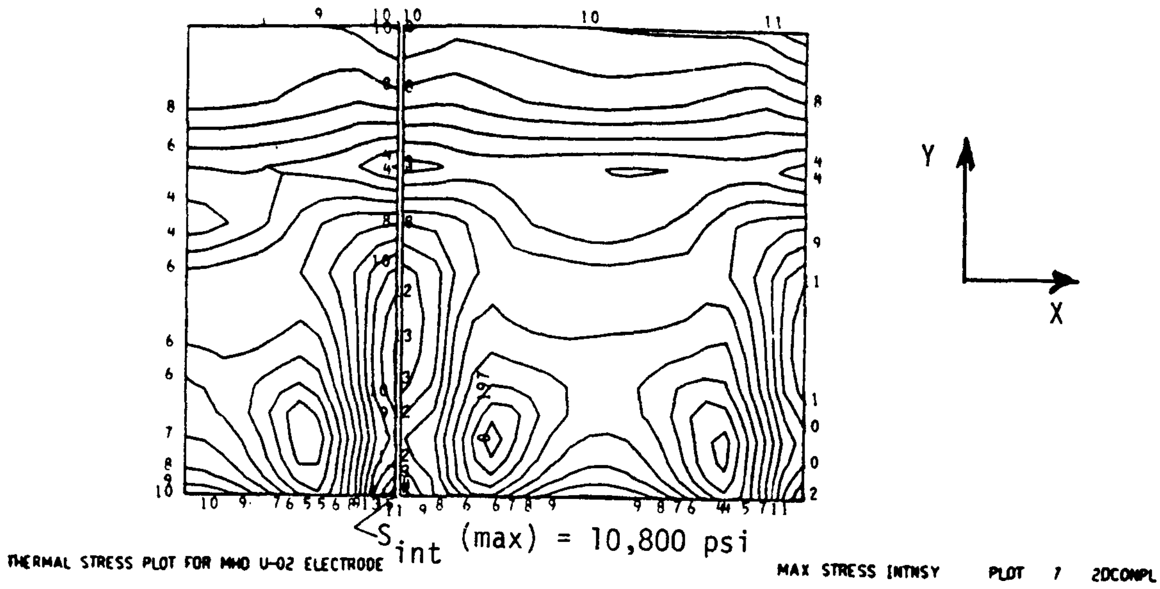

MAX STRESS INTNSY PLOT 7

MINIMUM	197 psi	
1	0	
2	750	
3	1500	- STRESS FREE AT 275°F (135°C)
4	2250	
5	3000	
6	3750	
7	4500	
8	5250	
9	6000	
10	6750	
11	7500	
12	8250	
13	9000	
14	9750	
15	10500	
MAXIMUM	10762	

Figure 49. Lanthanum Chromite Maximum Stress Intensity for the Lanthanum Chromite - Epoxy Bonded Electrode (Three Segment Electrode with Cuts Extending into Copper)

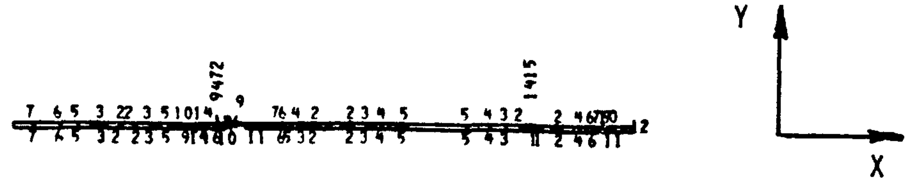

THERMAL STRESS PLOT FOR MHD U-02 ELECTRODE

MAX STRESS INTNSY PLOT 7 2DCONPL

MAX STRESS INTNSY PLOT 7

MINIMUM	1415 psi
1	1500
2	2000
3	2500
4	3000
5	3500
6	4000
7	4500
8	5000
9	5500
10	6000
11	6500
12	7000
13	7500
14	8000
15	8500
16	9000
MAXIMUM	9472

- STRESS FREE AT 275°F (135°C)

Figure 50. Epoxy Maximum Stress Intensity for the Lanthanum Chromite - Epoxy Bonded Electrode (Three Segment Design with Cuts Extending into Copper)

A further reduction in the component stress level was observed when the cuts were extended into the copper for a six segmented electrode (Figure 26). The potential interference of 0.005 inches between adjacent electrode segments is shown in Figure 51 for this design case and could easily be eliminated by making the cuts 0.005 inches thick. The stress reduction is most evident at the cold face of the ceramic (Figure 52) and the Epoxy bond (Figure 53). A comparison of Figures 52 and 49 demonstrates that the ceramic hot face stress hasn't changed significantly. The maximum stress intensity for the six segmented design occurs at the hot face (1487°C) and is equal to 7,840 psi. A significant reduction in Epoxy maximum stress intensity was observed for this design since it was computed to be 2,860 psi.

The analyzed design concepts for the Lanthanum Chromite-Epoxy bonded electrodes are best compared and evaluated when viewed in tabular form. Table 26 presents these results together with those of several traction free electrodes which were analyzed to compute the absolute minimum obtainable stress. The progressive reduction in operating stress level for this electrode by cutting the ceramic into three segments, extending the cuts into the cooling block, and cutting the ceramic into six segments is shown in the table. A comparison of these computed component stresses with the material strength data in Table 30 indicates the likelihood of electrode successful performance can be maximized by using a six segmented electrode with the cuts extending slightly into the copper.

The Lanthanum Chromite - Ni 205 mesh bonded electrode analysis results are shown in Table 27. The most significant reduction in bond stress level was achieved by extending the cuts into the copper for the three or six segmented ceramic. This is an important modification since bond stress is undoubtedly the most critical factor for this electrode. As with the Epoxy design, the three segmented Ni 205 mesh design should have cuts 0.010 inches thick and the six segmented design should have cuts 0.005 inches thick in order to preclude interference between adjacent segments.

Table 27 also contains the analysis results of the graded electrode analysis for the Lanthanum Chromite - Ni 205 mesh bonded electrode. For this analysis

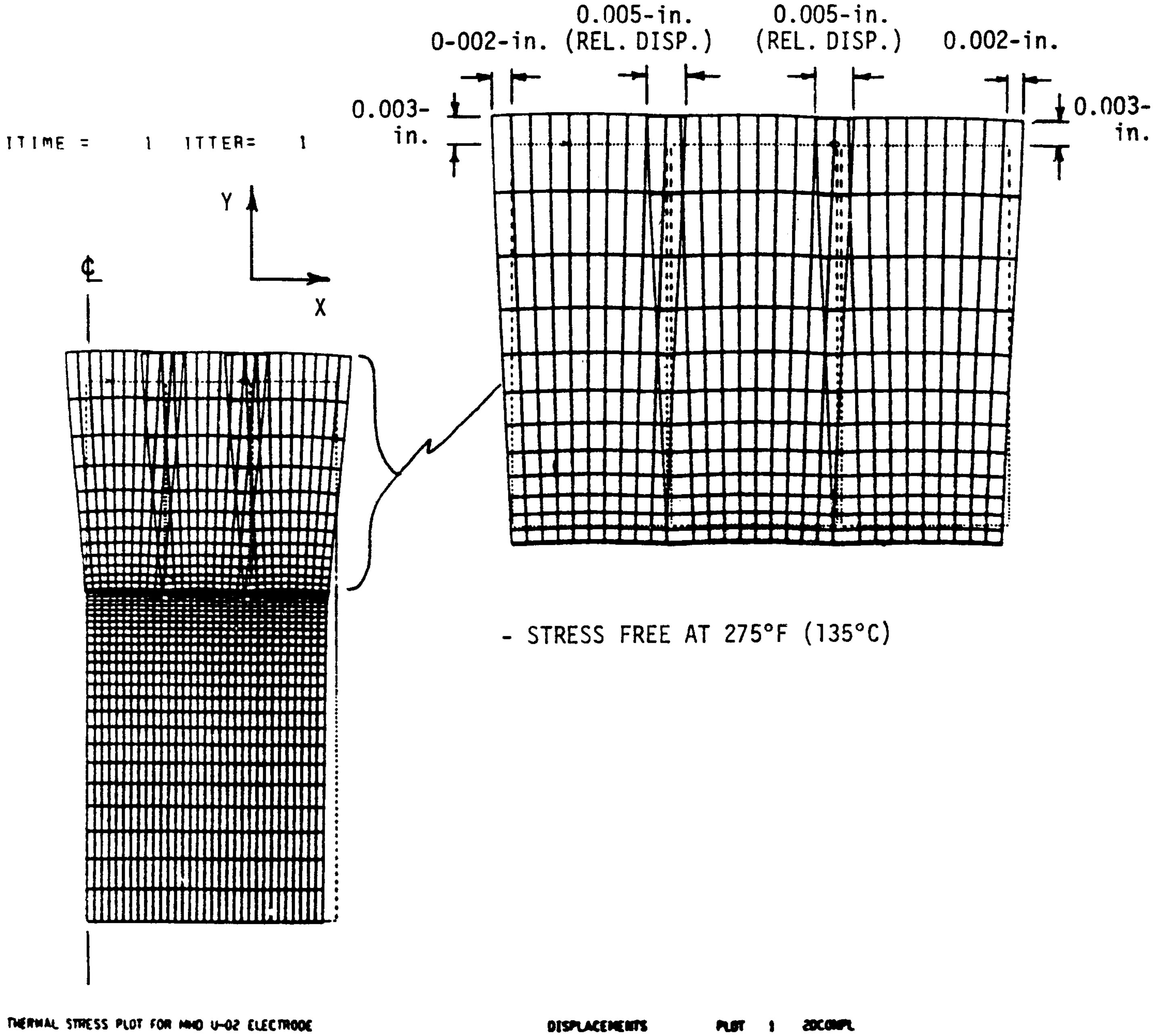

Figure 51. Lanthanum Chromite - Epoxy Bonded Electrode Displacement Plot (Six Segment Design with Cuts Extending into Copper)

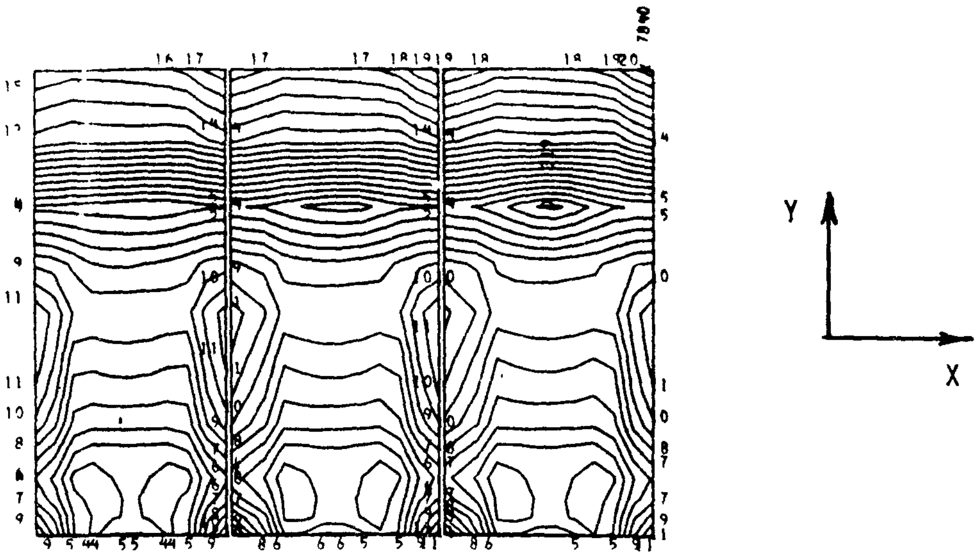

THERMAL STRESS PLOT FOR MHD U-02 ELECTRODE   MAX STRESS INTNSY   PLOT 7   2DCONPL

MAX STRESS INTNSY   PLOT 7

MINIMUM	319 psi
1	0
2	400
3	800
4	1200
5	1600
6	2000
7	2400
8	2800
9	3200
10	3600
11	4000
12	4400
13	4800
14	5200
15	5600
16	6000
17	6400
18	6800
19	7200
20	7600
MAXIMUM	7840

- STRESS FREE AT 275°F (135°C)

Figure 52. Lanthanum Chromite Maximum Stress Intensity for the Lanthanum Chromite - Epoxy Bonded Electrode (Six Segment Design with Cuts Extending into Copper)

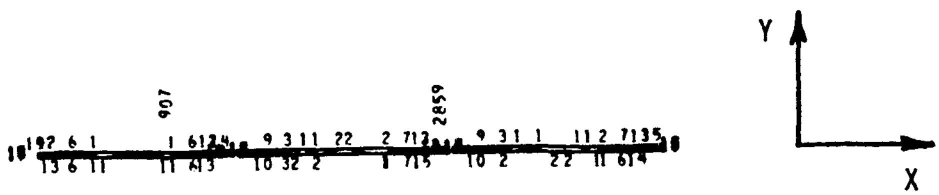

THERMAL, STRESS PLOT FOR MHD U-02 ELECTRODE

MAX STRESS INTNSY PLOT 7 2DCOMPL

MAX STRESS INTNSY PLOT 7

MINIMUM	907 psi
1	1000
2	1100
3	1200
4	1300
5	1400
6	1500
7	1600
8	1700
9	1800
10	1900
11	2000
12	2100
13	2200
14	2300
15	2400
16	2500
17	2600
18	2700
19	2800
MAXIMUM	2859

- STRESS FREE AT 275°F (135°C)

Figure 53. Epoxy Maximum Stress Intensity for the Lanthanum Chromite - Epoxy Bonded Electrode (Six Segment Design with Cuts Extending into the Copper)

TABLE 26

MAXIMUM STRESS INTENSITY [2 S_{shear}(max)] OF THE LANTHANUM CHROMITE ELECTRODE BONDED WITH 0.010-in. THICK EPOXY. JOULE HEATING IS INCLUDED AND THE HEAT FLUX IS EQUAL TO 16 w/cm^2.

ANALYSIS MODEL	S_{int} (psi)	STRESS FREE TEMPERATURE (°F)	COMPUTER RUN
*One Segment Bonded	S_{LaCrO_3} = 45,100 (301°F) S_{Epoxy} = 36,000 S_{cu} = 37,600	70	AN2GDZY AND AN3GD5Y
One Segment Traction Free	S_{LaCrO_3} = 8,050 (284°F)	70	AN7GDUO
Two Segments Traction Free	S_{LaCrO_3} = 7,560 (283°F)	70	AN9GDCX
Three Segments Traction Free	S_{LaCrO_3} = 6,810 (1350°F)	70	AN1GDIG
Six Segments Traction Free	S_{LaCrO_3} = 6,250 (2710°F)	70	AN1GDMZ
Three Segments Bonded	S_{LaCrO_3} = 19,900 (284°F) S_{Epoxy} = 8,280 S_{cu} = 7,700	70	AN3GD6G and AN9GD86
*Three Segments Bonded	S_{LaCrO_3} = 22,000 (284°F) S_{Epoxy} = 9,560 S_{cu} = 9,910	275 (135°C)	AN8GD39

*Plots included in report.

TABLE 26 (Continued)

ANALYSIS MODEL	S_{int} (psi)	STRESS FREE TEMPERATURE (°F)	COMPUTER RUN
Three Segments Bonded; Cuts Extend Into Copper	S_{LaCrO_3} = 13,700 (284°F) S_{Bond} = 8,850 S_x(Bond) = -3,430 S_y(Bond) = +4,550 S_{xy}(Bond) = 1,300 S_{cu} = 8,100	70	AN3GDAY
*Three Segments Bonded; Cuts Extend Into Copper	S_{LaCrO_3} = 10,800 (284°F) S_{Bond} = 9,470 S_x(Bond) = -2,410 S_y(Bond) = +4,620 S_{xy}(Bond) = 2,190 S_{cu} = 10,900	275 (135°C)	AN5GDPO
Six Segments Bonded; Cuts Extend Into Copper	S_{LaCrO_3} = 6,760 (284°F) S_{Bond} = 2,230 S_x(Bond) = -1,460 S_y(Bond) = +1,130 S_{xy}(Bond) = 573 S_{cu} = 2,310	70	AN5GD08
*Six Segments Bonded; Cuts Extend Into Copper	S_{LaCrO_3} = 7,840 (2710°F) S_{Bond} = 2,860 S_x(Bond) = +724 S_y(Bond) = +1,150 S_{xy}(Bond) = 1,150 S_{cu} = 3,700	275 (135°C)	AN4GDIQ and AN6GDUJ

*Plots included in report.

TABLE 27

MAXIMUM STRESS INTENSITY [2 S_{shear}(max)] OF THE LANTHANUM CHROMITE ELECTRODE BONDED WITH 0.093-in. THICK Ni-205 MESH. JOULE HEATING IS INCLUDED. HEAT FLUX = 16 w/cm^2.

ANALYSIS MODEL	S_{int} (psi)	STRESS FREE TEMPERATURE (°F)	COMPUTER RUN
One Segment Bonded	S_{LaCrO_3} = 5,520 (464°F) S_{Bond} = 7,680 S_{cu} = 2,610	70	AN4GD32
Three Segments Bonded	S_{LaCrO_3} = 5,180 (2794°F) S_{Bond} = 3,660 S_{cu} = 1,770	70	AN8GDH9
Three Segments Bonded	S_{LaCrO_3} = 7,220 (467°F) S_{Bond} = 3,080 S_{cu} = 1,420	932 (500°C)	AN7GD4B
Three Segments Bonded; Cuts Extend Into Copper	S_{LaCrO_3} = 5,180 (2794°F) S_{Bond} = 607 S_x(Bond) = -565 S_y(Bond) = +41 S_{xy}(Bond) = 94 S_{cu} = 220	70	AN1GDDN
Three Segments Bonded; Cuts Extend Into Copper	S_{LaCrO_3} = 6,280 (2794°F) S_{Bond} = 617 S_x(Bond) = +648 S_y(Bond) = +72 S_{xy}(Bond) = 216 S_{cu} = 653	932 (500°C)	AN1GDPC

TABLE 27(Continued)

ANALYSIS MODEL	S_{int} (psi)	STRESS FREE TEMPERATURE (°F)	COMPUTER RUN
Six Segments Bonded; Cuts Extend Into Copper	S_{LaCrO_3} = 4,870 (2794°F) S_{Bond} = 465 S_x(Bond) = -455 S_y(Bond) = +10.7 S_{xy}(Bond) = 69.4 S_{cu} = 220	70	AN4GD07
One Segment Bonded; With Graded Electrode Properties	S_{LaCrO_3} = 11,800 (469°F) S_{Bond} = 780 S_x(Bond) = +148 S_y(Bond) = +295 S_{xy}(Bond) = 197 S_{cu} = 970	70	AN9GD16
One Segment Bonded; With Graded Electrode Properties	S_{LaCrO_3} = 25,800 (469°F) S_{Bond} = 1,270 S_x(Bond) = -427 S_y(Bond) = +410 S_{xy}(Bond) = 449 S_{cu} = 1,830	932 (500°C)	AN2GD9K

the ceramic was assumed to have a thermal expansion coefficient which varies between that for Ni at the bond interface to that for Lanthanum Chromite at the ceramic hot face. In other words, the first row of finite elements in the ceramic were assigned the thermal expansion coefficient of Ni 205 and the last row of finite elements in the ceramic (hot face) were assigned the thermal expansion coefficient of Lanthanum Chromite. The thermal expansion coefficient assigned to the elements located between these two rows was obtained by incrementing between these two extremes. The analysis results from the graded electrode are presented in Table 27 for the one segmented design. A comparison with the analysis results for the nongraded electrode, which are also shown in Table 27, shows a reduction in bond stress from 7,680 psi to 780 psi by using a graded electrode. A significant increase in Lanthanum Chromite stress was also observed however. In light of achievements made by using a three or six segmented nongraded ceramic, it would seem that using a graded ceramic might only be advantageous from a fabrication standpoint; i.e., in obtaining a better Ni-205 mesh to ceramic braze.

Analysis results of the MAFF 31 - Hoskins 875 bonded electrode are shown in Table 28. The effect of including Joule heating in the analysis of the MAFF 31 electrode is shown in Table 28 to be a 10% or less increase in component stress level. The desired reduction in component stress level was not obtained by using a three segmented electrode instead of a one segment configuration. Upon analysis of the elevated stress free temperature case of 1436^{0}F (780^{0}C), the component stress levels were observed to significantly increase. Because of this, it is felt that the MAFF 31 electrode represents a less desirable selection than Lanthanum Chromite bonded with either the Epoxy or the Ni-205 mesh.

The analysis results for the Spinel insulator of the Lanthanum Chromite-Epoxy bonded are shown in Table 29. The stress level of 64,100 psi for the traction free case was felt to be excessive. One way to reduce this stress level would be to introduce five cuts at the base of the insulator as shown in Figure 37. The cuts could extend into the Spinel to an elevation that is just below that

TABLE 28

MAXIMUM STRESS INTENSITY [2 S_{shear}(max)] OF THE MAFF-31 ELECTRODE BONDED WITH 0.171-in. THICK HOSKINS 875 MESH. JOULE HEATING IS INCLUDED (EXCEPT WHERE NOTED). HEAT FLUX IS EQUAL TO 16 w/cm^2.

ANALYSIS MODEL	S_{int} (psi)	STRESS FREE TEMPERATURE (°F)	COMPUTER RUN
One Segment Bonded	S_{MAFF} = 8,470 (1647°F) S_{Bond} = 4,960 S_x(Bond) = -4,530 S_y(Bond) = +581 S_{xy}(Bond) = 1,120 S_{cu} = 3610	70	AN6GDBZ
Three Segments Bonded	S_{MAFF} = 8,300 (1638°F) S_{Bond} = 8,480 S_x(Bond) = -8,460 S_y(Bond) = +493 S_{xy}(Bond) = 1,150 S_{cu} = 3,160	70	AN2GD4K
Three Segments Bonded	S_{MAFF} = 39,200 (1638°F) S_{Bond} = 14,600 S_x(Bond) = -14,300 S_y(Bond) = +1,400 S_{xy}(Bond) = 2,880 S_{cu} = 9,680	1436 (780°C)	AN9GD94
Three Segments Bonded; Without Joule Heating	S_{MAFF} = 8,080 (1548°F) S_{Bond} = 7,790 S_x(Bond) = -7,770 S_y(Bond) = +448 S_{xy}(Bond) = 1,070 S_{cu} = 2,950	70	AN1GD72

TABLE 29

MAXIMUM STRESS INTENSITY [2 S_{shear}(max)] OF THE SPINEL INSULATOR FOR THE LANTHANUM CHROMITE - EPOXY BONDED ELECTRODE. JOULE HEATING IS INCLUDED AND THE HEAT FLUX IS EQUAL TO 16 w/cm^2.

ANALYSIS MODEL	S_{int} (psi)	STRESS FREE TEMPERATURE (°F)	COMPUTER RUN
One Segment Bonded (Copper Braze)	S_{spinel} = 73,900 (573°F) S_{braze} = 26,900 S_{Cu} = 25,600	70	AN5GDXY and AN6GD6E
One Segment Traction Free	S_{spinel} = 64,100 (128°F)	70	AN7GDF3 and AN4GDDX
One Vertical Cut at Base (Traction Free)	S_{spinel} = 44,900 (700°F)	70	AN5GDEX
Five Vertical Cuts at Base (Traction Free)	S_{spinel} = 20,800 (1100°F)	70	AN6GDN5

of the electrode bond. In addition to this modification, it was found that if the cold face were kept traction free, then the maximum stress intensity of the Spinel could be held to 20,800 psi. Insulator displacement data has indicated that these cuts need only be 0.004 inches thick at the cold face.

Conclusions

The following conclusions and recommendations were drawn from the conducted analysis:

- The Lanthanum Chromite electrode when used with the Epoxy or Ni-205 mesh bonds produces more favorable component stress distributions than the MAFF 31 electrode bonded with Hoskins 875.
- The Lanthanum Chromite - Epoxy bonded electrode design should perform its best when the ceramic has been out into six segments. The component stress levels would be minimized when the cuts extend through the Epoxy and slightly into the copper cooling block. The cuts dividing the electrode into segements should be at least 0.005 inches thick at the hot face to avoid segment interference.
- The Lanthanum Chromite - Ni 205 mesh bonded electrode would perform its best when cut into either three or six segments. Again the cuts should extend slightly into the copper. The cut thickness should be 0.010 inches for a three segment design or 0.005 inches for a six segment design.
- Grading the electrode properties for the Lanthanum Chromite - Ni 205 mesh bonded design would probably only be advantageous from a fabrication standpoint, i.e., in securing a good mesh braze to the ceramic.
- Spinel insulator analyses have indicated the desirability of keeping the interface between the insulator and cooling block in a traction free condition. The introduction of five vertical cuts 0.004 inches thick at the insulator base, which terminate just below the elevation of the electrode bond, also has been found to produce favorable results. The insulator could then be restrained through holes drilled in the insulator by the two electrically insulated bolts which now hold a group of elecerodes together. If needed, the insulator surface could be metalized in the region of the insulator-cooling block interface to promote heat transfer.
- Generally speaking, the effect of bonding the electrode components at an elevated temperature was to increase the operating stress levels of the components. Occasionally a decrease in component operating stress level was observed however.
- Joule heating was an insignificant factor for the Lanthanum Chromite electrodes and resulted in a maximum increase in stress of about 10% for the MAFF 31 design.

4.1.4 Proof Test Modules

Component parts are becoming available for the fabrication of the first U-02 proof test channel (WESTF Test No. 37).

The electrodes for this assembly will consist of paired groups of three electrodes each. One group will be sintered MAFF-31 "Flexbed" prepared by General Electric Company. Another group will be MAFF-31 plasma sprayed onto "BRUNSBOND" (Hoskins alloy 875 mesh) by Technetics Division of the Brunswick Corporation to which Westinghouse will add the interelectrode insulation to complete the assembly. The third group will consist of Hafnia based electrodes provided by Argonne National Laboratory. Westinghouse will provide three pairs of lanthanum chromite "guard" electrodes to complete the channel compliant of twelve electrodes per wall. The fabrication and assembly of component parts is in progress.

5.0 REFERENCES

1. Development, Testing and Evaluation of MHD Materials and Component Designs, Quarterly Report, January to March, 1977, on DOE Contract #EX-76-C-01-2248, Westinghouse Electric Corporation, April, 1977.

2. H. P. R. Frederikse et. al., "Spinels for MHD-Electrodes," Proc. of 15th Symposium on Engineering Aspects of MHD, Philadelphia, Pennsylvania, May, 1976.

3. A. M. George et. al., "Improved Lanthanum Chromite Ceramics for High Temperature Electrodes in Open Cycle MHD Systems," Proc. of 15th Symposium on Engineering Aspects of MHD, Philadelphia, Pennsylvania, May, 1976.

4. H. U. Andersson et. al., "Electrical Conductivity, Volatilization, and Preparation of $LaCrO_3$-Based Oxides," Proc. of Conf. on High Temperature Sciences Related to Open Cycle, Coal Fired MHD Systems, Argonne National Laboratory, April, 1977.

5. V. G. Gordon, High Temperature Institute, Moscow, 1975.

6. J. Jacobs et. al., "The Electrical Conductivity and Thermal Expansion of Potential MHD Electrodes Based on Mixed Perovskites of Lanthanum Strontium Chromite and Strontium Zirconate," Proc. of Conf. on High Temperature Sciences Related to Open Cycle Coal Fired MHD Systems, Argonne National Laboratory, April, 1977.

7. H. K. Bowen et. al., "Design and Performance of High Temperature Ceramic Electrode Modules," Proc. of 16th Symposium on Engineering Aspects of MHD, Pittsburgh, Pennsylvania, May, 1977.

8. I. K. Keles, Development of Physical and Chemical Basis for MHD Generator Oxide Electrode Materials, Proc. of the 3rd US-USSR Colloquium on MHD Electric Power Generation, Moscow, October, 1976.

9. Development, Testing and Evaluation of MHD-Materials," NBS Quarterly Report (to Department of Energy), September, 1977.

V. CONCLUSIONS

TASK 3 - TESTING AND EVALUATION OF PROTOTYPE ELECTRODE

Completion of Tests 35 and 36 in WESTF has shown the facility to be a reliable and flexible facility for the testing of electrode materials and systems. A total of 42 hours of operation at design conditions, from seed-on to seed-off, were achieved during testing of cold wall and hot wall test assemblies under clean firing conditions.

As a result of laboratory screening tests on MAFF, electrochemical corrosion tests, further insight has been gained on the degradation mechanisms encountered under slagging conditions. Analysis of these tests shows that electrochemical corrosion is a result of two separate but interrelated reactions - reactions that occur within the slag due to the passage of current and reactions between the "reacted" slag and the electrode materials themselves.

TASK 4 - TECHNICAL SUPPORT FOR THE COOPERATIVE US-USSR PROGRAM ON MHD

A total of 11 electrode/insulator systems have been identified as candidates for the U-02 Phase III Module Test and will be tested in a series of three proof tests to be completed in WESTF under clean firing conditions. Seven of these are based on $LaCrO_3$, three upon MAFF and one upon a HfO_2-metal composite. MgO and $MgAl_2O_4$ are included as interelectrode insulators; $SrZrO_2$ was eliminated as a candidate insulator. Candidate attachments include "FLEXBED", Ni mesh, silver filled epoxy and Hoskins 875 BRUNSBOND. The above reflects the results of a U-02 Phase III Module Status Review Meeting held in mid-July and attended by DOE-MHD and other program participants.

Coupled thermal-structural analyses have identified a number of design optimizations to be reflected in the electrode systems incorporated in the proof test series. Due to limitations in the available material property data these efforts have been limited to elastic stress analyses.

☆U.S. GOVERNMENT PRINTING OFFICE: 1978-740-094/1516